Tokyo Metropolitan University
The Graduate School of Science
The Department of physics

Universal nature of near-threshold exotic hadrons with compositeness

複合性を用いた閾値近傍のエキゾチックハドロンの普遍的性質

Tomona Kinugawa
衣川 友那

Abstract

Hadrons are particles composed of quarks and gluons interacting through the strong force. Most hadrons are classified into quark-antiquark pairs called mesons and three-quark states called baryons. In addition to these ordinary hadrons, states containing more than three quarks are called exotic hadrons. The number of experimental reports of exotic hadrons has been increasing year by year. Nevertheless, the proportion of exotic hadrons among all hadrons remains small. The fundamental theory of the strong interaction (quantum chromodynamics, QCD) does not explain the rarity of exotic hadrons. Moreover, the internal structure of exotic hadrons is not well established. Thus, the study of exotic hadrons is regarded as an important subject for understanding the low-energy phenomena in QCD. In recent hadron physics, exotic hadrons have been actively studied from both theoretical and experimental perspectives.

Exotic hadrons are mostly observed near the threshold energy above which the scattering of two hadrons occurs. Therefore, the internal structure of exotic hadrons should be studied with the consideration of the near-threshold nature. As a starting point to investigate the internal structure of the near-threshold exotic hadrons, an analogy with nuclear physics is useful. In nuclear physics, it is empirically known that the clustering phenomena emerge near the threshold of alpha particles (^{4}He nuclei), where nuclei consist of alpha particles as subunits rather than being constructed from protons and neutrons directly. This fact, known as the threshold rule, is regarded as a consequence of the low-energy universality which governs the near-threshold phenomena. By applying the threshold rule to hadron systems, it is naively expected that the near-threshold exotic hadrons have a hadronic molecular structure which consists of hadrons as subunits rather than directly consists of quarks.

The internal structure of exotic hadrons is expressed as a superposition of various possible components. The fraction of the hadronic molecular component is characterized by the quantitative measure called the compositeness. It is theoretically shown that the compositeness is unity (i.e., the state is a completely hadronic molecule) when the bound state exists exactly at the threshold, as a consequence of the low-energy universality. This suggests that the near-threshold states with a finite binding energy are dominated by the hadronic molecular component, which is in line with the threshold rule. However, the situation is not so straightforward, because a non-molecular component can always be mixed in, even for a shallow bound state. Thus, it is not theoretically clear why the threshold rule holds empirically. In other words, the theoretical basis of the threshold rule is not fully established. Furthermore, it is not clear how the threshold rule is affected by the decay and coupled channel contributions which are the peculiar features in hadron systems.

In this thesis, we aim to study the internal structure of the near-threshold states from the perspective of the low-energy universality. For this purpose, we introduce the effective field theory models to calculate the compositeness of the near-threshold states. We first examine the foundation of the threshold rule, by computing the probability of realizing a shallow non-composite bound state. We then quantitatively study the effect of decay width and channel coupling on the compositeness of the near-threshold states. We apply the present formulation to the renowned near-threshold exotic hadrons, $T_{cc}(3875)^+$ and $X(3872)$ to investigate their nature.

Contents

Chapter 1

Introduction

In this chapter, we present the background and aim of this thesis as an introduction. We first show an overview of hadrons and exotic hadrons in Section 1.1. Motivated by the recent observations of exotic hadrons, the study of the internal structure of exotic hadrons attracts significant interest. To characterize the internal structure of hadrons, we introduce a useful concept, called the compositeness (Section 1.2). A lot of exotic hadrons are observed in the near-threshold region, where the compositeness is model-independently determined as a consequence of the low-energy universality. We overview the low-energy universality in Section 1.3. Against this background, we finally describe the aim of this thesis in Section 1.4. In this thesis, we use the natural unit where $\hbar = c = 1$.

1.1 Exotic hadrons

Ordinary mesons and baryons

Elementary particles constitute the fundamental building blocks of matter in nature. Among them, quarks and gluons are governed by the strong interaction. The fundamental theory of the strong interaction is quantum chromodynamics (QCD). At low-energy scales, there arises difficulty in QCD because the perturbative methods do not work due to the strong coupling constant. One of the striking phenomena in low-energy QCD is color confinement. As a consequence of the confinement, the observed degrees of freedom are hadrons, not quarks and gluons. To elucidate low-energy phenomena in QCD, we focus on the study of hadrons.

Hadrons consist of quarks q and gluons g, except for top quarks t.[1] Specifically, all hadrons can be described as combinations of up u, down d, charm c, strange s, and bottom b quarks, together with gluons. In general, hadrons are classified into two categories, mesons and baryons. Mesons (baryons) typically consist of a pair of a quark and an anti-quark $q\bar{q}$ (three quarks qqq). For example, the proton $p \sim uud$ and neutron $n \sim udd$ are classified as baryons, while pions (e.g., $\pi^+ \sim u\bar{d}$) are categorized as mesons.

Let us demonstrate how the mesons are described as of $q\bar{q}$ using the nonrelativistic constituent quark model. The ground states are considered to have no angular momentum between q and $\bar{q}$. Because the spin-parity J^P of quarks (anti-quarks) is $1/2^+$ ($1/2^-$), the ground state mesons have

[1] Top quark t decays through the weak interaction before the hadronization.

$J^P = 0^-$ (pseudoscalar) or 1^- (vector). We can classify the combination of the u, d, s quarks by flavor SU(3) symmetry under the exchange of these quarks. By combining q ($\mathbf{3}$) representation and $\bar{q}$ ($\bar{\mathbf{3}}$), we obtain

$$\mathbf{3} \otimes \mathbf{3} = \mathbf{1} \oplus \mathbf{8}. \tag{1.1}$$

Thus, the mesons belong to either the singlet $\mathbf{1}$ or octet $\mathbf{8}$ representations. The ground state $J^P = 0^-$ octet mesons correspond to K^0, K^+, π^-, π^0, π^+, η_8, K^-, and $\bar{K}^0$. On the other hand, K^{*0}, K^{*+}, ρ^-, ρ^0, ρ^+, ω^0, ϕ^0, K^{*-}, and $\bar{K}^{*0}$ forms the ground state $J^P = 1^-$ nonet mesons. We note that the mass difference between s quark and u, d quarks induces SU(3) symmetry breaking. As a consequence, the mass splitting occurs among the octet mesons. Furthermore, symmetry breaking causes the mixing of η_8 state with the pseudoscalar singlet meson η_0, leading to the physical η and η' mesons. Similarly, in the vector mesons, physical ϕ and ω mesons are realized by the ideal mixing.

In the same way, the baryons qqq have the spin-parity $J^P = 1/2^+$ or $J^P = 3/2^+$ in the ground state. With flavor SU(3) symmetry, baryons are classified into the singlet, octet, and decuplet:

$$\mathbf{3} \otimes \mathbf{3} \otimes \mathbf{3} = \mathbf{1} \oplus \mathbf{8} \oplus \mathbf{8} \oplus \mathbf{10}. \tag{1.2}$$

Among all possible combinations of spin parity and flavor, only $1/2^+$ and $\mathbf{8}$, or $3/2^+$ and $\mathbf{10}$ are allowed so that the spin-flavor wavefunction is totally symmetric under the exchanges of quarks. Therefore, the ground state baryons are classified into $J^P = 1/2^+$ octet (n, p, Σ^-, Σ^0, Λ, Σ^+, Ξ^-, Ξ^0) and $J^P = 3/2^+$ decuplet states (Δ^-, Δ^0, Δ^+, Δ^{++}, Σ^{*-}, Σ^{*0}, Σ^{*+}, Ξ^{*-}, Ξ^{*0}, Ω^-).

For later discussion, we introduce the heavy-light mesons in the charm sector which contain one c quark. As before, the spin-parity of the ground state mesons is 0^- and 1^-. The u, d quarks and c quarks belong to the $\mathbf{2}$ and $\mathbf{1}$ representations of isospin SU(2) symmetry, respectively. Therefore, the ground state heavy-light mesons are classified into $(J^P, \text{flavor}) = (0^-, \mathbf{2})$ and $(1^-, \mathbf{2})$ states. The quark contents of the pseudoscalar mesons are:

$$D^0 \sim c\bar{u}, \tag{1.3}$$

$$D^+ \sim c\bar{d}, \tag{1.4}$$

and their anti-particles are:

$$\bar{D}^0 \sim \bar{c}u, \tag{1.5}$$

$$D^- \sim \bar{c}d. \tag{1.6}$$

The vector mesons are denoted with a superscript $*$, with the same quark contents but with spin 1 (e.g. $D^{*0} \sim c\bar{u}$).

It is usual to collectively denote the states belonging to the same isospin multiplet. For example, the proton p and neutron n are collectively expressed by the nucleon N:

$$N = \begin{pmatrix} p \\ n \end{pmatrix}. \tag{1.7}$$

In the same way, we use D and $\bar{D}$ for the heavy-light mesons

$$D = \begin{pmatrix} D^+ \\ D^0 \end{pmatrix}, \quad \bar{D} = \begin{pmatrix} \bar{D}^0 \\ D^- \end{pmatrix}, \tag{1.8}$$

$$D^* = \begin{pmatrix} D^{*+} \\ D^{*0} \end{pmatrix}, \quad \bar{D}^* = \begin{pmatrix} \bar{D}^{*0} \\ D^{*-} \end{pmatrix}. \tag{1.9}$$

With the isospin notation, for instance, $D\bar{D}$ stands for $D^+\bar{D}^0$, D^+D^-, $D^0\bar{D}^0$, or D^0D^-.

In this way, the quark model with $q\bar{q}$ and qqq predicts the quantum number of the ground state hadrons. These quantum numbers are consistent with those observed in the hadron spectra [1]. In addition to the ground states, the excited hadrons are described as the combination of the constituent quarks with finite angular momenta, which qualitatively reproduces the experimental data of excited hadrons [2, 3, 4]. Constituent quark models have been successfully applied to a wide range of hadrons, reproducing their properties in most cases. Therefore, it is broadly accepted that the internal structure of the ordinary hadrons is $q\bar{q}$ or qqq.

Classification of exotic hadrons

In QCD, quarks carry the color charge, but hadrons are realized as color singlet states. Color singlet states are constructed not only with $q\bar{q}$ or qqq but also with more than three quarks, such as $q\bar{q}q\bar{q}$, $qqq\bar{q}q$, and $qqqqqq$. States other than mesons ($q\bar{q}$) and baryons (qqq) are classified as exotic hadrons, as they differ from ordinary hadrons (mesons and baryons) [5, 6, 7].

In practice, the identification of exotic hadrons is performed by various criteria. Here we consider three exotics; (i) the quantum-number exotics (genuine exotics), (ii) the quarkonium-associated exotics, and (iii) the quark-model exotics [8]. In the following, we will show the details of these categories.

If the quantum number of a given hadron cannot be reached by the combination of $q\bar{q}$ or qqq, such hadron is identified as (i) the quantum-number exotic. The quantum number exotics are further categorized into the flavor exotics and the J^{PC} exotics. As an example of flavor exotics, let us show the case of $T_{cc}(3875)^+$, which is observed as the charm $C = 2$ state (i.e., containing two c quarks). To realize a color singlet hadron, we need two anti-quarks in this case, and $T_{cc}(3875)^+$ should contain at least four quarks $cc\bar{q}\bar{q}$ (q is different from c to have $C = 2$). In other words, $T_{cc}(3875)^+$ has two quark anti-quark pairs different from the mesons with one $q\bar{q}$ pair. In general, the hadrons with exotic flavor quantum numbers, such as $T_{cc}(3875)^+$ with $C = 2$, are called the flavor exotics. As of 2024, only five flavor exotic hadrons have been observed, $T^*_{cs0}(2870)^0$, $T^*_{cs1}(2900)^0$, $T^*_{c\bar{s}0}(2900)$, $T_{cc}(3875)^+$, $T_{b\bar{s}}(5568)^+$ [1].

In a similar way to the flavor exotics, J^{PC} exotic states are identified based on the combination of the spin J, parity P, and charge conjugation C. Because of the rotation and parity symmetry of QCD, the spin J and parity P serve as conserved quantum numbers. The charge conjugation $C = \pm$ is also defined, if the state transforms into itself under the charge conjugation which changes q with $\bar{q}$. Under this transformation, only the mesons consisting of the same flavor remain unchanged up to sign, such as $|c\bar{c}\rangle \sim |\bar{c}c\rangle$, while that of mesons with a different flavor and that of baryons do not transform into their antiparticles (e.g., $|u\bar{d}\rangle \neq |\bar{u}d\rangle$ and $|qqq\rangle \neq |\bar{q}\bar{q}\bar{q}\rangle$). To obtain the relation among charge conjugation C, spin of the quark pair S, and angular momentum between quarks L, let us consider the replacement of q with $\bar{q}$. In this case, the sign of the total wavefunction corresponds to the product of these of the spatial wavefunction, the spin wavefunction, and the charge conjugate C. The sign of the spatial wavefunction changes as $(-1)^L$ because the wavefunction is antisymmetric for odd numbers of L. The spin wavefunction also changes as $(-1)^{S+1}$ by recalling that the spin wavefunction is antisymmetric with $S = 0$. Because q and $\bar{q}$ are fermions, the total wavefunction should be antisymmetric with the

replacement, namely, the sign of the total wavefunction is -1:

$$-1 = C \times (-1)^L \times (-1)^{1+S}. \tag{1.10}$$

From this relation, we find that

$$C = (-1)^{L+S}. \tag{1.11}$$

By making a combination of a quark q ($J^P = 1/2^+$) and an anti-quark $\bar{q}$ ($J^P = 1/2^-$) with $L \geq 0$, the possible J^{PC} of $q\bar{q}$ mesons are found to be $J^{PC} = 0^{-+}, 1^{--}, 1^{+-}, 0^{++}, 1^{++}, 2^{++}, 2^{-+}, 1^{--}, 2^{--}, 3^{--}, ...$ Thus, the following J^{PC} states cannot be realized by $q\bar{q}$ but require $q\bar{q}q\bar{q}$, $q\bar{q}q\bar{q}q\bar{q}$, etc.:

$$J^{PC} = 0^{--}, 0^{+-}, 1^{-+}, ... \tag{1.12}$$

Only three J^{PC} exotic states are observed so far, $\pi^1(1400)$ ($J^{PC} = 1^{-+}$), $\pi^1(1600)$ ($J^{PC} = 1^{-+}$), and $\eta^1(1855)$ ($J^{PC} = 1^{-+}$) [1]. We emphasize that the quantum number exotics have more than four quarks already at the level of their minimal quark content, as shown above. This is a qualitative difference from other exotic hadrons (ii) and (iii).

On the other hand, some states are considered exotic, even though their minimal quark content is $q\bar{q}$ or qqq. These states are identified as exotic based on the hidden heavy quark pairs [(ii) the quarkonium-associated exotics] and the quark models [(iii) quark-model exotics].

If the state has the heavy $c\bar{c}$ or $b\bar{b}$ pairs in addition to the meson $q\bar{q}$ or baryon qqq structures with the light quarks, they are regarded as (ii) the quarkonium-associated exotics. At the level of the minimal quark content, such states have the same structure as the mesons or baryons considering the annihilation of $c\bar{c}$ or $b\bar{b}$. However, it is known that the heavy-quark pair is hardly created in the decay process from the OZI rule [9, 10, 11, 12]. Thus, if the hadrons observed in the decay process containing $c\bar{c}$ or $b\bar{b}$ pairs in addition to the $q\bar{q}$ or qqq with light quarks, the heavy-quark pair is intrinsically contained in the quark content of hadrons. For example, $P_{c\bar{c}}(4312)^+$ is observed as the state decaying into $J/\psi p$ whose quark content is $c\bar{c}uud$ [13, 14]. By annihilating the $c\bar{c}$ pair, the minimal quark content of $P_{c\bar{c}}(4312)^+$ is uud, the same as ordinary baryons. However, from OZI rule, $P_{c\bar{c}}(4312)^+$ is considered as a pentaquark state including $c\bar{c}$.

In addition to (i) the quantum number and (ii) the presence of $c\bar{c}$ or $b\bar{b}$ pair, the constituent quark models are sometimes used as criteria to identify the exotic hadrons. As discussed above, the constituent quark models with $q\bar{q}$ and qqq have largely succeeded in explaining the spectrum of a majority of hadrons. However, there are several exceptions that do not fit well within the quark-model framework. These exceptions are expected to have a different internal structure from $q\bar{q}$ or qqq, and are considered the exotic hadrons. For example, in the $C = 0$ sector, a lot of charmonium states including $c\bar{c}$ are predicted by the quark-model calculations. However, these predictions agree well only with the states below the $D\bar{D}$ threshold (Fig. 1.1) [5]. From this viewpoint, the states above the $D\bar{D}$ threshold are considered as candidates of exotic hadrons (XYZ mesons) [15, 5, 7].

The quantum-number exotics (i) are qualitatively different from other categories (ii) and (iii) because they are defined by the model-independent criterion, conserved quantum numbers. This is why the quantum-number exotics are also called the "genuine" exotic. Although (ii) and (iii) are not genuine exotics in this sense, they are regarded to be helpful to understand the nature of genuine exotic hadrons. Thus, quarkonium-associated exotics (ii) and quark model exotics (iii) are also actively studied in addition to quantum-number exotics (i).

In summary, exotic hadrons are identified by following viewpoints;

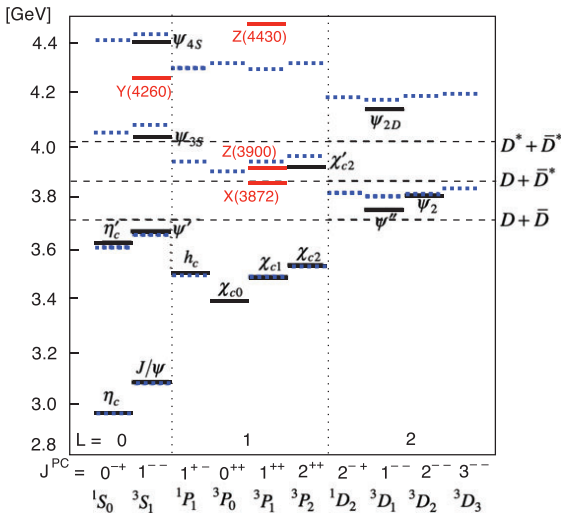

Figure 1.1: The spectrum of the observed hadrons in the charm sector, adapted from Ref. [5].

(i) quantum-number exotic (genuine exotic): the state whose minimal quark content is not $q\bar{q}$ or qqq. These exotic states are further categorized as;

- flavor exotics: the states whose quark contents are not $q\bar{q}$ or qqq in terms of the flavor [e.g. $T_{cc}(3875)^+$]
- J^{PC} exotics: the states whose combination of spin J, parity P, and charge conjugation C cannot be realized by $q\bar{q}$ [e.g. $\pi^1(1400)$ [1]],

(ii) quarkonium-associated exotics: the states which are considered to practically include the hidden $c\bar{c}$ or $b\bar{b}$ pairs [e.g. $Z_c(3900)$, $P_{c\bar{c}}(4312)^+$ [1]];

(iii) quark model exotics: the state with the minimal quark content $q\bar{q}$ or qqq, but whose nature does not agree with the results from the $q\bar{q}$ or qqq picture by the standard quark models [e.g. XYZ mesons].

We note that these categories are not mutually exclusive. For example, Z mesons are considered as exotics not only from the viewpoint of (ii) the quarkonium-associated exotics but also (iii) the quark model exotics.

Internal structure of exotic hadrons

In this way, exotic hadrons contain more quarks than ordinary hadrons. This suggests that exotic hadrons can have complex internal structures. Let us now consider the possible internal structure of exotic hadrons composed of $q\bar{q}q\bar{q}$ or $qqq\bar{q}q$.

The most straightforward example is the so-called multi-quark states which are compact states of more than three quarks. In this case, the strong interaction acts to attract all quarks through the gluons. Therefore, the size of multiquark states is expected to be ~ 1 fm, which is roughly estimated from the typical length scale of the strong interaction.

On the other hand, it is possible to make the combinations of two mesons ($q\bar{q}$ and $q\bar{q}$) or one baryon and one meson (qqq and $q\bar{q}$) from $q\bar{q}q\bar{q}$ or $qqqq\bar{q}$, respectively. In this case, the quarks form compact mesons or baryons as the subunits at first, and then these subunits interact through the strong interaction. These states are known as the hadronic molecular state. The typical example is the deuteron, where the subunits p and n are bound with the nuclear force through the π exchange. From the analogy of the nuclear force, the attraction between the subunits is considered to occur through the meson exchange. Therefore, the size of the hadronic molecule is estimated as larger than the typical length scale of the strong interaction $\gtrsim 1$ fm. In fact, the radius of the wavefunction of the deuteron is 4.32 fm, which is larger than the typical length scale of the strong interaction.[2]

In actual cases, it is natural that the internal structure of hadrons is described not as a pure multiquark state or hadronic molecule, but as a superposition of these components. In general, for a given hadron, all possible components having the same quantum numbers mix in. For example, the deuteron wavefunction does not purely contain the s-wave pn molecular component, but the small d-wave component exists (~ 5 %) [16]. To establish the internal structure of hadrons, we need to extract the fraction of these components. However, the conserved quantum numbers cannot be used to distinguish the multiquarks and the hadronic molecules. Therefore, some quantities should be introduced to classify the hadron structure. This is the motivation to employ the compositeness to characterize the internal structure of exotic hadrons.

As a characteristic phenomenon in hadron physics, the mixing associated with the $q\bar{q}$ creation occurs. Let us consider this mixing from the viewpoint of the baryon number B, defined as the conservation quantity from U(1) symmetry in QCD [17]. Using the baryon number, the meson (baryon) is defined as the state with $B = 0$ ($B = 1$). Because the baryon number of $q\bar{q}$ pair is zero, $q\bar{q}q\bar{q}$ also has $B = 0$ and is regarded as a meson. Therefore, wavefunction of a meson is given by $|\text{meson}\rangle = |q\bar{q}\rangle + |q\bar{q}q\bar{q}\rangle + ...$ Similarly, a baryon with $B = 1$ is expressed by $|\text{baryon}\rangle = |qqq\rangle + |qqqq\bar{q}\rangle + ...$

The picture with the $q\bar{q}$ creation can reproduce the spectra of excited hadrons, which allows the hadrons to have an exotic structure with more than four quarks. Furthermore, the spectra can be described also with the internal excitation of quarks. In this case, the excited hadrons is considered by the constituent quark models with the finite angular momentum between quarks. In this way, various possible components can contribute to the internal structure of hadrons (Fig. 1.2).

Because we cannot extract bare quarks due to the quark confinement, the asymptotic degrees of freedom are hadrons. This means that the internal structure of exotic hadrons cannot be observed in terms of the degrees of freedom of quarks. This feature of the strong interaction complicates the investigation of the internal structure of exotic hadrons. In this way, the study of the internal structure of exotic hadrons is challenging but important for gaining insight into low-energy phenomena in QCD.

Example of exotic hadrons

Before discussing the hadron wavefunction, here we show several examples of the exotic hadrons. The total number of observed hadrons has been getting larger every year. According to the Particle Data Group (PDG) [1], 227 kinds of mesons and 188 kinds of baryons have been found so far, and 10 mesons and 11 baryons have been newly discovered since 2022. In Fig. 1.3 and 1.4, we show the summary of observed hadrons so far. The shaded hadrons have been newly observed in the past two years,

[2] In addition to multi-quark and hadronic molecule, the gluonic hybrid state and glueball with the constituent gluon can be realized as the internal structure of exotic hadrons.

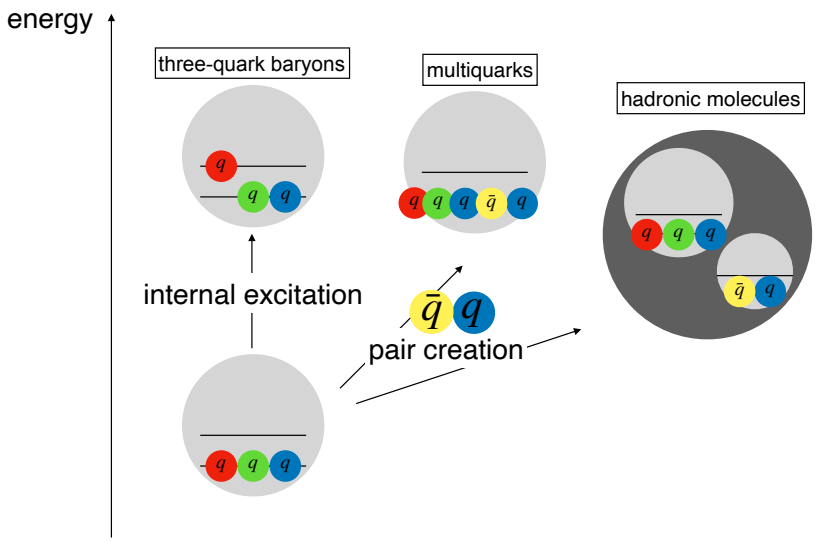

Figure 1.2: The schematic illustration of the possible internal structure of excited baryons.

and the enclosed hadrons by solid and dotted lines are the quantum-number exotics and J^{PC} exotics, respectively. As shown in these tables, the number of exotic hadrons is still smaller than that of ordinary hadrons but also increasing year by year. In the last two years, three kinds of quantum-number exotics [$\eta_1(1855)$, $T^*_{cs0}(2870)^+$ and $T_{cc}(3875)^+$] have been newly discovered in addition to the five exotic hadrons observed by 2022. In addition to these quantum-number exotic hadrons, there are various observations of the quarkonium-associated and quark-model exotic hadrons, whose number also increases every year. It is considered that the study of these hadrons leads to the understanding of the quantum-number exotic hadrons.

Let us show some examples of exotic hadrons. Even before the establishment of the concept of the exotic hadrons, the candidate of the exotic hadron $\Lambda(1405)$ has already been observed [18, 19, 20, 8, 21]. $\Lambda(1405)$ is not a quantum-number exotic state with the minimal quark content uds. However, it is regarded as the quark model exotic [category (iii)] due to the following reasons. In Ref. [3], the mass of $\Lambda(1405)$ is calculated using the constituent quark model by taking into account the excitations of quarks.[3] That work shows that the calculated spectrum of $\Lambda(1405)$ does not agree with the experimental data, while the model works well for other hadrons (Fig. 1.5). Furthermore, it is also shown that $\Lambda(1405)$ is lighter than the first excited states of nuclei [$N(1535)$] which consists only of the light quarks u and d. These results suggest that the qqq picture is not suitable to reproduce $\Lambda(1405)$. Therefore, $\Lambda(1405)$ is regarded as having an exotic structure.

Not only in the strange sector, the candidates of the exotic hadron have also been discovered in the charm sector with heavy c quarks, as shown above. As a representative XYZ mesons, we focus on $X(3872)$.[4] $X(3872)$ is the first observed XYZ mesons discovered in 2003 by the Belle experiment [22].

[3] $\Lambda(1405)$ cannot be produced only by the ground state three quarks with $1/2^+$, because of its negative parity $J^P = 1/2^-$.

[4] In PDG, $X(3872)$ is named as $\chi_{c1}(3872)$. However, we use $X(3872)$ due to a conventional reason. Similarly, almost all of the XYZ mesons are nowadays not named as X, Y, or Z in PDG, but we still call them XYZ mesons. Originally, "X" is assigned to the neutral states, and "Z" to charged states [7]. "Y" corresponds to the states produced by the

LIGHT UNFLAVORED ($S = C = B = 0$)

	$I^G(J^{PC})$
• $\pi^{\pm}$	$1^-(0^{-+})$
• π^0	$1^-(0^{-+})$
• η	$0^+(0^{-+})$
• $f_0(500)$	$0^+(0^{++})$
• $\rho(770)$	$1^+(1^{--})$
• $\omega(782)$	$0^-(1^{--})$
• $\eta'(958)$	$0^+(0^{-+})$
• $f_0(980)$	$0^+(0^{++})$
• $a_0(980)$	$1^-(0^{++})$
• $\phi(1020)$	$0^-(1^{--})$
• $h_1(1170)$	$0^-(1^{+-})$
• $b_1(1235)$	$1^+(1^{+-})$
• $a_1(1260)$	$1^-(1^{++})$
• $f_2(1270)$	$0^+(2^{++})$
• $f_1(1285)$	$0^+(1^{++})$
• $\eta(1295)$	$0^+(0^{-+})$
• $\pi(1300)$	$1^-(0^{-+})$
• $a_2(1320)$	$1^-(2^{++})$
• $f_0(1370)$	$0^+(0^{++})$
• $\pi_1(1400)$	$1^-(1^{-+})$
• $\eta(1405)$	$0^+(0^{-+})$
• $h_1(1415)$	$0^-(1^{+-})$
• $f_1(1420)$	$0^+(1^{++})$
• $\omega(1420)$	$0^-(1^{--})$
$f_2(1430)$	$0^+(2^{++})$
• $a_0(1450)$	$1^-(0^{++})$
• $\rho(1450)$	$1^+(1^{--})$
• $\eta(1475)$	$0^+(0^{-+})$
• $f_0(1500)$	$0^+(0^{++})$
$f_1(1510)$	$0^+(1^{++})$
• $f_2'(1525)$	$0^+(2^{++})$
• $f_2(1565)$	$0^+(2^{++})$
$\rho(1570)$	$1^+(1^{--})$
$h_1(1595)$	$0^-(1^{+-})$
• $\pi_1(1600)$	$1^-(1^{-+})$
• $a_1(1640)$	$1^-(1^{++})$
$f_2(1640)$	$0^+(2^{++})$
• $\eta_2(1645)$	$0^+(2^{-+})$
• $\omega(1650)$	$0^-(1^{--})$
• $\omega_3(1670)$	$0^-(3^{--})$
• $\pi_2(1670)$	$1^-(2^{-+})$
• $\phi(1680)$	$0^-(1^{--})$
• $\rho_3(1690)$	$1^+(3^{--})$

	$I^G(J^{PC})$
• $\rho(1700)$	$1^+(1^{--})$
• $a_2(1700)$	$1^-(2^{++})$
$a_0(1710)$	$1^-(0^{++})$
• $f_0(1710)$	$0^+(0^{++})$
$X(1750)$	$?^-(1^{--})$
$\eta(1760)$	$0^+(0^{-+})$
$f_0(1770)$	$0^+(0^{++})$
• $\pi(1800)$	$1^-(0^{-+})$
$f_2(1810)$	$0^+(2^{++})$
$X(1835)$	$0^+(0^{-+})$
• $\phi_3(1850)$	$0^-(3^{--})$
$\eta_1(1855)$	$0^+(1^{-+})$
• $\eta_2(1870)$	$0^+(2^{-+})$
• $\pi_2(1880)$	$1^-(2^{-+})$
$\rho(1900)$	$1^+(1^{--})$
$f_2(1910)$	$0^+(2^{++})$
$a_0(1950)$	$1^-(0^{++})$
• $f_2(1950)$	$0^+(2^{++})$
• $a_4(1970)$	$1^-(4^{++})$
$\rho_3(1990)$	$1^+(3^{--})$
$\pi_2(2005)$	$1^-(2^{-+})$
• $f_2(2010)$	$0^+(2^{++})$
• $f_0(2020)$	$0^+(0^{++})$
• $f_4(2050)$	$0^+(4^{++})$
$\pi_2(2100)$	$1^-(2^{-+})$
$f_0(2100)$	$0^+(0^{++})$
$f_2(2150)$	$0^+(2^{++})$
$\rho(2150)$	$1^+(1^{--})$
• $\phi(2170)$	$0^-(1^{--})$
$f_0(2200)$	$0^+(0^{++})$
$f_J(2220)$	$0^+(2^{++}$ or $4^{++})$
$\omega(2220)$	$0^-(1^{--})$
$\eta(2225)$	$0^+(0^{-+})$
$\rho_3(2250)$	$1^+(3^{--})$
• $f_2(2300)$	$0^+(2^{++})$
$f_4(2300)$	$0^+(4^{++})$
$f_0(2330)$	$0^+(0^{++})$
• $f_2(2340)$	$0^+(2^{++})$
$\rho_5(2350)$	$1^+(5^{--})$
$X(2370)$	$?^?(?^{??})$
$f_0(2470)$	$0^+(0^{++})$
$f_6(2510)$	$0^+(6^{++})$

STRANGE ($S = \pm1$, $C = B = 0$)

	$I(J^P)$
• $K^{\pm}$	$1/2(0^-)$
• K^0	$1/2(0^-)$
• K_S^0	$1/2(0^-)$
• K_L^0	$1/2(0^-)$
• $K_0^*(700)$	$1/2(0^+)$
• $K^*(892)$	$1/2(1^-)$
• $K_1(1270)$	$1/2(1^+)$
• $K_1(1400)$	$1/2(1^+)$
• $K^*(1410)$	$1/2(1^-)$
• $K_0^*(1430)$	$1/2(0^+)$
• $K_2^*(1430)$	$1/2(2^+)$
• $K(1460)$	$1/2(0^-)$
$K_2(1580)$	$1/2(2^-)$
$K(1630)$	$1/2(?^?)$
• $K_1(1650)$	$1/2(1^+)$
• $K^*(1680)$	$1/2(1^-)$
• $K_2(1770)$	$1/2(2^-)$
• $K_3^*(1780)$	$1/2(3^-)$
• $K_2(1820)$	$1/2(2^-)$
$K(1830)$	$1/2(0^-)$
• $K_0^*(1950)$	$1/2(0^+)$
• $K_2^*(1980)$	$1/2(2^+)$
• $K_4^*(2045)$	$1/2(4^+)$
$K_2(2250)$	$1/2(2^-)$
$K_3(2320)$	$1/2(3^+)$
$K_5^*(2380)$	$1/2(5^-)$
$K_4(2500)$	$1/2(4^-)$
$K(3100)$	$?^?(?^{??})$

CHARMED ($C = \pm1$)

	$I(J^P)$
• $D^{\pm}$	$1/2(0^-)$
• D^0	$1/2(0^-)$
• $D^*(2007)^0$	$1/2(1^-)$
• $D^*(2010)^{\pm}$	$1/2(1^-)$
• $D_0^*(2300)$	$1/2(0^+)$
• $D_1(2420)$	$1/2(1^+)$
• $D_1(2430)^0$	$1/2(1^+)$
• $D_2^*(2460)$	$1/2(2^+)$
$D_0(2550)^0$	$1/2(0^-)$
$D_1^*(2600)^0$	$1/2(1^-)$
$D^*(2640)^{\pm}$	$1/2(?^?)$
$D_2(2740)^0$	$1/2(2^-)$
• $D_3^*(2750)$	$1/2(3^-)$
$D_1^*(2760)^0$	$1/2(1^-)$
$D(3000)^0$	$1/2(?^?)$

CHARMED, STRANGE ($C = \pm1$, $S = \pm1$)

	$I(J^P)$
• $D_s^{\pm}$	$0(0^-)$
• $D_s^{*\pm}$	$0(1^-)$
• $D_{s0}^*(2317)^{\pm}$	$0(0^+)$
• $D_{s1}(2460)^{\pm}$	$0(1^+)$
• $D_{s1}(2536)^{\pm}$	$0(1^+)$
• $D_{s2}^*(2573)$	$0(2^+)$

CHARMED, STRANGE continued

	$I(J^P)$
$D_{s0}(2590)^+$	$0(0^-)$
• $D_{s1}^*(2700)^{\pm}$	$0(1^-)$
$D_{s1}^*(2860)^{\pm}$	$0(1^-)$
• $D_{s3}^*(2860)^{\pm}$	$0(3^-)$
$D_{sJ}(3040)^{\pm}$	$0(?^?)$

BOTTOM ($B = \pm1$)

	$I(J^P)$
• $B^{\pm}$	$1/2(0^-)$
• B^0	$1/2(0^-)$
• $B^{\pm}/B^0$ ADMIXTURE	
• $B^{\pm}/B^0/B_s^0/b$-baryon ADMIXTURE	
V_{cb} and V_{ub} CKM Matrix Elements	
• B^*	$1/2(1^-)$
• $B_1(5721)$	$1/2(1^+)$
$B_J^*(5732)$	$?(?^?)$
• $B_2^*(5747)$	$1/2(2^+)$
$B_J(5840)$	$1/2(?^?)$
• $B_J(5970)$	$1/2(?^?)$

BOTTOM, STRANGE ($B = \pm1$, $S = \mp1$)

	$I(J^P)$
• B_s^0	$0(0^-)$
• B_s^*	$0(1^-)$
• $B_{s1}(5830)^0$	$0(1^+)$
• $B_{s2}^*(5840)^0$	$0(2^+)$
$B_{sJ}^*(5850)$	$?(?^?)$
$B_{sJ}(6063)^0$	$0(?^?)$
$B_{sJ}(6114)^0$	$0(?^?)$

BOTTOM, CHARMED ($B = C = \pm1$)

	$I(J^P)$
• $B_c^{\pm}$	$0(0^-)$
• $B_c(2S)^{\pm}$	$0(0^-)$

$c\bar{c}$

	$I^G(J^{PC})$
• $\eta_c(1S)$	$0^+(0^{-+})$
• $J/\psi(1S)$	$0^-(1^{--})$
• $\chi_{c0}(1P)$	$0^+(0^{++})$
• $\chi_{c1}(1P)$	$0^+(1^{++})$
• $h_c(1P)$	$0^-(1^{+-})$
• $\chi_{c2}(1P)$	$0^+(2^{++})$
• $\eta_c(2S)$	$0^+(0^{-+})$
• $\psi(2S)$	$0^-(1^{--})$
• $\psi(3770)$	$0^-(1^{--})$
• $\psi_2(3823)$	$0^-(2^{--})$
• $\psi_3(3842)$	$0^-(3^{--})$
$\chi_{c0}(3860)$	$0^+(0^{++})$
• $\chi_{c1}(3872)$	$0^+(1^{++})$
• $\chi_{c0}(3915)$	$0^+(0^{++})$
• $\chi_{c2}(3930)$	$0^+(2^{++})$
$X(3940)$	$?^?(?^{??})$
• $\psi(4040)$	$0^-(1^{--})$
• $\chi_{c1}(4140)$	$0^+(1^{++})$
• $\psi(4160)$	$0^-(1^{--})$
$X(4160)$	$?^?(?^{??})$

$c\bar{c}$ continued

	$I^G(J^{PC})$
• $\psi(4230)$	$0^-(1^{--})$
• $\chi_{c1}(4274)$	$0^+(1^{++})$
$X(4350)$	$0^+(?^{?+})$
• $\psi(4360)$	$0^-(1^{--})$
• $\psi(4415)$	$0^-(1^{--})$
$\chi_{c0}(4500)$	$0^+(0^{++})$
$X(4630)$	$0^+(?^{?+})$
• $\psi(4660)$	$0^-(1^{--})$
$\chi_{c1}(4685)$	$0^+(1^{++})$
$\chi_{c0}(4700)$	$0^+(0^{++})$

$b\bar{b}$

	$I^G(J^{PC})$
• $\eta_b(1S)$	$0^+(0^{-+})$
• $\Upsilon(1S)$	$0^-(1^{--})$
• $\chi_{b0}(1P)$	$0^+(0^{++})$
• $\chi_{b1}(1P)$	$0^+(1^{++})$
• $h_b(1P)$	$0^-(1^{+-})$
• $\chi_{b2}(1P)$	$0^+(2^{++})$
$\eta_b(2S)$	$0^+(0^{-+})$
• $\Upsilon(2S)$	$0^-(1^{--})$
• $\Upsilon_2(1D)$	$0^-(2^{--})$
• $\chi_{b0}(2P)$	$0^+(0^{++})$
• $\chi_{b1}(2P)$	$0^+(1^{++})$
• $h_b(2P)$	$0^-(1^{+-})$
• $\chi_{b2}(2P)$	$0^+(2^{++})$
• $\Upsilon(3S)$	$0^-(1^{--})$
• $\chi_{b1}(3P)$	$0^+(1^{++})$
• $\chi_{b2}(3P)$	$0^+(2^{++})$
• $\Upsilon(4S)$	$0^-(1^{--})$
$\Upsilon(10753)$	$?^?(1^{--})$
• $\Upsilon(10860)$	$0^-(1^{--})$
• $\Upsilon(11020)$	$0^-(1^{--})$

OTHER

$T_{cs0}^*(2870)^0$	$?(0^+)$
$T_{cs1}^*(2900)^0$	$?(1^-)$
$T_{c\bar{s}0}^*(2900)$	$1(0^+)$
$T_{cc}(3875)^+$	$?(?^?)$
$T_{c\bar{c}1}(3900)$	$1^+(1^{+-})$
$T_{c\bar{c}s1}(4000)$	$1/2(1^+)$
• $T_{c\bar{c}}(4020)$	$1^+(?^{?-})$
$T_{c\bar{c}}(4050)^+$	$1^-(?^{?+})$
$T_{c\bar{c}}(4055)^+$	$1^+(?^{?-})$
$T_{c\bar{c}}(4100)^+$	$1^-(?^{?+})$
$T_{c\bar{c}1}(4200)^+$	$1^+(1^{+-})$
$T_{c\bar{c}s1}(4220)^+$	$1/2(1^+)$
$T_{c\bar{c}0}(4240)^+$	$1^+(0^{--})$
$T_{c\bar{c}}(4250)^+$	$1^-(?^{?+})$
• $T_{c\bar{c}1}(4430)^+$	$1^+(1^{+-})$
$T_{b\bar{s}}(5568)^+$	$1(?^?)$
$T_{cc\bar{c}\bar{c}}(6900)^0$	$0^+(?^{?+})$
• $T_{b\bar{b}1}(10610)$	$1^+(1^{+-})$
• $T_{b\bar{b}1}(10650)^+$	$1^+(1^{+-})$

Further States

Figure 1.3: The list of observed mesons and their quantum numbers adapted from PDG [1]. The shaded mesons are newly discovered states in the past two years. The hadrons enclosed by the solid (dotted) lines are the quantum-number exotic hadrons (J^{PC} exotic hadrons). The particle with • is well established by the experiments.

p	$1/2^+$	****	$\Delta(1232)$	$3/2^+$	****	Σ^+	$1/2^+$	****	Λ_c^+	$1/2^+$	****	Λ_b^0	$1/2^+$	***
n	$1/2^+$	****	$\Delta(1600)$	$3/2^+$	****	Σ^0	$1/2^+$	****	$\Lambda_c(2595)^+$	$1/2^-$	***	$\Lambda_b(5912)^0$	$1/2^-$	***
$N(1440)$	$1/2^+$	****	$\Delta(1620)$	$1/2^-$	****	Σ^-	$1/2^+$	****	$\Lambda_c(2625)^+$	$3/2^-$	***	$\Lambda_b(5920)^0$	$3/2^-$	***
$N(1520)$	$3/2^-$	****	$\Delta(1700)$	$3/2^-$	****	$\Sigma(1385)$	$3/2^+$	****	$\Lambda_c(2765)^+$		*	$\Lambda_b(6070)^0$	$1/2^+$	***
$N(1535)$	$1/2^-$	****	$\Delta(1750)$	$1/2^+$	*	$\Sigma(1580)$	$3/2^-$	*	$\Lambda_c(2860)^+$	$3/2^+$	***	$\Lambda_b(6146)^0$	$3/2^+$	***
$N(1650)$	$1/2^-$	****	$\Delta(1900)$	$1/2^-$	***	$\Sigma(1620)$	$1/2^-$	*	$\Lambda_c(2880)^+$	$5/2^+$	***	$\Lambda_b(6152)^0$	$5/2^+$	***
$N(1675)$	$5/2^-$	****	$\Delta(1905)$	$5/2^+$	****	$\Sigma(1660)$	$1/2^+$	***	$\Lambda_c(2910)^+$		*	Σ_b	$1/2^+$	***
$N(1680)$	$5/2^+$	****	$\Delta(1910)$	$1/2^+$	****	$\Sigma(1670)$	$3/2^-$	****	$\Lambda_c(2940)^+$	$3/2^-$	***	Σ_b^*	$3/2^+$	***
$N(1700)$	$3/2^-$	***	$\Delta(1920)$	$3/2^+$	***	$\Sigma(1750)$	$1/2^-$	***	$\Sigma_c(2455)$	$1/2^+$	****	$\Sigma_b(6097)^+$		***
$N(1710)$	$1/2^+$	****	$\Delta(1930)$	$5/2^-$	***	$\Sigma(1775)$	$5/2^-$	****	$\Sigma_c(2520)$	$3/2^+$	***	$\Sigma_b(6097)^-$		***
$N(1720)$	$3/2^+$	****	$\Delta(1940)$	$3/2^-$	**	$\Sigma(1780)$	$3/2^+$	*	$\Sigma_c(2800)$		***	Ξ_b^-	$1/2^+$	***
$N(1860)$	$5/2^+$	**	$\Delta(1950)$	$7/2^+$	****	$\Sigma(1880)$	$1/2^+$	**	Ξ_c^+	$1/2^+$	***	Ξ_b^0	$1/2^+$	***
$N(1875)$	$3/2^-$	***	$\Delta(2000)$	$5/2^+$	**	$\Sigma(1900)$	$1/2^-$	**	Ξ_c^0	$1/2^+$	****	$\Xi_b'(5935)^-$	$1/2^+$	***
$N(1880)$	$1/2^+$	***	$\Delta(2150)$	$1/2^-$	*	$\Sigma(1910)$	$3/2^-$	***	$\Xi_c'^+$	$1/2^+$	***	$\Xi_b(5945)^0$	$3/2^+$	***
$N(1895)$	$1/2^-$	****	$\Delta(2200)$	$7/2^-$	***	$\Sigma(1915)$	$5/2^+$	****	$\Xi_c'^0$	$1/2^+$	***	$\Xi_b(5955)^-$	$3/2^+$	***
$N(1900)$	$3/2^+$	****	$\Delta(2300)$	$9/2^+$	**	$\Sigma(1940)$	$3/2^+$	*	$\Xi_c(2645)$	$3/2^+$	***	$\Xi_b(6087)^0$	$3/2^-$	***
$N(1990)$	$7/2^+$	**	$\Delta(2350)$	$5/2^-$	*	$\Sigma(2010)$	$3/2^-$	*	$\Xi_c(2790)$	$1/2^-$	***	$\Xi_b(6095)^0$	$3/2^-$	***
$N(2000)$	$5/2^+$	**	$\Delta(2390)$	$7/2^+$	*	$\Sigma(2030)$	$7/2^+$	****	$\Xi_c(2815)$	$3/2^-$	***	$\Xi_b(6100)^-$	$3/2^-$	***
$N(2040)$	$3/2^+$	*	$\Delta(2400)$	$9/2^-$	**	$\Sigma(2070)$	$5/2^+$	*	$\Xi_c(2882)$		*	$\Xi_b(6227)^-$		***
$N(2060)$	$5/2^-$	***	$\Delta(2420)$	$11/2^+$	****	$\Sigma(2080)$	$3/2^+$	*	$\Xi_c(2923)$		**	$\Xi_b(6227)^0$		***
$N(2100)$	$1/2^+$	***	$\Delta(2750)$	$13/2^-$	**	$\Sigma(2100)$	$7/2^-$	*	$\Xi_c(2930)$		**	$\Xi_b(6327)^0$		***
$N(2120)$	$3/2^-$	***	$\Delta(2950)$	$15/2^+$	**	$\Sigma(2110)$	$1/2^-$	*	$\Xi_c(2970)$	$1/2^+$	***	$\Xi_b(6333)^0$		***
$N(2190)$	$7/2^-$	****				$\Sigma(2230)$	$3/2^+$	*	$\Xi_c(3055)$		***	Ω_b^-	$1/2^+$	***
$N(2220)$	$9/2^+$	****	Λ	$1/2^+$	****	$\Sigma(2250)$		**	$\Xi_c(3080)$		***	$\Omega_b(6316)^-$		***
$N(2250)$	$9/2^-$	****	$\Lambda(1380)$	$1/2^-$	**	$\Sigma(2455)$		*	$\Xi_c(3123)$		*	$\Omega_b(6330)^-$		***
$N(2300)$	$1/2^+$	**	$\Lambda(1405)$	$1/2^-$	****	$\Sigma(2620)$		*	Ω_c^0	$1/2^+$	***	$\Omega_b(6340)^-$		***
$N(2570)$	$5/2^-$	**	$\Lambda(1520)$	$3/2^-$	****	$\Sigma(3000)$		*	$\Omega_c(2770)^0$	$3/2^+$	***	$\Omega_b(6350)^-$		***
$N(2600)$	$11/2^-$	***	$\Lambda(1600)$	$1/2^+$	****	$\Sigma(3170)$		*	$\Omega_c(3000)^0$		***			
$N(2700)$	$13/2^+$	**	$\Lambda(1670)$	$1/2^-$	****				$\Omega_c(3050)^0$		***	$P_{c\bar{c}}(4312)^+$		*
			$\Lambda(1690)$	$3/2^-$	****	Ξ^0	$1/2^+$	****	$\Omega_c(3065)^0$		***	$P_{c\bar{c}s}(4338)^0$	$1/2^-$	*
			$\Lambda(1710)$	$1/2^+$	*	Ξ^-	$1/2^+$	****	$\Omega_c(3090)^0$		***	$P_{c\bar{c}}(4380)^+$		*
			$\Lambda(1800)$	$1/2^-$	***	$\Xi(1530)$	$3/2^+$	****	$\Omega_c(3120)^0$		***	$P_{c\bar{c}}(4440)^+$		*
			$\Lambda(1810)$	$1/2^+$	***	$\Xi(1620)$		**	$\Omega_c(3185)^0$		***	$P_{c\bar{c}}(4457)^+$		*
			$\Lambda(1820)$	$5/2^+$	****	$\Xi(1690)$		***	$\Omega_c(3327)^0$		***	$P_{c\bar{c}s}(4459)^0$		*
			$\Lambda(1830)$	$5/2^-$	****	$\Xi(1820)$	$3/2^-$	***						
			$\Lambda(1890)$	$3/2^+$	****	$\Xi(1950)$		***	Ξ_{cc}^+		*			
			$\Lambda(2000)$	$1/2^-$	*	$\Xi(2030)$	$\geq \frac{5}{2}$?	***	Ξ_{cc}^{++}		***			
			$\Lambda(2050)$	$3/2^-$	*	$\Xi(2120)$		*						
			$\Lambda(2070)$	$3/2^+$	*	$\Xi(2250)$		**						
			$\Lambda(2080)$	$5/2^-$	*	$\Xi(2370)$		**						
			$\Lambda(2085)$	$7/2^+$	**	$\Xi(2500)$		*						
			$\Lambda(2100)$	$7/2^-$	****									
			$\Lambda(2110)$	$5/2^+$	***	Ω^-	$3/2^+$	****						
			$\Lambda(2325)$	$3/2^-$	*	$\Omega(2012)^-$	$?^-$	***						
			$\Lambda(2350)$	$9/2^+$	***	$\Omega(2250)^-$		***						
			$\Lambda(2585)$		*	$\Omega(2380)^-$		**						
						$\Omega(2470)^-$		**						

Figure 1.4: The list of observed baryons and their quantum numbers adapted from PDG [1]. The shaded baryons are newly discovered states in the past two years. The number of $*$ represents the degree of the evidence of existence of the particle. $*$ evidence of existence is poor; $**$ evidence of existence is only fair; $***$ evidence ranges from very likely to certain, but further confirmation is desirable, and/or some properties are not well determined; $****$ existence is certain and properties are well known.

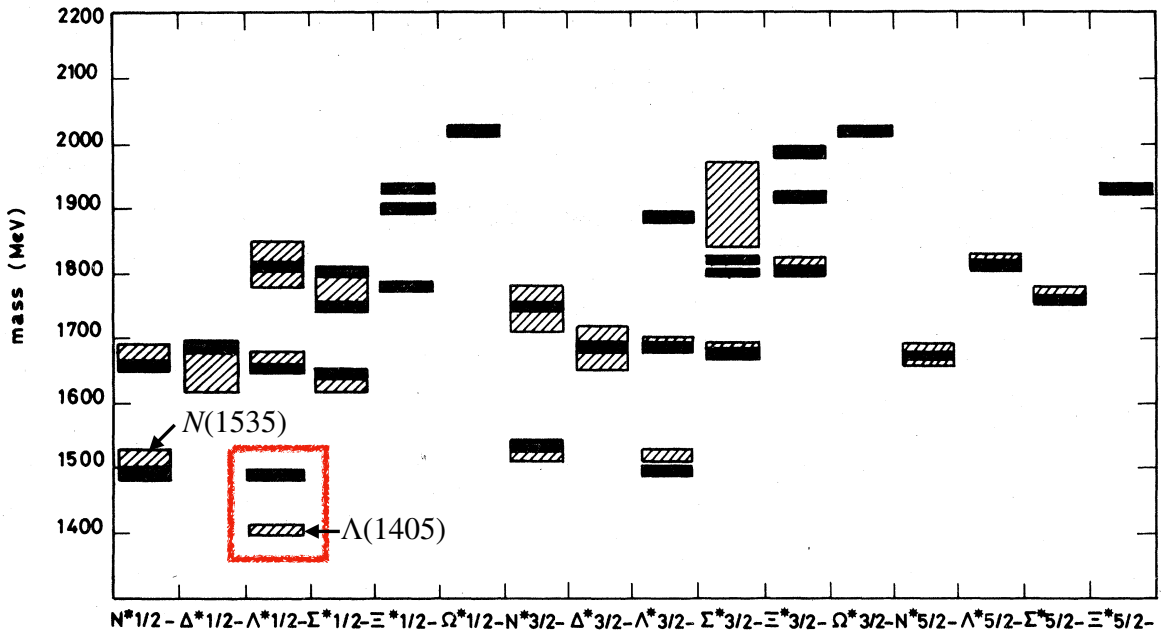

Figure 1.5: The mass of the negative parity baryons obtained from the constituent quark model (shaded square) and experiment (hatched square). The surrounded region shows the result of $\Lambda(1405)$. The original figure is adapted from Ref. [3], but some explanations are added.

The experiment observed the decay process of $B^{\pm} \to K^{\pm}\pi^{+}\pi^{-}J/\psi$, and found the charmonium-like state $X(3872)$ which decays to $\pi^{+}\pi^{-}J/\psi$ (left panel in Fig. 1.6). Because the quark content of $\pi^{+}\pi^{-}J/\psi$ is $u\bar{d}+\bar{u}d+c\bar{c}$, $X(3872)$ is not a quantum-number exotic state. However, it is considered as quark model exotic due to the lack of the corresponding prediction by the quark model [4]. After the first observation of $X(3872)$, more detailed features of $X(3872)$ were observed such as the spin parity $J^{PC} = 1^{++}$ [23] and isospin $I = 1$ [24]. In the recent experiments, the mass and width of $X(3872)$ was precisely observed in the $B^{+} \to K^{+}\pi^{+}\pi^{-}J/\psi$ decay process [25]. One of the significant feature of $X(3872)$ is its small binding energy $B = 0.04$ MeV with respect to the $D^{0}\bar{D}^{*0}$ threshold [1]. Based on the threshold rule discussed below, $X(3872)$ is considered to be the hadronic molecule-dominant state. At the same time, the experiment suggests that the $c\bar{c}$ core plays an important role to the $X(3872)$ structure [26, 27, 28]. Therefore, the internal structure of $X(3872)$ is now considered as the mixture of the molecular state and $c\bar{c}$ state.

In $C = 2$ sector with two c quarks, the LHCb collaboration has reported the existence of the genuine tetra-quark exotic state $T_{cc}(3875)^{+}$ in 2021 [30, 29]. They observed the $D^{0}D^{0}\pi^{+}$ mass distribution produced by the pp collision, and found the narrow peak just below the $D^{0}D^{*+}$ threshold (right panel of Fig. 1.6). This means that $T_{cc}(3875)^{+}$ decays into the $D^{0}D^{0}\pi^{+} \sim c\bar{u}c\bar{u}d\bar{}$, and therefore $T_{cc}(3875)^{+}$ is concluded as the flavor exotic state with the minimal quark contents $cc\bar{u}\bar{d}$. Motivated by the first observation by LHCb, many experimental groups are now performing additional experiments on $T_{cc}(3875)^{+}$. Before the first experimental report, the existence of the $cc\bar{u}\bar{d}$ state has already been extensively studied [31, 32, 33, 34, 35, 36, 37, 38, 39, 40, 41, 42, 43, 44, 45, 46, 47, 48, 49, 50, 51, 52,

initial state radiation, where the Y mesons have the common quantum number to the photon $J^{PC} = 1^{--}$ [5].

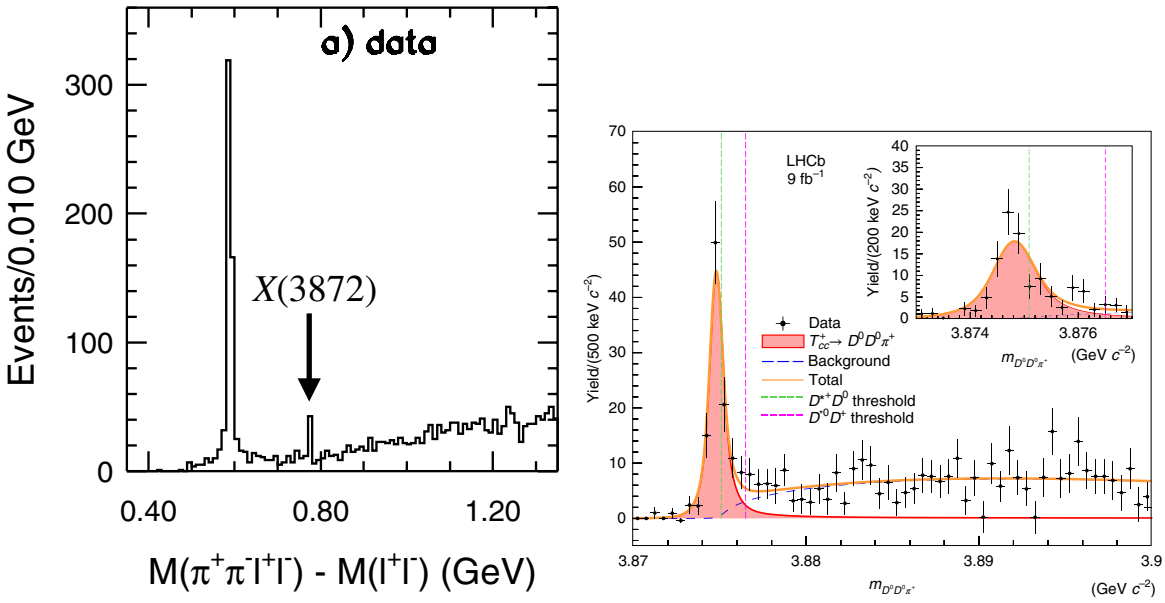

Figure 1.6: (Left) The spectrum of $X(3872)$ in $\pi^+\pi^- J/\psi$ mass distribution. The peak near the 0.80 GeV corresponds to the signal of $X(3872)$ (another large peak corresponds to ψ'). The original result is adopted from Ref. [22], but some explanations are added. (Right) The spectrum of $T_{cc}(3875)^+$ in the $D^0D^0\pi^+$ mass distribution, adapted from Ref. [29]. The peak below the D^0D^{*+} threshold (green dashed line) corresponds to the signal of $T_{cc}(3875)^+$.

53, 54, 55, 56, 57, 58, 59, 60, 61, 62, 63]. After the observation, a lot of studies of $T_{cc}(3875)^+$ has been continued not only as the multiquark states but also as the viewpoint of the hadronic molecular picture [64, 65, 66, 67, 68, 69, 70].

In the last part of this thesis, we focus on the internal structure of $X(3872)$ and $T_{cc}(3875)^+$, by focusing on their similarities and differences. Both $T_{cc}(3875)^+$ and $X(3872)$ are the near-threshold state of DD^*, and their binding energies are prominently small among the near-threshold exotic hadrons.[5] Furthermore, as seen above, both of them have the decay width and coupling to the isospin partner channel. It is also interesting to note that the $X(3872)$ is the oldest exotic hadrons in the charm sector, in contrast to the very newly observed $T_{cc}(3875)^+$. In addition to these similarities, we also find some differences between the two systems by comparing both systems. We see the decay width of $T_{cc}(3875)^+$ is relatively smaller than that of $X(3872)$, and the threshold energy difference $\Delta\omega$ of $X(3872)$ is relatively larger than that of $T_{cc}(3875)^+$. We summarize the system in Fig. 1.7.

1.2 Compositeness

In the above discussion, we see that the internal structure of exotic hadrons is written as a superposition of the various possible components, such as the hadronic molecule and the multiquark. Because these components cannot be distinguished using quantum numbers, as mentioned above, we need another

[5] In fact, the binding energy of $\Lambda(1405)$ is of the order of 10 MeV, which is considered as the usual energy scale of the near-threshold hadrons.

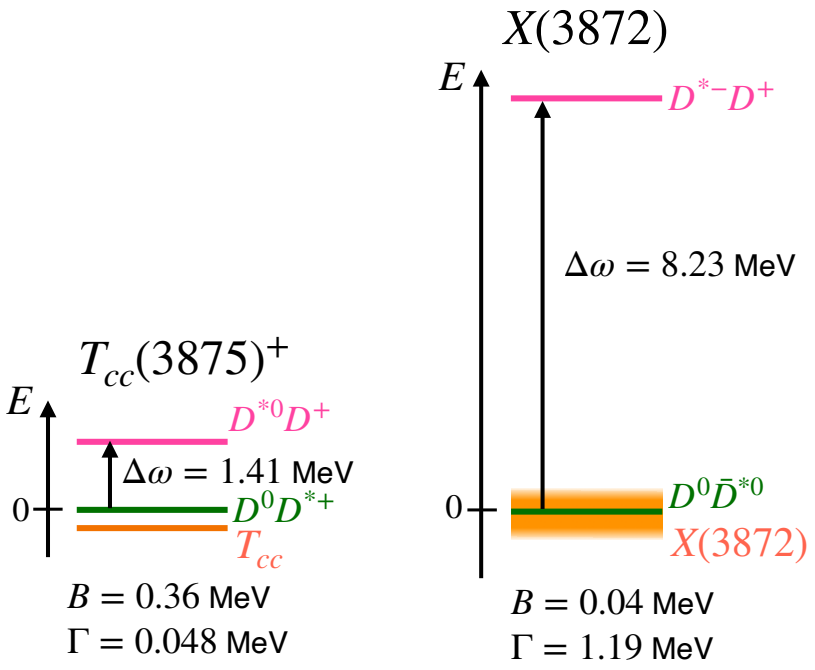

Figure 1.7: The schematic illustration of the system of $T_{cc}(3875)^+$ (left) and $X(8372)$ (right). The B is the binding energy, Γ is the decay width, and $\Delta\omega$ is the threshold energy difference between the threshold channel and the nearest coupled channel. This figure is adapted from Ref. [71].

quantity to characterize the internal structure of exotic hadrons. In this thesis, we introduce the measure called the compositeness, to study the fraction of the hadronic molecular component [72, 17, 73, 74].

While the formal definition of the compositeness will be given in Chapter 5, here let us briefly introduce the notion of the compositeness. The compositeness X is schematically represented as the square of the coefficient of the molecular component $|\text{molecular}\rangle$ in the bound state $|B\rangle$:

$$|B\rangle = \sqrt{X}\,|\text{molecular}\rangle + \sqrt{Z}\,|\text{non molecular}\rangle\,. \tag{1.13}$$

Here we denote the components other than molecular as $|\text{non molecular}\rangle$. For example, a multi-quark component is included in the non-molecular components. The fraction $Z = 1 - X$ is called the elementarity or elementariness. From Eq. (1.13), we see the compositeness is the probability of finding the molecular component $|\text{molecular}\rangle$ in the bound state $|B\rangle$:

$$X = |\,\langle B|\text{molecular}\rangle\,|^2. \tag{1.14}$$

By calculating the compositeness, we can quantitatively investigate the internal structure of bound states, determining whether they are molecule-dominant states with $X > 50\%$ or non-molecule-dominant states with $X < 50\%$.

Historically, the compositeness has been introduced in the works by S. Weinberg [75, 76, 72]. By estimating the compositeness model independently, he shows the deuteron is a composite state of p and n. After four decades, the notion of the compositeness has been applied to consider the internal structure of exotic hadrons (see also Sections 5.1 and 5.8).

The compositeness of the weakly bound states can be estimated only from the observables. In principle, the compositeness is a model-dependent quantity. However, when the binding energy is much smaller than the typical energy scale of the system, the compositeness X is model-independently related to the observables. This relation is called the weak-binding relation [72]. This model-independent nature of the weak-binding relation is associated with the low-energy universality discussed below.

1.3 Low-energy universality

As discussed above, many exotic hadrons are observed near the threshold, such as $T_{cc}(3875)^+$ and $X(3872)$. Therefore, to understand the nature of exotic hadrons, it is necessary to focus on the near-threshold states. In the near-threshold energy region, it is known that the low-energy universality holds [77, 78, 79, 80, 81, 82, 83], and phenomena follow the common laws irrespective of the microscopic details of the system. The mechanism of the universality is associated with the divergence of the scattering length. The scattering length is the physical observable characterizing the low-energy scatterings in the system (see Section 2.3.3). If the binding energy B decreases, the scattering length becomes larger. In the s-wave scattering, the scattering length diverges, and other scales become negligible in the $B = 0$ limit. In this case, all physical quantities are scale invariant.

Let us consider the realization of the universality with the following example. By comparing hadron and atomic systems, they have different typical energy scales, which can be estimated from the interaction in the system. For instance, the typical scale of hadrons (atoms) is estimated by the strong interaction ~ 1 fm $= 10^{-15}$ m (the Coulomb interaction ~ 1 Å$= 10^{-10}$ m). Even with this difference, however, the physical quantities in both systems can be estimated by the same equation as shown in the following. Here we consider the deuteron and ^{4}He dimer as the shallow bound states near the threshold.[6] As a consequence of the low-energy universality, the binding energy B of the shallow bound state is written only by the scattering length a_0:

$$B \sim \frac{1}{2\mu a_0^2}. \tag{1.15}$$

By substituting the scattering length of the deuteron ($a_0 = 1.75$ fm) [84] and that of ^{4}He dimer [$a_0 = 189$ Bohr radius (B.R.)] [85] to Eq. (1.15), the binding energy is estimated as [80, 77]

$$B_d^{\text{estimated}} = 1.41 \text{ [MeV]} \quad \text{(deuteron)}, \tag{1.16}$$

$$B_{^4\text{He}}^{\text{estimated}} = 1.21 \text{ [mK]} \quad (^4\text{He dimer}). \tag{1.17}$$

where unit mK means the millikelvin. For comparison, we also show the observed binding energy:

$$B_d^{\text{observed}} = 2.22 \text{ [MeV]} \quad \text{(deuteron)}, \tag{1.18}$$

$$B_{^4\text{He}}^{\text{observed}} = 1.30 \text{ [mK]} \quad (^4\text{He dimer}), \tag{1.19}$$

The ratios R_B of the estimated binding energies $B^{\text{estimated}}$ to the observed ones B^{observed} are obtained as follows

$$R_B = \frac{|B^{\text{observed}} - B^{\text{estimated}}|}{B^{\text{observed}}}, \tag{1.20}$$

[6] ^{4}He dimer is the shallow bound state of the two-body ^{4}He atom by the van der Waals force.

$$R_{B,d} = 0.36 \quad \text{(deuteron)}, \tag{1.21}$$

$$R_{B,^4\mathrm{He}} = 0.07 \quad (^4\text{He dimer}), \tag{1.22}$$

Equations (1.21) and (1.22) show that the deviation between the observed and estimated binding energies is small. This indicates that the binding energy of shallow bound states can be roughly estimated using Eq. (1.15), while the deuteron and ^{4}He dimer have very different scales such as $\sim$ MeV and $\sim$ mK. In this way, the realization of the universality is demonstrated. We note that B^{ratio} of the deuteron is not negligible when compared to that of ^{4}He dimer case. As shown below, this suggests the necessity of the range correction to the deuteron, where the contribution of higher-order terms is important.

We then apply the idea of the low-energy universality to discuss the nature of near-threshold hadrons by focusing on the radius of the wavefunction. When a bound state exists near the threshold to the extent that universality holds, the radius of the wavefunction R also becomes large with the scattering length a_0:

$$R = \frac{1}{\sqrt{2\mu B}} \sim a_0. \tag{1.23}$$

In this sense, the size of the shallow bound state is naively expected to be large. Intuitively, this fact seems to suggest that the shallow bound state is the hadronic molecular state, whose size is larger than the typical scale of hadrons.

In fact, this expectation is empirically supported by the α-clustering phenomena in nuclear physics. It is known that in the energy region near the threshold of α particles (the ^{4}He nuclei), the molecular-like structure of α particles is observed as the clustering phenomenon. In the clustering phenomena, the nucleons first form α particle as a subunit, and then these subunits compose the molecular-like nuclei, in contrast to the ordinary nuclei directly composed of nucleons. For example, the ^{8}Be nucleus exists near the two-α threshold, and it is known as the tw0-α composite state [86, 87]. Another well-known example is the excited state of the ^{12}C nucleus near the three-α threshold, called the Hoyle state. The Hoyle state is the weakly bound state of three α particles, while the ^{12}C ground state is the tightly bound state of twelve nucleons [88]. Based on the various observations of the clustering phenomena, it is expected that

> molecular-like structure is formed in a near-threshold state as a consequence of the clustering phenomena.

This idea is called the threshold rule [89, 90], and empirically confirmed by the above examples in nuclear physics. As an analogy to the clustering phenomena in nuclear physics, the hadronic molecules can be formed by the clustering of quarks. It is known that the clustering phenomena are widely observed across the hierarchy of matters, from hadrons to molecules (Fig. 1.8).

1.4 Aim of this thesis

As outlined so far, the establishment of the internal structure of the exotic hadrons such as $T_{cc}(3875)^+$ and $X(3872)$ attracts much interest. The structure of exotic hadrons can be characterized using the compositeness, the fraction of the hadronic molecular component in the wavefunction. Because most

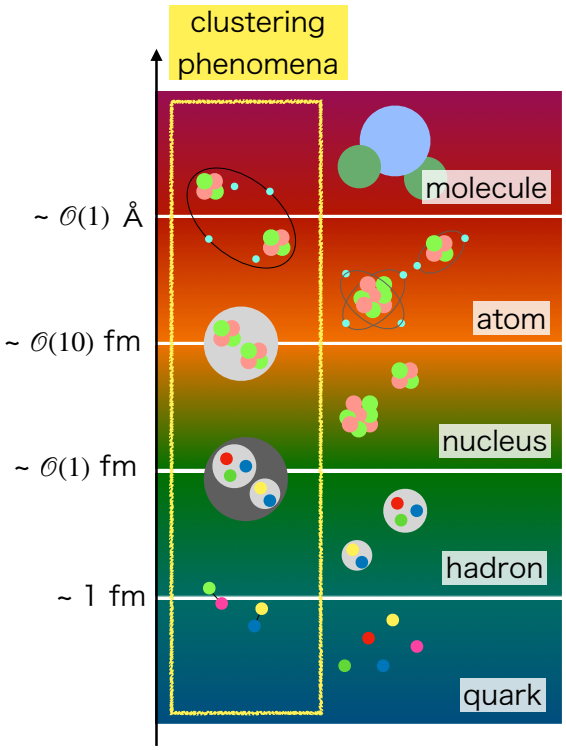

Figure 1.8: The illustration of the hierarchical structure of the matter in nature and the clustering phenomena.

of the exotic hadrons are observed in the near-threshold energy region, the low-energy universality is helpful in understanding the nature of exotic hadrons.

Against this background, we will discuss the universal nature of the near-threshold bound states using the compositeness. To study the internal structure of shallow bound states, let us start by recalling the threshold rule in nuclear physics, which states that the molecular-like structure appears in the near-threshold energy region. By applying the threshold rule to hadron systems, the near-threshold exotic hadrons are naively expected to have a hadronic molecular structure. In the context of the compositeness X, shallow bound states are expected to have $X \sim 1$. However, the threshold rule is empirical and not established in a theoretical manner. In fact, Refs. [91, 92] show that in the energy region other than on the threshold, it is possible to have the arbitrary value of the compositeness within $0 < X < 1$, even if the binding energy is small. In other words, the non-composite shallow bound states can always be realized, contrary to the expectation from the threshold rule. There arises a question: why does the threshold rule appear to align with the observations in nuclear physics? In this context, we aim to establish the theoretical foundation of the threshold rule and provide a theoretical justification for considering shallow bound states as having a molecular-like structure, in analogy with nuclear physics.

As an initial step, we consider the compositeness of shallow bound states in the simplest case, the single-channel system, from the viewpoint of the low-energy universality. We then move on to more realistic situations, by recalling that exotic hadrons have the decay and couplings to other

channels. References [93, 94] indicate that the compositeness of the shallow bound states is affected by contributions of decay and higher coupled channels. In light of this, we qualitatively investigate the contributions of decay and channel couplings to the compositeness of near-threshold states. Finally, we apply this framework to the representative near-threshold exotic hadrons, $T_{cc}(3875)^+$ and $X(3872)$. We calculate the compositeness of these exotic hadrons and discuss the internal structure. In summary, the following four topics are discussed in this thesis;

(a) the universal nature of shallow bound states in a single-channel system using the compositeness;

(b) how the compositeness is affected by the presence of the decay;

(c) how the compositeness is affected by the presence of the channel coupling; and

(d) the internal structure of $T_{cc}(3875)^+$ and $X(3872)$.

This thesis is organized as follows. In the next Chapter 2, we introduce the scattering theory and the definition of resonances. We then present the Feshbach method to describe coupled channel systems in Chapter 3 [74]. To discuss the universal nature of near-threshold states, we introduce the effective field theory models (Chapter 4) [95, 71, 74]. In Chapter 5, using the above formulations, we define the compositeness of bound states and resonances together with the useful expressions [95, 96, 74]. The evaluations of the compositeness of hadrons in previous works are summarized [74].

As the main topic of this thesis, we study the internal structure of the near-threshold states in Chapter 6 [71]. In the first Section 6.1, we discuss the threshold rule from the viewpoint of the low-energy universality in relation to the problem (a) discussed above. Here we employ the effecrive field theory model in Section 4.1 and the expression of the compositeness of bound states in Section 5.3. In the next Sections 6.3 and 6.4, we examine the contributions of the decay and channel coupling to the compositeness of shallow bound states to address the issues (b) and (c) using the model developed in Section 4.2. As an application of these formulations, in Section 6.5, we discuss the internal structure of the exotic hadrons $T_{cc}(3875)^+$ and $X(3872)$ [topic (d)] [96]. The last chapter is devoted to a summary.

Chapter 2

Scattering theory and resonances

Here we introduce the basic concepts to consider exotic hadron systems. Historically, hadron interactions have been studied through scattering experiments. Therefore, the scattering theory has been used to extract hadron interaction from the experimental observables. Here we formulate the non-relativistic two-body scattering theory. In Section 2.1, we first summarize the eigenstates of the Hamiltonian. The t-matrix and scattering amplitude are used to describe the scattering process. The definition and useful expressions of the t-matrix and scattering amplitude are given in Section 2.2 and Section 2.3. Furthermore, most exotic hadrons are unstable states which decay into the ground state hadrons through the strong interaction, as mentioned in the introduction. Unstable states are called resonances in the scattering theory. In the Schrödinger equation, resonances are described as the generalized discrete eigenstates of the Hamiltonian. Through the classification of the eigenstates of the Hamiltonian, we summarize the properties of resonances in Section 2.4. The unstable nature of resonances prevents us from normalizing their wavefunctions. Thus, we introduce the generalized eigenvector (the Gamow vector) to define meaningful expectation values in Section 2.5.

2.1 Hamiltonian and eigenstates

We discuss the non-relativistic, two-body, and single-channel s-wave scatterings with short-range potential. In this formulation, we consider the particles without the internal degrees of freedom such as the spin and isospin. We introduce the stationary scattering states (Section 2.1.1) and eigenstates of the free Hamiltonian (Section 2.1.2), which are used to define the compositeness in later sections. The relation between the scattering eigenstates is shown as the Lippmann-Schwinger equation in Section 2.1.3.

2.1.1 Asymptotic eigenstates

We formulate the non-relativistic two-body scatterings based on the Hamiltonian which satisfies the following time-dependent Schrödinger equation:

$$i\frac{\partial}{\partial t}\psi(t,\boldsymbol{r}) = \hat{H}\psi(t,\boldsymbol{r}). \tag{2.1}$$

If the Hamiltonian does not explicitly depend on time, the system can be described by the time-independent scattering problem. In this case, the wavefunction can be factorized as

$$\psi(t, \boldsymbol{r}) = \phi(t)\Psi(\boldsymbol{r}). \tag{2.2}$$

The time-dependent part $\phi(t)$ is obtained from Eq. (2.1) as

$$\phi(t) = Ce^{-iE_h t}, \tag{2.3}$$

with a constant C and the eigenenergy E_h which is given by the time-independent Schrödinger equation:

$$\hat{H}\Psi(\boldsymbol{r}) = E_h\Psi(\boldsymbol{r}). \tag{2.4}$$

In the following, we focus on the coordinate space wavefunction $\Psi(\boldsymbol{r})$.

We denote the state vector as $|\Psi\rangle$ such that $\langle \boldsymbol{r}|\Psi\rangle = \Psi(\boldsymbol{r})$. Using the state vector, the Schrödinger equation is written as

$$\hat{H}\,|\Psi\rangle = E_h\,|\Psi\rangle\,. \tag{2.5}$$

For a short-range potential, the asymptotic (stationary) scattering states $|\boldsymbol{p}, \pm\rangle$ exist in the Hilbert space, with the eigenmomentum $\boldsymbol{p}$ being a continuous valiable[1]. Here we assume that the system also has one bound state $|B\rangle$. In this setup, Eq. (2.5) reads

$$\hat{H}\,|\boldsymbol{p}, \pm\rangle = E_p\,|\boldsymbol{p}, \pm\rangle\,, \quad E_p = \frac{\boldsymbol{p}^2}{2\mu}, \tag{2.6}$$

$$\hat{H}\,|B\rangle = -B\,|B\rangle\,, \tag{2.7}$$

where μ is the reduced mass of the system and $B > 0$ is the binding energy of $|B\rangle$.

The bound state can be normalized as

$$\langle B|B\rangle = 1, \tag{2.8}$$

because its wavefunction $\langle \boldsymbol{r}|B\rangle$ vanishes at large distance $r \to \infty$. For the normalization of the interacting scattering states, we use the following condition[2]

$$\langle \boldsymbol{p}', \pm|\boldsymbol{p}, \pm\rangle = \delta(\boldsymbol{p}' - \boldsymbol{p}). \tag{2.9}$$

Because $|\boldsymbol{p}, \pm\rangle$ and $|B\rangle$ are the eigenstates of the same Hamiltonian $\hat{H}$ with different eigenvalues, they are orthogonal:

$$\langle B|\boldsymbol{p}, \pm\rangle = 0. \tag{2.10}$$

We assume the validity of the following completeness relation [97]:

$$1 = \int d\boldsymbol{p}\ \ |\boldsymbol{p}, \pm\rangle\,\langle \boldsymbol{p}, \pm| + |B\rangle\,\langle B|\,. \tag{2.11}$$

[1] The interacting scattering state asymptotically behaves as the free scattering state at the large distance [97].

[2] We use this normalization in quantum mechanics in Chapters 2 and 3, while we adopt a different normalization in the field theory framework in Chapter 4. See Section 2.3.2 for the summary of differences.

2.1.2 Free eigenstates

For later discussions, we decompose the full Hamiltonian $\hat{H}$ intro the free Hamiltonian $\hat{H}_0$ and interaction $\hat{V}$:

$$\hat{H} = \hat{H}_0 + \hat{V}. \tag{2.12}$$

The explicit forms of $\hat{H}_0$ and $\hat{V}$ can be chosen depending on the specific context under consideration. As a simple example, we consider the following free Hamiltonian:

$$\hat{H}_0 |\boldsymbol{p}\rangle = -\frac{\nabla^2}{2\mu} |\boldsymbol{p}\rangle = E_p |\boldsymbol{p}\rangle \tag{2.13}$$

Here $|\boldsymbol{p}\rangle$ are the free scattering states with the eigenenergy E_p, which are normalized as

$$\langle \boldsymbol{p}'|\boldsymbol{p}\rangle = \delta(\boldsymbol{p}' - \boldsymbol{p}). \tag{2.14}$$

The completeness relation in this case is given only with the free scattering states:

$$1 = \int d\boldsymbol{p} \, |\boldsymbol{p}\rangle \langle \boldsymbol{p}| \,. \tag{2.15}$$

The solution of Eq. (2.13) in the coordinate space $\langle \boldsymbol{r}|\boldsymbol{p}\rangle$ is the plane wave

$$\langle \boldsymbol{r}|\boldsymbol{p}\rangle \sim e^{i\boldsymbol{p}\cdot\boldsymbol{r}}. \tag{2.16}$$

While the free scattering states $\langle \boldsymbol{r}|\boldsymbol{p}\rangle$ have the same eigenenergy E_p with interacting scattering states $\langle \boldsymbol{r}|\boldsymbol{p}, \pm\rangle$, their wavefunctions are different from each other because the latter contains the effect of the interaction.

Here we emphasize that the decomposition of the full Hamiltonian into $\hat{H}_0$ and $\hat{V}$ is not unique. As a decomposition suitable for introducing the compositeness, we consider a different case where free Hamiltonian $\hat{H}_0$ has not only the scattering eigenstates $|\boldsymbol{p}\rangle$ but also a discrete eigenstate $|\phi\rangle$ with the eigenenergy ν_0. Namely, this Hamiltonian leads to the Schrödinger equations

$$\hat{H}_0 |\boldsymbol{p}\rangle = E_p |\boldsymbol{p}\rangle \,, \tag{2.17}$$

$$\hat{H}_0 |\phi\rangle = \nu_0 |\phi\rangle \,. \tag{2.18}$$

The discrete state $|\phi\rangle$ is sometimes called the bare state, in analogy with the quantum field theory. This setup essentially corresponds to the coupled-channel system, as shown in the Feshbach method in Chapter 3. The completeness relation in this case is given by

$$1 = \int d^3\boldsymbol{p} \, |\boldsymbol{p}\rangle \langle \boldsymbol{p}| + |\phi\rangle \langle \phi| \,. \tag{2.19}$$

The free scattering states and the discrete bare state are also orthogonal with each other and normalized as

$$\langle \phi|\boldsymbol{p}\rangle = 0, \tag{2.20}$$

$$\langle \boldsymbol{p}'|\boldsymbol{p}\rangle = \delta(\boldsymbol{p}' - \boldsymbol{p}), \tag{2.21}$$

$$\langle \phi|\phi\rangle = 1. \tag{2.22}$$

In general, $\hat{H}_0$ and $\hat{V}$ can be chosen arbitrarily without modifying the full Hamiltonian $\hat{H}$ [98, 75]. It is shown that the formulation with $\hat{H}_0$ in Eq. (2.13) can be converted to another formulation with $\hat{H}_0$ in Eqs. (2.17) and (2.18) by adjusting the interaction $\hat{V}$ appropriately.

2.1.3 Lippmann-Schwinger equation for eigenstates

Let us consider the relation between the scattering eigenstates of the full Hamiltonian $|\boldsymbol{p}, \pm\rangle$ and those of the free Hamiltonian $|\boldsymbol{p}\rangle$. This relation called the Lippmann-Schwinger equation (L-S equation), can be derived from the Schrödinger equation (2.6). Using Eq. (2.12), the Schrödinger equation (2.6) can be written by $\hat{H}_0$ and $\hat{V}$:

$$\hat{V}\,|\boldsymbol{p}, \pm\rangle = (E_p - \hat{H}_0)\,|\boldsymbol{p}, \pm\rangle\,. \tag{2.23}$$

The Schrödinger equation for the free Hamiltonian $\hat{H}_0$ (2.13) leads

$$-(E_p - \hat{H}_0)\,|\boldsymbol{p}\rangle = 0. \tag{2.24}$$

Combining these two, we then obtain

$$\hat{V}\,|\boldsymbol{p}, \pm\rangle = (E_p - \hat{H}_0)(|\boldsymbol{p}, \pm\rangle - |\boldsymbol{p}\rangle). \tag{2.25}$$

Here we define the free Green's operator as

$$\hat{G}_0(z) = (z - \hat{H}_0)^{-1}, \tag{2.26}$$

which satisfies

$$\hat{G}_0(z)\,|\boldsymbol{p}\rangle = \frac{1}{z - E_p}\,|\boldsymbol{p}\rangle\,. \tag{2.27}$$

Using $\hat{G}_0$, Eq. (2.25) can be written as

$$|\boldsymbol{p}, \pm\rangle = |\boldsymbol{p}\rangle + \hat{G}_0(E_p)\hat{V}\,|\boldsymbol{p}, \pm\rangle\,. \tag{2.28}$$

This is called the L-S equation for the wavefunction. We note that Eq. (2.28) with operators does not depend on the explicit form of $\hat{H}_0$, while its coordinate representation can be different depending on the completeness relation.

2.2 Expressions of t-matrix

The stationary scatterings are formulated using the T-operator and Green's operator, which will be introduced in this section. Here we present the definition of T-operator and t-matrix, the matrix element of the T-operator (Section 2.2.1). Then we show several equations for the t-matrix with free and full Hamiltonians (Section 2.2.2 and 2.2.3).

2.2.1 T-operator and t-matrix

The T-operator is defined for an arbitrary energy z as [97]

$$\hat{T}(z) = \hat{V} + \hat{V}\hat{G}(z)\hat{V}. \tag{2.29}$$

Here $\hat{V}$ is the interaction defined in Eq. (2.12). $\hat{G}(z)$ is the full Green's operator:

$$\hat{G}(z) = (z - \hat{H})^{-1}, \tag{2.30}$$

which corresponds to the propagator with the full Hamiltonian. This definition shows that when $\hat{G}(z)$ diverges, $\hat{T}(z)$ also diverges. Namely, $\hat{G}(z)$ and $\hat{T}(z)$ have poles at the same energy z. Here we define the free Green's operator $\hat{G}^0(z)$ [97]

$$\hat{G}^0(z) = (z - \hat{H}_0)^{-1}, \tag{2.31}$$

which is the propagator with the free Hamiltonian. It is shown that these operators are related to each other as follows [97]:

$$\hat{G}(z)\hat{V} = \hat{G}^0(z)\hat{T}(z). \tag{2.32}$$

Substituting Eq. (2.32) into the definition (2.29), T-operator is shown to satisfy the relation with G^0

$$\hat{T}(z) = \hat{V} + \hat{V}\hat{G}^0(z)\hat{T}(z). \tag{2.33}$$

This is called the L-S equation for the T-operator. By substituting $\hat{T}(z)$ in the left-hand side into that in the right-hand side iteratively, we find the T-operator is expressed by an infinite sum of $\hat{V}$ and $\hat{G}^0$

$$\hat{T} = \hat{V} + \hat{V}\hat{G}^0\hat{V} + \hat{V}\hat{G}^0\hat{V}\hat{G}^0\hat{V} + ... \tag{2.34}$$

This expansion shows that the T-operator represents the sum of the multiple scatterings (the Born series).

To discuss the scattering problem, it is convenient to consider the t-matrix. The off-shell t-matrix is defined as the matrix element of $\hat{T}(z)$ with the initial momentum $\boldsymbol{p}$ and final momentum $\boldsymbol{p}'$:

$$t(z; \boldsymbol{p}, \boldsymbol{p}') = \langle \boldsymbol{p}'|\hat{T}(z)|\boldsymbol{p}\rangle\,, \tag{2.35}$$

where the matrix element is taken by the free scattering states in Eq. (2.17). The energy z and momenta $\boldsymbol{p}$, $\boldsymbol{p}'$ can be chosen arbitrary in the off-shell t-matrix. On the other hand, to describe physical scatterings, the energy should be conserved $|\boldsymbol{p}| = |\boldsymbol{p}'|$, and the magnitude of momentum should satisfy $|\boldsymbol{p}| = \sqrt{2\mu z}$ (the on-shell condition) with a real and positive energy $z = E_p$. By imposing these conditions, we obtain the on-shell t-matrix $t(E_p)$:

$$t(E_p) = \langle \boldsymbol{p}'|\hat{T}(E_p + i0^+)|\boldsymbol{p}\rangle\Big|_{E_p = E_p'}\,. \tag{2.36}$$

Note that the on-shell t-matrix does not depend on the scattering angle $\cos\theta = \boldsymbol{p}'\cdot\boldsymbol{p}/|\boldsymbol{p}|^2$ in the s-wave case that we consider in this thesis.

In the following, we derive the two expressions of the on-shell t-matrix for later discussion;

- the L-S equation for t-matrix which is derived from Eq. (2.33) using the completeness relation of the eigenstates of the free Hamiltonian (2.15); and

- the Low-equation which is derived from Eq. (2.29) using the completeness relation of the eigenstates of the full Hamiltonian (2.11).

2.2.2 Lippmann-Schwinger equation for t-matrix

Here we derive the L-S equation for the on-shell t-matrix. By calculating the matrix element of the L-S equation for the T-operator (2.33), the equation for the off-shell t-matrix is obtained as

$$t(z;\boldsymbol{p},\boldsymbol{p}') = \langle \boldsymbol{p}|\hat{V}|\boldsymbol{p}'\rangle + \int d\boldsymbol{q}\ \frac{\langle \boldsymbol{p}|\hat{V}|\boldsymbol{q}\rangle}{z-E_q} t(z;\boldsymbol{q},\boldsymbol{p}'), \tag{2.37}$$

where we use the completeness relation (2.15). In general, the L-S equation is an integral equation for $t(Z;\boldsymbol{p},\boldsymbol{p}')$ due to the second term. When the free Hamiltonian $\hat{H}_0$ and the interaction $\hat{V}$ are given, we can calculate the t-matrix using Eq. (2.37).

It is known that when the interaction is separable, the L-S equation can be reduced to the algebraic equation, which is tractable to solve. If the matrix element of $\hat{V}$ can be factorized as the product of functions of $\boldsymbol{p}$ and $\boldsymbol{p}'$, the interaction is called separable:

$$\langle \boldsymbol{p}|\hat{V}|\boldsymbol{p}'\rangle = VF(p)F(p'), \tag{2.38}$$

where $F(p)$ is the form factor normalized at the on-shell momentum as

$$F(p)|_{p=\sqrt{2\mu E_p}} = 1. \tag{2.39}$$

When the interaction V is separable, it is shown from Eq. (2.29) that the t-matrix becomes also separable with the same form factors:

$$t(z;\boldsymbol{p},\boldsymbol{p}') = \tau(z)F(p)F(p'), \tag{2.40}$$

where we denote the energy-dependent part as $\tau(z)$. By substituting this expression into the L-S equation (2.37), we find that $\tau(z)$ satisfies the following algebraic equation:

$$\tau(z) = V + VG^0(z)\tau(z), \tag{2.41}$$

with the Green's function $G^0(z)$ defined as

$$G^0(z) = \int d\boldsymbol{q} \frac{|F(\boldsymbol{q})|^2}{z-E_q+i0^+}. \tag{2.42}$$

In this way, we obtain the explicit form of the off-shell t-matrix for the separable potential. Imposing the on-shell condition, we obtain

$$t(E_p) = \tau(E_p)|F(\boldsymbol{p})|^2 = \tau(E_p). \tag{2.43}$$

Therefore, the L-S equation for the on-shell t-matrix with the separable potential is derived as

$$t(E_p) = V + VG^0(E_p)t(E_p). \tag{2.44}$$

This leads to the on-shell t-matrix $t(E_p)$ as the following closesd form:

$$t(E_p) = [V^{-1} - G^0(E_p)]^{-1}. \tag{2.45}$$

The L-S equation (2.45) cannot be directly applied to the system with a discrete bare state $|\phi\rangle$ (2.19) introduced in Sec. 2.1, because Eq. (2.45) is derived based on the completeness relation (2.15). The

systems with $|\phi\rangle$ can be reduced to the systems only with $|\boldsymbol{p}\rangle$ where the L-S equation is applicable, by embedding the contribution of $|\phi\rangle$ into the interaction V (the channel elimination). In this case, the interaction V is replaced by the effective interaction $V_{\rm eff}(E_p)$ with the implicit contribution from $|\phi\rangle$, and the L-S equation becomes:

$$t(E_p) = [V_{\rm eff}^{-1}(E_p) - G^0(E_p)]^{-1}, \tag{2.46}$$

if the effective interaction is separable. In general, $V_{\rm eff}$ has an energy dependence due to the channel elimination. The detailed derivation of $V_{\rm eff}$ is shown in Chapters 3 and 4.

With the L-S equation, we obtain the on-shell t-matrix from the free Hamiltonian $\hat{H}_0$ and interaction $\hat{V}$. The eigenenergy of the full Hamiltonian is extracted from the pole of the on-shell t-matrix in this case. In the later discussion, we will mainly use the L-S equation (2.46) to calculate the scattering amplitude and compositeness.

2.2.3 Low equation

We also derive the integral equation for t-matrix, called the Low equation [99], by using the completeness relation (2.11). By calculating the matrix element of $\hat{T}(z)$ (2.29) in terms of $|\boldsymbol{p}\rangle$, we obtain the following relation

$$\begin{aligned} t(z;\boldsymbol{p},\boldsymbol{p}') &= \langle \boldsymbol{p}'|\hat{V}|\boldsymbol{p}\rangle + \langle \boldsymbol{p}'|\hat{V}\hat{G}(z)\hat{V}|\boldsymbol{p}\rangle \\ &= \langle \boldsymbol{p}'|\hat{V}|\boldsymbol{p}\rangle + \langle \boldsymbol{p}'|\,\hat{V}\,|B\rangle\,\langle B|\,\frac{1}{z-\hat{H}}\hat{V}\,|\boldsymbol{p}\rangle + \int d\boldsymbol{q}\ \langle \boldsymbol{p}'|\,\hat{V}\,|\boldsymbol{q},\pm\rangle\,\langle \boldsymbol{q},\pm|\,\frac{1}{z-\hat{H}}\hat{V}\,|\boldsymbol{p}\rangle \\ &= \langle \boldsymbol{p}'|\hat{V}|\boldsymbol{p}\rangle + \frac{\langle \boldsymbol{p}'|\,\hat{V}\,|B\rangle\,\langle B|\,\hat{V}\,|\boldsymbol{p}\rangle}{z+B} + \int d\boldsymbol{q}\ \frac{\langle \boldsymbol{p}'|\,\hat{V}\,|\boldsymbol{q},\pm\rangle\,\langle \boldsymbol{q},\pm|\,\hat{V}\,|\boldsymbol{p}\rangle}{z-E_q}. \end{aligned} \tag{2.47}$$

From this equation, the integral equation for the t-matrix is obtained by rewriting the third term:

$$t(z;\boldsymbol{p},\boldsymbol{p}') = \langle \boldsymbol{p}'|\hat{V}|\boldsymbol{p}\rangle + \frac{\langle \boldsymbol{p}'|\,\hat{V}\,|B\rangle\,\langle B|\,\hat{V}\,|\boldsymbol{p}\rangle}{z+B} + \int d\boldsymbol{q}\ \frac{\langle \boldsymbol{p}'|\,\hat{T}(E_q \pm i0^+)\,|\boldsymbol{q}\rangle\,\langle \boldsymbol{q}|\,\hat{T}(E_q \mp i0^-)\,|\boldsymbol{p}\rangle}{z-E_q} \tag{2.48}$$

$$= \langle \boldsymbol{p}'|\hat{V}|\boldsymbol{p}\rangle + \frac{\langle \boldsymbol{p}'|\,\hat{V}\,|B\rangle\,\langle B|\,\hat{V}\,|\boldsymbol{p}\rangle}{z+B} + \int d\boldsymbol{q}\ \frac{t(E_q \pm i0^+;\boldsymbol{p}',\boldsymbol{q})t(E_q \mp i0^+;\boldsymbol{q},\boldsymbol{p})}{z-E_q}, \tag{2.49}$$

where we use the relation between the asymptotic and free scattering states [97]:

$$\hat{V}\,|\boldsymbol{p},\pm\rangle = \hat{T}(E_p \pm i0^+)\,|\boldsymbol{p}\rangle\,. \tag{2.50}$$

The sign is determined to be + when the initial state is the interacting scattering states:

$$\langle \boldsymbol{p}'|\hat{T}(E_p+i0^+)|\boldsymbol{p}\rangle = \langle \boldsymbol{p}'|\hat{V}|\boldsymbol{p},+\rangle\,, \quad \langle \boldsymbol{p}'|\hat{T}(E_p+i0^+)|\boldsymbol{p}\rangle = \langle \boldsymbol{p}',-|\hat{V}|\boldsymbol{p}\rangle\,. \tag{2.51}$$

One of the solutions of Eq. (2.49) is obtained as the on-shell t-matrix which satisfies the following equation [72, 17]:

$$t(E_p) = \langle \boldsymbol{p}|\,\hat{V}\,|\boldsymbol{p}\rangle + \frac{|\,\langle \boldsymbol{p}|\,\hat{V}\,|B\rangle\,|^2}{E_p+B} + 4\pi\sqrt{2\mu^3}\int_0^\infty dE_q\ \frac{\sqrt{E'}|t(E_q)|^2}{E_p-E_q+i0^+}. \tag{2.52}$$

This is called the Low equation.

The Low equation is utilized to derive the weak-binding relation for the compositeness in Weinberg's pioneering work [72] and related papers such as Refs. [17, 100]. In the s-wave scatterings, the transition from the bound state to the scattering states $\langle \boldsymbol{p}| \hat{V} |B\rangle$ is written as

$$\langle \boldsymbol{p}| \hat{V} |B\rangle = g_{\rm th} F(E_p), \tag{2.53}$$

where $F(E_p)$ is the form factor which is normalized as $F(0) = 1$ and $g_{\rm th}$ is the coupling constant of the bound state pole at the threshold $E_p = 0$. The form factor should vanish at large E_p for the finite-range interaction. The Low-equation is then given by

$$t(E_p) = \langle \boldsymbol{p}| \hat{V} |\boldsymbol{p}\rangle + \frac{g_{\rm th}^2 |F(E_p)|^2}{E_p + B} + 4\pi\sqrt{2\mu^3} \int_0^\infty dE_q \, \frac{\sqrt{E_q}|t(E_q)|^2}{E_p - E_q + i0^+}. \tag{2.54}$$

Note that the Low equation explicitly contains the binding energy B, in contrast to the L-S equation. Therefore, the Low equation is useful when the binding energy is given. For example, the residue of the t-matrix at the bound state pole g^2 can be calculated from Eq. (2.54):

$$g^2 = \lim_{E \to -B} (E + B) t(E) \tag{2.55}$$

$$= g_{\rm th}^2 |F(-B)|^2. \tag{2.56}$$

We will use these relations to derive the expressions of the compositeness in Chapter 5.

2.3 Scattering amplitude

In this section, we first define the scattering amplitude (Section 2.3.1) and show the relation between the on-shell t-matrix and the scattering amplitude (Section 2.3.2). In Section 2.3.3, we then introduce the effective range expansion and the optical theorem.

2.3.1 Definition of scattering ampllitude

In general, the scattering amplitude $f(E_p, \theta)$ depends on the energy E_p and scattering angle θ. The scattering amplitude can be extracted from the asymptotic scattering wavefunction at large distance $r \to \infty$ [97]:

$$\langle \boldsymbol{r}|\boldsymbol{p}, +\rangle \to (2\pi)^{-3/2} \left[e^{i\boldsymbol{p}\cdot\boldsymbol{r}} + f(E_p, \theta) \frac{e^{ipr}}{r} \right] \quad (r \to \infty). \tag{2.57}$$

The first (second) term represents the incoming plane wave (outgoing spherical wave), and $f(E_p, \theta)$ controls E_p and θ dependence of the outgoing waves. Therefore, the information of the scattering is contained in the scattering amplitude.

The scattering amplitude is expanded using the Legendre polynomial P_l (partial-wave expansion) [97]

$$f(E, \theta) = \sum_{l=0}^{\infty} (2l + 1) f_l(E) P_l(\cos\theta), \tag{2.58}$$

where l is the angular momentum. In this expansion, $f_l(E)$ is called the partial-wave amplitude. In this thesis, we focus on the s-wave scattering near the threshold, where the contribution from higher partial waves can be neglected. We simply denote the s-wave amplitude $f_0(E)$ as $f(E)$ in the following.

2.3.2 Relation between on-shell t-matrix and scattering amplitude

It is known that the on-shell t-matrix $t(k)$ is related to the scattering amplitude $f(E)$ by the following relation [97]:

$$f(E) = -\mu(2\pi)^2 t(E) \quad \text{(quantum mechanics)}. \tag{2.59}$$

The coefficient $-\mu(2\pi)^2$ is chosen to be consistent with the convention of the normalization of the continuum states (2.21). We may adopt a different convention, for example, the normalization which is often used in the non-relativistic quantum field theory

$$\langle \boldsymbol{p}' | \boldsymbol{p} \rangle|_{\rm FT} = (2\pi)^3 (\boldsymbol{p}' - \boldsymbol{p}) \quad \text{(field theory)}. \tag{2.60}$$

The continuum states in Eq. (2.60) ($|\boldsymbol{p}\rangle|_{\rm FT}$) is related with those in Eq. (2.21) ($|\boldsymbol{p}\rangle|_{\rm QM}$) as

$$|\boldsymbol{p}\rangle|_{\rm FT} = (2\pi)^{3/2} |\boldsymbol{p}\rangle|_{\rm QM}\,. \tag{2.61}$$

Because the t-matrix (2.36) is defined by the matrix element with $|\boldsymbol{p}\rangle$, the relation between $f(E)$ and $t(E)$ in this convention becomes different from Eq. (2.59) by a $(2\pi)^3$ factor:

$$f(E) = -\frac{\mu}{2\pi} t(E) \quad \text{(field theory)}. \tag{2.62}$$

In the same way, the Green's function $G^0(z)$ is given by

$$G^0(z) = \int \frac{d\boldsymbol{q}}{(2\pi)^3} \frac{|F(\boldsymbol{q})|^2}{z - E_q + i0^+} \quad \text{(field theory)}. \tag{2.63}$$

We use Eq. (2.21) in this chapter and Chapter 3 where we work in the framework of the quantum mechanics, and Eqs. (2.60) and (2.62) in Chapter 4 and 6 where the effective field theory is utilized. We note that while the choice of the convention modifies the relations containing $|\boldsymbol{p}\rangle$ such as the completeness relation (2.15), the observables and compositeness remain unchanged [74].

2.3.3 Effective range expansion and optical theorem

In general, the denominator of the s-wave scattering amplitude can be expressed by the phase shift δ:

$$f(p) = \frac{1}{p\cot\delta - ip}. \tag{2.64}$$

It is known that $p\cot\delta$ can be expanded in powers of p^2:

$$f(p) = \left[-\frac{1}{a_0} + \frac{r_e}{2} p^2 + \mathcal{O}(p^4) - ip \right]^{-1}. \tag{2.65}$$

This expansion of the denominator of $f(p)$ is called the effective range expansion (ERE).[3] Here the coefficients a_0 and r_e are called the scattering length and effective range, respectively. The ERE (2.65)

[3]The expansion (2.65) is the expression for the s-wave with the angular momentum $l = 0$. For arbitrary l, the effective range expansion is given by

$$f_l(p) = \frac{p^{2l}}{-\frac{1}{a_l} + \frac{r_l}{2} p^2 + \mathcal{O}(p^4) - ip^{2l+1}}.$$

provides the general form of the scattering amplitude in the low-energy region, and a_0 and r_e characterize that behavior. We note that the sign convention of a_0 can be different from that in Eq. (2.65). For example, in hadron physics, a definition with the opposite sign $a_0 = f(0)$ is also used. In this thesis, we adopt the definition in Eq. (2.65), namely, $a_0 = -f(0)$.

It is known that the imaginary part of the scattering amplitude $f(E)$ is related to the s-wave cross section $\sigma(E)$ (the optical theorem for partial waves) [97]:

$$\mathrm{Im}\, f(E) = \frac{p}{4\pi}\sigma(E), \tag{2.66}$$

$$\sigma(E) = 4\pi|f(E)|^2, \tag{2.67}$$

which is derived from the unitarity of the s-matrix. By writing Eqs. (2.66) and (2.67) with $f(E)$ and $f^*(E)$, it is shown that

$$\mathrm{Im}\,\frac{1}{f(E)} = -p. \tag{2.68}$$

Thus, the $-ip$ term in the denominator of the scattering amplitude (2.64) is required by the unitarity through Eq (2.68).

2.4 Discrete eigenstates of Hamiltonian

From now on, we discuss the eigenstates of the Hamiltonian. In Section 2.1, only the bound state is considered as the discrete eigenstate of the Hamiltonian, for simplicity. However, in addition to the bound states, there are also eigenstates classified into the virtual states and resonances, according to their eigenenergy. As a preparation to show the properties of these eigenstates, we first consider how to obtain the bound state solution from the asymptotic wavefunction in Section 2.4.1. We then summarize the classification of the eigenstates in Section 2.4.2. We finally present the typical behavior of wavefunctions of different eigenstates and discuss their properties in Section 2.4.3.

2.4.1 outgoing boundary condition

For the classification of the eigenstates, let us first consider the boundary condition for the bound states using the general solution of the Schrödinger equation. In the $r \to \infty$ limit, the potential is assumed to vanish, and the solution corresponds to the superposition of plane waves. Because the eigenenergy of the scattering states is real and positive $E > 0$, the eigenmomentum of the scattering states $p = \sqrt{2\mu E}$ is also real and positive. Using the eigenmomentum, the asymptotic behavior of the scattering state is written as

$$u(r) \to A^-(p)e^{-ipr} + A^+(p)e^{+ipr}, \quad (r \to \infty), \tag{2.69}$$

where $u(r)$ is defined as the s-wave component of the radial wavefunction $u_l(r)$ with $l = 0$:

$$\langle \boldsymbol{r}|\Psi\rangle = \frac{u_l(r)}{r}Y_m^l(\theta,\phi). \tag{2.70}$$

As seen in Eq. (2.69), the wavefunction of the scattering states is written as a linear combination of the incoming wave e^{-ipr} and outgoing wave e^{+ipr}.

We then consider expressing a bound state wavefunction by starting from the general solution (2.69). As is known, bound states have a negative binding energy $E = -B < 0$. If we define real and positive $\kappa = \sqrt{2\mu B}$, the asymptotic behavior of $u(r)$ is written as

$$u(r) \to A^-(i\kappa)e^{+\kappa r} + A^+(i\kappa)e^{-\kappa r} \quad (r \to \infty). \tag{2.71}$$

To obtain the bound state solution, we impose the boundary condition $A^-(i\kappa) = 0$ so that the diverging component $e^{+\kappa r}$ vanishes.

By comparing Eqs. (2.69) and (2.71), we find that Eq. (2.71) corresponds to Eq. (2.69) with the complex eigenmomentum $p = i\kappa$. This indicates that Eq. (2.71) can also be regarded as Eq. (2.69) with the analytic continuation of the momentum p in the complex plane $p \in \mathbb{C}$ which is originally defined as a real quantity. Here we focus on the discrete eigenstates obtained by imposing the condition

$$A^-(p) = 0, \tag{2.72}$$

to Eq. (2.69) with a complex p as in the bound state cases [101]. This condition is called the outgoing boundary condition, with which only the outgoing wave e^{+ipr} remains. The outgoing boundary condition is equivalently expressed by the Siegert boundary condition [102, 103, 101]:

$$\frac{du(r)}{dr} = ipu(r). \quad (r \to \infty). \tag{2.73}$$

The coefficient of the incoming wave $A^-(p)$ is proportional to the Jost function [97]. It can be shown that the scattering amplitude $f(p)$ is related to $A^-(p)$ as

$$f(p) \propto \frac{1}{A^-(p)}. \tag{2.74}$$

From this relation, we find that the pole position of the scattering amplitude in the complex momentum plane corresponds to the eigenmomentum of the Hamiltonian.

2.4.2 Classification of eigenstates

Let us classify generalized eigenstates of Hamiltonian obtained from the outgoing boundary condition. In the discussion above, we see that bound states have pure imaginary eigenmomenta $p = i\kappa$ in the complex momentum plane. Discrete eigenstates with a general eigenmomentum $p = |p|e^{i\theta_p}$ are classified into

- bound states: positive-pure-imaginary eigenmomentum $p = i\kappa$ ($\theta_p = \pi/2$);
- virtual (anti-bound) states: negative-pure-imaginary eigenmomentum $p = -i\kappa_V$ with $\kappa_V > 0$ ($\theta_p = 3\pi/2$);
- resonances: complex eigenmomentum in the $7\pi/4 < \theta_p < 2\pi$ region; and
- anti-resonances: complex eigenmomentum in the $\pi < \theta_p < 5\pi/4$ region.

In Fig 2.1, we show the classification of the eigenstates in the complex momentum plane. The states in $3\pi/2 < \theta_p < 7\pi/4$ are called virtual states with width or resonance below the threshold, and $5\pi/4 < \theta_p < 3\pi/2$ are the conjugate states of them.

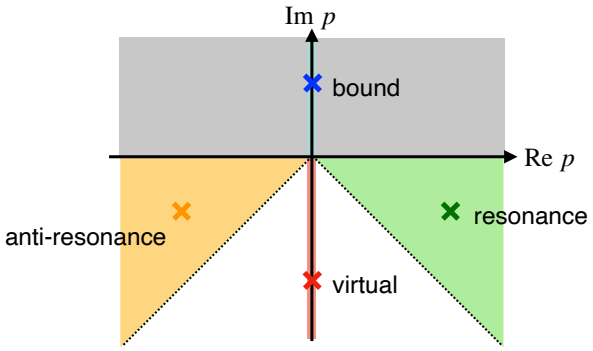

Figure 2.1: The classification of their eigenstates by the eigenmomentum (poles of the scattering amplitude) in the complex momentum p plane.

The eigenstates are also classified by the eigenenergy $E = p^2/(2\mu)$. The eigenmomentum $p = |p|e^{i\theta_p}$ is related to the eigenenergy $E = |E|e^{i\theta_E}$ as

$$|E|e^{i\theta_E} = \frac{|p|^2 e^{2i\theta_p}}{2\mu}. \tag{2.75}$$

From this relation, we find $2\theta_p = \theta_E$. Therefore, the argument of the momentum in the $0 \le \theta_p < 2\pi$ region corresponds to that of the energy in the $0 \le \theta_E < 4\pi$ region. This means that to express the whole complex momentum plane, we need two Riemann sheets for the complex energy plane. The energy plane with $0 \le \theta_E < 2\pi$ ($2\pi \le \theta_E < 4\pi$) is called the first (second) Riemann sheet, which corresponds to the upper (lower) half of the momentum p plane. From this relation, we now show the classification of the eigenstates in terms of the complex eigenenergy $E = |E|e^{i\theta_E}$. Here we denote the argument of the first and second Riemann sheets $\theta_E^I = \theta_E$ and $\theta_E^{II} = \theta_E - 2\pi$, respectively.

- Bound states: real and negative eigenenergy $E = -B = -\kappa^2/(2\mu) < 0$ ($\theta_E^I = \pi$) in the *first* Riemann sheet;
- virtual (anti-bound) states: real and negative eigenenergy $E = -E_V = -\kappa_V^2/(2\mu) < 0$ ($\theta_E^{II} = \pi$) in the *second* Riemann sheet;
- resonances: complex eigenenergy in the $3\pi/2 < \theta_E^{II} < 2\pi$ region of the *second* Riemann sheet;
- anti-resonances: complex eigenenergy in the $0 < \theta_E^{II} < \pi/2$ region of the *second* Riemann sheet;

In this way, only the bound states exist in the first Riemann sheet. We show the classification of the eigenstates in Fig. 2.2. We note that on the positive real axis Re $E > 0$, $A^-(p)$ is discontinuous. The branch cut associated with this discontinuity is called the unitary cut. Because the t-matrix and scattering amplitude have the same analytic properties with $A^-(p)$ as shown in Eq. (2.74), they also have the unitarity cut on the positive real axis.

Here we emphasize that the position of the eigenmoomentum is restricted to the region on the imaginary axis or the lower half of the momentum plane. This region corresponds to the negative real axis in the first Riemann sheet or the second Riemann sheet in the energy plane. This relation is understood by the square integrability of the wavefunction. By imposing the outgoing boundary

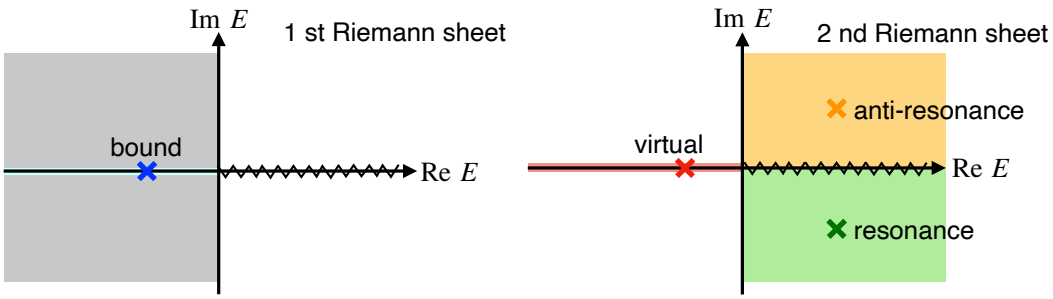

Figure 2.2: The classification of the eigenstates by their eigenenergy (poles of the scattering amplitude) in the complex energy E plane. The left (right) panel shows the first (second) Riemann sheet which corresponds to the upper (lower) half of the p plane. The wiggly lines stand for the unitarity cut.

condition to Eq. (2.69), we see the wavefunction $u(r)$ behaves at large distance as

$$u(r) \to A^+(p)e^{i(\mathrm{Re}\, p + i\, \mathrm{Im}\, p)r} = A^+(p)e^{i\, \mathrm{Re}\, p\cdot r - \mathrm{Im}\, p\cdot r} \quad (r \to \infty). \tag{2.76}$$

In the upper half of the momentum plane Im $p > 0$, the r integration of $|u(r)|^2$ converges thanks to the dumping term $e^{-\mathrm{Im}\, p\cdot r}$. This means that the wavefunction is square integrable in the upper half of the momentum plane (first Riemann sheet of the energy plane). The Hamiltonian is Hermitian with the square-integrable functions, and the eigenvalue, in this case, must be real. Therefore, the eigenstates are not allowed to exist in the upper half of the momentum plane, except for the imaginary axis. On the other hand, in the lower half of the momentum plane with Im $p < 0$ (second Riemann sheet of the energy plane), the integration of $|u(r)|^2$ diverges due to the factor $e^{-\mathrm{Im}\, p\cdot r} = e^{+|\,\mathrm{Im}\, p|r}$. Therefore, the Hamiltonian becomes non-Hermitian with non-integrable functions, and it is possible to have a complex eigenvalue. Because unstable resonances have a complex eigenenergy as shown below, we classify the poles in the lower half of the momentum plane into resonances. At the same time, this non-Hermitian nature of Hamiltonian induces some difficulties; Eq. (2.76) indicates that the wavefunction of the states in the lower half of the momentum plane diverges at a large distance, which is explicitly demonstrated in the next subsection. In this sense, the virtual states, resonances, and anti-resonances should be regarded as the generalized discrete eigenstates of the Hamiltonian, because they have a qualitatively different nature from bound states.

2.4.3 Wavefunction of discrete eigenstates

Here we show the difference among bound states, virtual states, and resonances from the viewpoint of the wavefunction. For demonstration, we adopt the rectangular potential to calculate the wavefuction setting $\mu = 1$, all the quantities are measured in powers of length.

Bound states

When two particles are bound together to form a stable composite state by the attractive interaction, such state is called the bound state $|B\rangle$. From Eq. (2.69), the asymptotic behavior of the wavefunction of discrete eigenstates is proportional to e^{+ipr} under the outgoing boundary condition (2.72). Because the eigenmomentum of the bound state is $p = i\kappa$ with $\kappa > 0$, the asymptotic form of the wavefunction

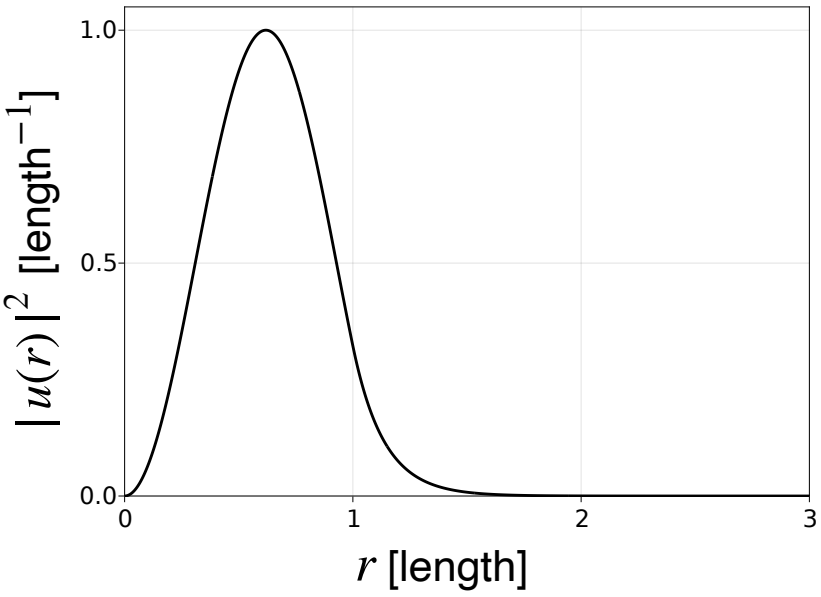

Figure 2.3: The wavefunction of the bound state with the binding energy $B = 6.8$ [length^{-2}] in the attractive square well potential. The width of the well is 1 [length], and the depth is 10 [length^{-2}].

of the bound state is written as

$$\langle \boldsymbol{r}|B\rangle = \frac{1}{\sqrt{4\pi}}\frac{u(r)}{r} \to \frac{1}{\sqrt{4\pi}}\frac{e^{-\kappa r}}{r} \quad (r \to \infty), \tag{2.77}$$

where $\kappa = \sqrt{2\mu B}$ with the binding energy B. As seen in Eq. (2.77), the bound state wavefunction decreases exponentially at large distance ($r \to \infty$). We plot the absolute value square of the bound state wavefunction $|u(r)|^2$ in Fig. 2.3. In fact, we see that $|u(r)|^2 \sim 0$ at large r. Thanks to this property, the wavefunction of the bound state is square integrable:

$$\langle B|B\rangle = \int d\boldsymbol{r}\ |\langle \boldsymbol{r}|B\rangle|^2 = \int d\boldsymbol{r}\ |u(r)|^2 < \infty. \tag{2.78}$$

Therefore, the bound state wavefunction can be normalized as $\langle B|B\rangle = 1$. We note that $|u(r)|^2$ is localized in the interaction region ($r < 1$).

Virtual states

An attractive interaction does not always generate bound states. For example, if the attraction of the square-well potential is not strong enough, we obtain a virtual state rather than a bound state. As in the bound state case, the asymptotic form of the wavefunction of the virtual state at $E = -E_V$ is governed by the virtual state eigenmomentum $p = -i\kappa_V$:

$$\langle \boldsymbol{r}|V\rangle \sim \frac{e^{+\kappa_V r}}{r} \quad (r \to \infty), \tag{2.79}$$

where $\kappa_V = \sqrt{2\mu E_V} > 0$. From this equation, $|u(r)|^2$ exponentially diverges at infinity. In Fig. 2.4, we show the absolute value square of the virtual state wavefunction $|u(r)|^2$. In fact, $|u(r)|^2$ increases

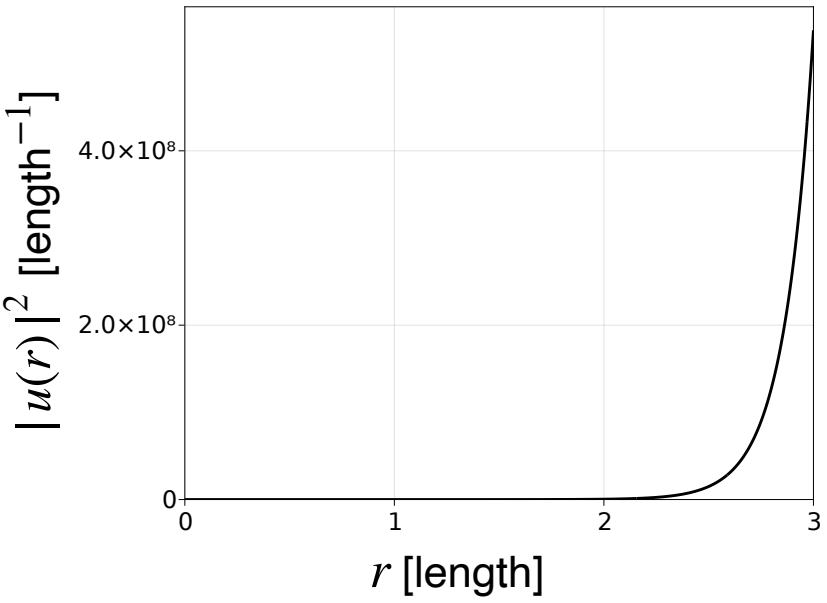

Figure 2.4: The wavefunction of the virtual state with the eigenenergy $E_V = 6.4$ [length^{-2}] in the attractive square well potential. The width of the well is 1 [length], and the depth is 0.02 [length^{-2}].

with r. In contrast to the bound states, the virtual states are not localized in the interaction region. Instead, the virtual states can be regarded as the states localized at infinity, and they are also called the anti-bound states. From Eq. (2.79), the norm of the virtual state diverges:

$$\langle V|V\rangle = \int d\boldsymbol{r}\ |\langle \boldsymbol{r}|V\rangle|^2 \to \infty. \tag{2.80}$$

Therefore, the wavefunction of the virtual state cannot be normalized.

Furthermore, it is known that the metric of the virtual states is negative [104]. For example, the completeness relation of the system with only one virtual eigenstate is written as

$$1 = \int d^3\boldsymbol{p}\ \ |\boldsymbol{p},\pm\rangle\langle\boldsymbol{p},\pm| - |V\rangle\langle V|\,. \tag{2.81}$$

In the scattering amplitude, this nature is reflected as the negative residue of the virtual state pole. The divergence of the virtual state norm (2.80) indicates that the expectation value of an operator with the virtual states cannot be calculated. In this sense, the virtual states have a different nature from the bound states and are regarded as generalized eigenstates.

When a virtual state exists near the threshold, it can affect the observables above the threshold. For example, the attraction in the two-neutron system does not produce a bound state but a virtual state near the threshold as indicated by the nn scattering length. This fact is important to understand the nature of the nuclear force. Furthermore, the existence of the near-threshold virtual states in coupled-channel scatterings is considered to affect the spectrum as the enhancement of the threshold cusp [105].

Resonances

A resonance is an *unstable* composite state of two particles while the bound state is *stable*. Unstable resonances eventually decay into lower-energy scattering channels as time passes. Resonances appear as the discrete eigenstates $|R\rangle$ in the same way with bound and virtual states but with a complex eigenenergy E_R:

$$\hat{H}\,|R\rangle = E_R\,|R\rangle\,. \tag{2.82}$$

The real part of E_R is regarded as the mass of the resonance M, and the imaginary part is related to the decay width of the resonance $\Gamma > 0$ as:

$$E_R = M - \frac{\Gamma}{2}i. \tag{2.83}$$

Note that the imaginary part of E_R is negative as shown in Fig. 2.2.

While the norm of stable bound states is constant in time, that of resonances depends on time t. From Eq. (2.83), the time-dependent part of the resonance wavefunction (2.3) is written as

$$\phi(t) \sim e^{-iE_Rt} = e^{-iMt-(\Gamma/2)t}. \tag{2.84}$$

In this case, the square of the wavefunction decreases with Γ:

$$|\phi(t)|^2 \propto e^{-\Gamma t}. \tag{2.85}$$

This represents the exponential decay of unstable resonances and justifies the identification of Γ as the decay width. As seen in Eq. (2.76), the resonance wavefunction is not square integrable in r due to the growing component with $\mathrm{Im}\,p_R < 0$. We visualize this property by showing the square of the wavefunction of a resonance in the repulsive square well potential [106, 107] (Fig. 2.5). We see that the resonance wavefunction increases with r at a large distance, similar to virtual states. As a consequence, the norm of the resonance diverges:

$$\langle R|R\rangle = \int d\boldsymbol{r}\ |\,\langle \boldsymbol{r}|R\rangle\,|^2 \to \infty. \tag{2.86}$$

Because of this non-square integrable nature, the wavefunction of the resonance cannot be normalized in the standard nammer. However, there is a prescription to normalize the resonance wavefunction by introducing the Gamow vector, as discussed in the next section. In the interaction region ($r < 1$), $|u(r)|^2$ is found to be localized in Fig. 2.5. The localization of the resonance wavefunction shows similarity with the bound state wavefunction.

The states with $E_R = M + \Gamma/2$ ($\mathrm{Re}\,p_R < 0$) are called the anti-resonances. In contrast to resonances with decay, the square of the wavefunction of the anti-resonance increases with time:

$$|\phi(t)|^2 \propto e^{+\Gamma t}. \tag{2.87}$$

In this thesis, we do not consider anti-resonances.

2.5 Non-Hermitian Hamiltonian and Gamow vector

In this section, we introduce the Gamow vector to consider the expectation value of the resonances $|R\rangle$ which is the eigenstate of a non-Hermitian Hamiltonian. When the Hamiltonian is non-Hermitian

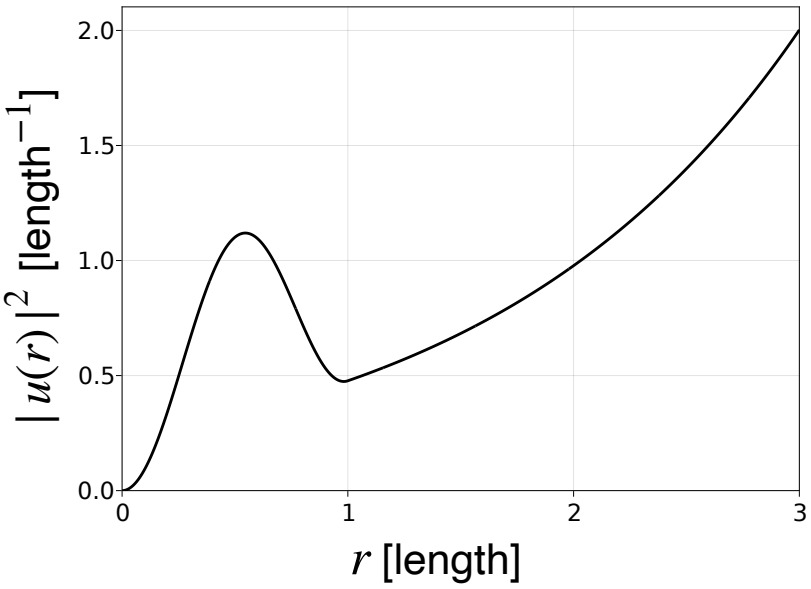

Figure 2.5: The wavefunction of the resonance with the eigenenergy $E_R = 14 - 1.9i$ [length^{-2}] in the square well potential with the repulsive square well potential. The width of the well is 1 [length], and the height is 10 [length^{-2}].

$\hat{H}^\dagger \neq \hat{H}$, it is shown that the Hermite conjugate state $\langle R| = |R\rangle^\dagger$[4] is not a left eigenstate of $\hat{H}$ but that of $\hat{H}^\dagger$:

$$(\hat{H}\,|R\rangle)^\dagger = \langle R|\,\hat{H}^\dagger = \langle R|\,E_R^*. \tag{2.88}$$

Let us turn to the expectation value of resonances. It is clear that the standard expectation value $\langle R|\hat{H}|R\rangle\,/\,\langle R|R\rangle$ has some problems because the inner product $\langle R|R\rangle$ should be finite and both $\langle R|$ and $|R\rangle$ should be the eigenstates of $\hat{H}$ to give a sensible expectation value. These are not satisfied by the resonances $|R\rangle$ as shown in Eqs. (2.86) and (2.88).

To solve this problem, we define the Gamow vector $\langle\tilde{R}|$ as the left eigenstate of $\hat{H}$ having the same eigenvalue E_R of $|R\rangle$ [108, 109, 103, 110, 111, 106, 17, 112, 113]:

$$\langle\tilde{R}|\,\hat{H} = \langle\tilde{R}|\,E_R. \tag{2.89}$$

By introducing the Gamow vector $\langle\tilde{R}|$, a sensible normalization and expectation value can be defined. As shown in Eq. (2.86), the standard norm of resonances $\langle R|R\rangle$ diverges. However, if we define the inner product of resonances as $\langle\tilde{R}|R\rangle$, it is normalizable using the regularization procedure (Zel'dovich' s method) [108]:

$$\langle\tilde{R}|R\rangle = \int d\boldsymbol{r}\,\langle\tilde{R}|\boldsymbol{r}\rangle\,\langle\boldsymbol{r}|R\rangle\,, \tag{2.90}$$

$$|\,\langle\tilde{R}|R\rangle\,| = \int d\boldsymbol{r}|\,\langle\tilde{R}|\boldsymbol{r}\rangle\,\langle\boldsymbol{r}|R\rangle\,| < \infty. \tag{2.91}$$

[4]For an infinite-dimensional space, dagger † represents the generalization of the Hermite conjugate in finite-dimensional vector space.

Let us show that the inner product with the Gamow vector is obtained by the complex square of the wavefunction:

$$\langle \tilde{R}|R\rangle = \int d\boldsymbol{r}[\Psi_R(\boldsymbol{r})]^2. \tag{2.92}$$

From Eq. (2.82), the Schrödinger equation for $|R\rangle$ in the coordinate space is written as

$$\hat{H}_r\Psi_R(\boldsymbol{r}) = E_R\Psi_R(\boldsymbol{r}), \quad \langle \boldsymbol{r}|R\rangle = \Psi_R(\boldsymbol{r}), \tag{2.93}$$

where $\hat{H}_r$ is the space coordinate representation of the Hamiltonian operator. In the same way, the Schrödinger equation for $|\tilde{R}\rangle$ is derived from Eq. (2.89)

$$\hat{H}_r\Psi^*_{\tilde{R}}(\boldsymbol{r}) = E_R\Psi^*_{\tilde{R}}(\boldsymbol{r}), \quad \langle \tilde{R}|\boldsymbol{r}\rangle = \Psi^*_{\tilde{R}}(\boldsymbol{r}). \tag{2.94}$$

By comparing Eqs. (2.93) with (2.94), the wavefunction of the left eigenstate $\Psi^*_{\tilde{R}}(\boldsymbol{r})$ is equivalent to that of $\Psi_{\tilde{R}}(\boldsymbol{r})$ up to a constant C:

$$\langle \tilde{R}|\boldsymbol{r}\rangle = C\langle \boldsymbol{r}|R\rangle = C\Psi_R(\boldsymbol{r}). \tag{2.95}$$

By absorbing the constant C by the normalization, Eq. (2.90) can be rewritten as Eq. (2.92). It should be noted that by normalizing $\langle \tilde{R}|R\rangle = 1$, the phase of the wavefunction is uniquely determined in contrast to the standard normalization. With this normalization, the expectation value can be consistently defined:

$$\langle \tilde{R}|\hat{H}|R\rangle = E_R \in \mathbb{C}. \tag{2.96}$$

At the same time, the expectation value of any operator using the Gamow vector $\langle \tilde{R}|$ becomes, in general, complex for resonances. This feature induces the complex compositeness of resonances as shown in Chapter 5.

For bound states, the Gamow vector $|\tilde{B}\rangle$ is equivalent to $|B\rangle$ up to a constant. In this case, the Schrödinger equation with the left eigenstate $\langle \tilde{B}|$ is written with $M = -B$ and $\Gamma = 0$ in Eq. (2.89):

$$\langle \tilde{B}|\,\hat{H} = -B\,\langle \tilde{B}|\,. \tag{2.97}$$

Taking Hermite conjugate to both sides of this equation, we obtain

$$\hat{H}^\dagger\,|\tilde{B}\rangle = -B^*\,|\tilde{B}\rangle\,. \tag{2.98}$$

Because the Hamiltonian is Hermitian for bound states and B is real, this reduces to

$$\hat{H}\,|\tilde{B}\rangle = -B\,|\tilde{B}\rangle\,. \tag{2.99}$$

Comparing with the Schrödinger equation of $|B\rangle$ (2.7), we find that the relation between $|B\rangle$ and $|\tilde{B}\rangle$ is

$$|\tilde{B}\rangle = C\,|B\rangle\,, \tag{2.100}$$

with a constant C. Therefore, normalization with $\langle \tilde{B}|$ provides the same expectation value with the standard one with $\langle B|$:

$$\frac{\langle \tilde{B}|\hat{H}|B\rangle}{\langle \tilde{B}|B\rangle} = \frac{C^*\,\langle B|\hat{H}|B\rangle}{C^*\,\langle B|B\rangle} = \frac{\langle B|\hat{H}|B\rangle}{\langle B|B\rangle}. \tag{2.101}$$

By focusing on the wavefunction, we find a difference in the remaining degrees of freedom with the normalization conditions. From Eq. (2.92), the normalization with the Gamow vector $\langle \tilde{B}|$ is

$$\langle \tilde{B}|B\rangle = 1 = \int d\boldsymbol{r}[\Psi(\boldsymbol{r})]^2, \tag{2.102}$$

which indicates that $\Psi(\boldsymbol{r})$ has to be real. On the other hand, the standard renormalization is defined as

$$\langle B|B\rangle = 1 = \int d\boldsymbol{r}|\Psi(\boldsymbol{r})|^2, \tag{2.103}$$

where the wavefunction can have an arbitrary phase. Thus, the normalization with the Gamow vector imposes a stronger condition. In this way, the use of the Gamow vector provides the same expectation value as the standard one for bound states, and it can be applied also to resonances. Therefore, the expectation value with the Gamow vector can be regarded as a natural extension of the standard one.

Chapter 3

Feshbach method

In this chapter, we consider one of the useful formulations to introduce the compositeness in quantum mechanics. It is the Feshbach method [114, 115] that describes bound states in two-channel systems with P and Q channels. In this framework, a bound state wavefunction is composed of the components of P and Q channels. By performing the channel elimination, the two-channel problem can be reduced to the single-channel problem with an effective Hamiltonian. With the Feshbach method, we can describe the system introduced in Section 2.1.

The Feshbach method was originally introduced by H. Feshbach to discuss nuclear reactions around 1960 [114, 115]. Not only in nuclear physics but the same formulation has been widely applied also in high-energy physics, atomic physics, solid-state physics and so on [116, 117, 118, 119, 120, 121]. In particular, in cold atom physics, the idea of the Feshbach method serves as the foundation of the experiments to vary the strength of the interaction between two atoms through the adjustment of the external magnetic field (the Feshbach resonance) [122, 118, 120, 80].

We start with the general formulation with the two-channel Hamiltonian and calculate the useful relations of operators in Section 3.1. We then focus on the single resonance approach which describes the couplings of the single discrete state coupled to the free scattering states in Section 3.2. This approach is useful to introduce the compositeness in later chapters.

3.1 Formulation

In this section, the formulation of the Feshbach method is presented. We first introduce the coupled-channel Hamiltonian and eigenstates in the first Section 3.1.1. Then the effective Hamiltonian is derived by eliminating the Q channel in Section 3.1.2. In Section 3.1.3, we calculate the T-operators for later discussion.

3.1.1 Hamiltonian with channel coupling

Here we consider the Schrödinger equation in a general two-channel problem with the Feshbach method. Let us start with considering the Hamiltonian $\hat{H}$ and its eigenstate $|\Psi\rangle$ which follow the Schrödinger equation:

$$\hat{H}\,|\Psi\rangle = E\,|\Psi\rangle\,, \tag{3.1}$$

where E is the eigenenergy. The explicit form of the Hamiltonian and eigenvector will be given in later sections, by specifying the model. We consider two spaces P and Q, and schematically denote their basis as $|P_{\rm base}\rangle$ and $|Q_{\rm base}\rangle$. For example, if P (Q) space contains $N_c^{\rm P}$ ($N_c^{\rm Q}$) continuum channels and $N_d^{\rm P}$ ($N_d^{\rm Q}$) discrete states the basis vectors are collectively represented as

$$|P_{\rm base}\rangle = \{|\boldsymbol{p}_j\rangle, |\phi_i\rangle \,|1 \le j \le N_c^{\rm P}, 1 \le i \le N_d^{\rm P}\}, \tag{3.2}$$

$$|Q_{\rm base}\rangle = \{|\boldsymbol{p}_j\rangle, |\phi_i\rangle \,|N_c^{\rm P}+1 \le j \le N_c^{\rm P}+N_c^{\rm Q}, N_d^{\rm P}+1 \le i \le N_d^{\rm P}+N_d^{\rm Q}\} \tag{3.3}$$

P and Q basis are normalized and orthogonal with each other:

$$\langle P_{\rm base}|P_{\rm base}\rangle = 1, \tag{3.4}$$

$$\langle Q_{\rm base}|Q_{\rm base}\rangle = 1, \tag{3.5}$$

$$\langle P_{\rm base}|Q_{\rm base}\rangle = \langle Q_{\rm base}|P_{\rm base}\rangle = 0. \tag{3.6}$$

We define $\hat{P}$ and $\hat{Q}$ as the projection operators to the P and Q spaces, respectively:

$$\hat{P} = |P_{\rm base}\rangle \langle P_{\rm base}|, \tag{3.7}$$

$$\hat{Q} = |Q_{\rm base}\rangle \langle Q_{\rm base}|. \tag{3.8}$$

With the example of Eqs. (3.2) and (3.3), the projection operators are given by

$$\hat{P} = \sum_{j=1}^{N_c^{\rm P}} \int d\boldsymbol{p}_j \, |\boldsymbol{p}_j\rangle \langle \boldsymbol{p}_j| + \sum_{i=1}^{N_d^{\rm P}} |\phi_i\rangle \langle \phi_i|, \tag{3.9}$$

$$\hat{Q} = \sum_{j=N_c^{\rm P}+1}^{N_c^{\rm P}+N_c^{\rm Q}} \int d\boldsymbol{p}'_j \, |\boldsymbol{p}'_j\rangle \langle \boldsymbol{p}'_j| + \sum_{i=N_d^{\rm P}+1}^{N_d^{\rm P}+N_d^{\rm Q}} |\phi_i\rangle \langle \phi_i|. \tag{3.10}$$

It is clear that $\hat{P}$ and $\hat{Q}$ satisfy the properities of the projection operators:

$$\hat{P}^2 = \hat{P}, \tag{3.11}$$

$$\hat{Q}^2 = \hat{Q}, \tag{3.12}$$

$$\hat{P}\hat{Q} = \hat{Q}\hat{P} = 0. \tag{3.13}$$

Using these operators, the completeness relation of the whole Hilbert space is also written as

$$1 = \hat{P} + \hat{Q} = |P_{\rm base}\rangle \langle P_{\rm base}| + |Q_{\rm base}\rangle \langle Q_{\rm base}|. \tag{3.14}$$

With this setup, a state vector $|B\rangle$ can be expanded with the bases in P and Q spaces:

$$|\Psi\rangle = \langle P_{\rm base}|\Psi\rangle \, |P_{\rm base}\rangle + \langle Q_{\rm base}|\Psi\rangle \, |Q_{\rm base}\rangle. \tag{3.15}$$

We now consider the expression of the Hamiltonian $\hat{H}$ in terms of the P and Q spaces given in Eq. (3.15). Acting $\hat{P}$ from left-hand-side to the Schrödinger equation (3.1) and using the completeness relation (3.14), we obtain

$$\hat{P}\hat{H}(\hat{P}+\hat{Q})\,|\Psi\rangle = \hat{P}E\,|\Psi\rangle$$

$$\hat{P}\hat{H}(\hat{P}^2+\hat{Q}^2)\,|\Psi\rangle = E\hat{P}\,|\Psi\rangle$$

$$\hat{P}\hat{H}\hat{P}(\hat{P}\,|\Psi\rangle) + \hat{P}\hat{H}\hat{Q}(\hat{Q}\,|\Psi\rangle) = E\hat{P}\,|\Psi\rangle \tag{3.16}$$

A similar equation is also obtained by acting $\hat{Q}$:

$$\hat{Q}\hat{H}\hat{P}(\hat{P}\,|\Psi\rangle) + \hat{Q}\hat{H}\hat{Q}(\hat{Q}\,|\Psi\rangle) = E\hat{Q}\,|\Psi\rangle \tag{3.17}$$

Equations (3.16) and (3.17) can be summarized in the matrix form:

$$\begin{pmatrix} \hat{H}_{PP} & \hat{H}_{PQ} \\ \hat{H}_{QP} & \hat{H}_{QQ} \end{pmatrix} \begin{pmatrix} |P\rangle \\ |Q\rangle \end{pmatrix} = E \begin{pmatrix} |P\rangle \\ |Q\rangle \end{pmatrix}, \quad \hat{H}_{XY} = \hat{X}\hat{H}\hat{Y}, \tag{3.18}$$

where $|P\rangle$ and $|Q\rangle$ are the state vector projected onto the P and Q spaces defined as

$$|P\rangle = \hat{P}\,|\Psi\rangle = \langle P_{\text{base}}|\Psi\rangle\,|P_{\text{base}}\rangle\,, \tag{3.19}$$

$$|Q\rangle = \hat{Q}\,|\Psi\rangle = \langle Q_{\text{base}}|\Psi\rangle\,|Q_{\text{base}}\rangle\,. \tag{3.20}$$

In this way, the Schrödinger equation is regarded as the two-channel problem based on P and Q spaces. For later discussion, we decompose each element into the free Hamiltonian and the interaction as follows

$$\hat{H}_{PP} = \hat{H}^0_{PP} + \hat{V}_{PP}, \tag{3.21}$$

$$\hat{H}_{PQ} = \hat{V}_{PQ}, \tag{3.22}$$

$$\hat{H}_{QP} = \hat{V}_{QP}, \tag{3.23}$$

$$\hat{H}_{QQ} = \hat{H}^0_{QQ} + \hat{V}_{QQ}. \tag{3.24}$$

Usually, the off-diagonal components do not contain the free part. The explicit form of the free Hamiltonians and the interactions are chosen depending on the system considered. As an example, we will present the case in the single resonance approach in Section 3.2.

3.1.2 Effective Hamiltonian

To solve the two-component Schrödinger equation (3.18), we employ the prescription called the channel elimination. From the two-component Hamiltonian (3.18), the matrix Schrödinger equation leads to the set of equations for $|P\rangle$ and $|Q\rangle$:

$$\hat{H}_{PP}\,|P\rangle + \hat{H}_{PQ}\,|Q\rangle = E\,|P\rangle\,, \tag{3.25}$$

$$\hat{H}_{QP}\,|P\rangle + \hat{H}_{QQ}\,|Q\rangle = E\,|Q\rangle\,. \tag{3.26}$$

Equation. (3.26) can be schematically solved for $|Q\rangle$ as

$$|Q\rangle = (E - \hat{H}_{QQ})^{-1}\hat{H}_{QP}\,|P\rangle\,. \tag{3.27}$$

By substituting this into Eq. (3.25), we then obtain the Schrödinger equation only for the P channel:

$$[\hat{H}_{PP} + \hat{H}_{PQ}(E - \hat{H}_{QQ})^{-1}\hat{H}_{QP}]\,|P\rangle = E\,|P\rangle\,, \tag{3.28}$$

where the contribution of the Q channel is not explicitly present. In this way, the Schrödinger equation for the single P channel can be derived by the Q channel elimination. The operator in the left-hand side of Eq. (3.28) is called the effective Hamiltonian of the P channel $[\hat{H}_{\text{eff}}(E)]$:

$$\hat{H}_{\text{eff}}(E) = \hat{H}_{PP} + \hat{H}_{PQ}(E - \hat{H}_{QQ})^{-1}\hat{H}_{QP}. \tag{3.29}$$

Because no approximations were made in the derivation, the Schrödinger equation with $\hat{H}_{\rm eff}(E)$ provides the equivalent result with that of two-component Hamiltonian (3.18) as long as the P space is concerned:

$$\hat{H}_{\rm eff}(E)\,|P\rangle = E\,|P\rangle\,. \tag{3.30}$$

Because $\hat{H}_{\rm eff}$ depends on the energy E, the eigenenergy of $|P\rangle$ should be obtained by self-consistently solving this equation. As shown in the expression of the effective Hamiltonian (3.29), $\hat{H}_{\rm eff}(E)$ has the energy dependence even though the original Hamiltonian in Eq. (3.1). This energy dependence originates from the second term in Eq. (3.29), which is induced by the channel elimination. With the channel elimination, the contribution of the Q channel is effectively included in the second term, where the Q space contribution in the matrix Hamiltonian in Eq. (3.18). When the Q space contains a lower energy channel than the P space, this term causes the non-Hermitian nature of the effective Hamiltonian [123, 101].

3.1.3 T-operator

From now on, we assume that the P space consists of a single scattering channel in the Feshbach method, while the Q channel remains unspecified. We recall that in Chapter 2, the scattering problem in the single-channel system can be solved by decomposing the Hamiltonian into the free and interaction parts. In the previous subsection, we showed that the coupled-channel problem can be reduced to the single-channel problem with the effective Hamiltonian $\hat{H}_{\rm eff}$ by the channel elimination. In this subsection, we introduce the T-operator as in Chapter 2, by decomposing $\hat{H}_{\rm eff}$ into free and interaction parts. We also derive the expression of the T-operator by the self-energy operator.

Effective interaction $\hat{V}_{\rm eff}$

To calculate the T-operator of P channel scatterings, we first decompose the effective Hamiltonian $\hat{H}_{\rm eff}$ (3.29) into free and interaction parts. Because $\hat{H}_{PP}$ in the effective Hamiltonian contains the free part $\hat{H}^0_{PP}$ as shown in Eq. (3.21), the remaining part of $\hat{H}_{\rm eff}$ is regarded as the effective interaction $\hat{V}_{\rm eff}(E)$:

$$\hat{H}_{\rm eff}(E) = \hat{H}^0_{PP} + \hat{V}_{\rm eff}(E), \tag{3.31}$$

$$\hat{V}_{\rm eff}(E) = \hat{V}_{PP} + \hat{V}_{PQ}(E - \hat{H}_{QQ})^{-1}\hat{V}_{QP}. \tag{3.32}$$

We find that the interaction part depends on the energy, which is different from the single-channel problem with Eq. (2.12). This energy dependence arises in the effective Hamiltonian, as a consequence of the channel elimination, as discussed above. Furthermore, we see that the Q channel contribution is contained only in the second term of $\hat{V}_{\rm eff}(E)$, while the first term corresponds to the original interaction in the P channel. In this sense, the effective interaction is further decomposed into the interaction within the P channel and that induced by the P and Q channel contributions denoted as $\hat{V}_{PQP}(E)$:

$$\hat{V}_{\rm eff}(E) = \hat{V}_{PP} + \hat{V}_{PQP}(E), \tag{3.33}$$

$$\hat{V}_{PQP}(E) = \hat{H}_{PQ}(E - \hat{H}_{QQ})^{-1}\hat{H}_{QP}. \tag{3.34}$$

This decomposition is useful to define the self-energy operator, which will be shown below.

L-S equation with effective interaction $\hat{V}_{\rm eff}(E_p)$

The Lippmann-Schwinger (L-S) equation for operators (see Section 2.2.2) can be used to calculate the T-operator using the effective interaction $\hat{V}_{\rm eff}(E)$. By substituting $V_{\rm eff}(E)$ (3.33) into the L-S equation (2.46), the T-operator is written as

$$\hat{T}(E) = \{[\hat{V}_{PP} + \hat{V}_{PQP}(E)]^{-1} - \hat{G}^0_P(E)\}^{-1}. \tag{3.35}$$

Here we denote the free Green's operator in the P channel as $\hat{G}^0_P(z)$:

$$\hat{G}^0_P(z) = (z - \hat{H}^0_{PP})^{-1}. \tag{3.36}$$

As shown in later sections, this expression of the T-operator is useful for a separable interaction, because the t-matrix from Eq. (3.35) reduces to the algebraic equation.

T-operators with decomposition $T_P + T_{PQP}$

Here we show an alternative expression of the T-operator which was used in the original work by H. Feshbach [114, 115]. In Eq. (3.33), the effective interaction can be decomposed into two parts, $\hat{V}_{PP}$ without the Q channel contribution and $\hat{V}_{PQP}$ with the Q channel contribution. Based on this viewpoint, we consider decomposing the T-operator into two parts, $\hat{T}_P$ and $\hat{T}_{PQP}$:

$$\hat{T}(E) = \hat{T}_P(E) + \hat{T}_{PQP}(E), \tag{3.37}$$

where $\hat{T}_P(E)$ corresponds to the T-operator only with the P channel contribution, and $\hat{T}_{PQP}(E)$ expresses all the remaning contributions. It is shown that these operators are given by [115, 114, 116]

$$\hat{T}_P(E) = [\hat{V}^{-1}_{PP} - \hat{G}^0_P(E)]^{-1}, \tag{3.38}$$

$$\hat{T}_{PQP}(E) = \hat{T}_P \hat{V}^{-1}_{PP}[\hat{V}^{-1}_{PQP}(E) - \hat{G}_P(E)]^{-1}\hat{V}^{-1}_{PP}\hat{T}_P. \tag{3.39}$$

Here $\hat{G}_P$ represents the full Green's operator in the P space:

$$\hat{G}_P(z) = (z - \hat{H}_{PP})^{-1}. \tag{3.40}$$

Note that $\hat{T}_{PQP}$ is not simply given by the $\hat{V}_{PQP}$ contribution $[\hat{V}^{-1}_{PQP}(E) - \hat{G}_P(E)]^{-1}$, but also contains the effect of $\hat{V}_{PP}$. As shown below, the T-operator in Eq. (3.37) is used to derive the useful relation to obtain the binding energy from the self energy.

Self-energy operator

When the system has a bound state, the binding energy is obtained as the pole of the on-shell t-matrix as mentioned in Section 2.4. To calculate the binding energy in the later discussion, here we derive the bound state condition (pole condition) in terms of the self-energy operator. It is shown that the pole of $\hat{T}_{PQP}$ (3.39) corresponds to the pole of the whole T-operator, while that of $\hat{T}_P$ (3.38) does not [115, 114, 116]. Therefore, the bound state condition is given by the pole condition of $[\hat{V}^{-1}_{PQP}(E) - \hat{G}_P(E)]^{-1}$ operator:

$$\begin{aligned} 0 = \hat{V}^{-1}_{PQP}(E) - \hat{G}_P(E) &= [\hat{H}_{PQ}(E - \hat{H}_{QQ})^{-1}\hat{H}_{QP}]^{-1} - \hat{G}_P(E) \\ &= \hat{H}^{-1}_{QP}(E - \hat{H}_{QQ})\hat{H}^{-1}_{PQ} - \hat{G}_P(E) \end{aligned}$$

$$= \hat{H}_{QP}^{-1}[E - \hat{H}_{QQ} - \hat{H}_{QP}\hat{G}_P(E)\hat{H}_{PQ}]\hat{H}_{PQ}^{-1}$$
$$= \hat{H}_{QP}^{-1}[E - \hat{H}_{QQ} - \hat{\Sigma}(E)]\hat{H}_{PQ}^{-1}. \tag{3.41}$$

In the last line, we define the self-energy operator $\hat{\Sigma}$:

$$\hat{\Sigma}(E) = \hat{H}_{QP}\hat{G}_P(E)\hat{H}_{PQ}. \tag{3.42}$$

Because the transition components $\hat{H}_{QP}$ and $\hat{H}_{PQ}$ do not give a pole, the bound state condition for operators is given by

$$E - \hat{H}_{QQ} - \hat{\Sigma}(E) = 0. \tag{3.43}$$

The expectation value of Eq. (3.43) in terms of the Q channel state corresponds to the bound state condition as shown in the later discussion.

3.2 Single resonance approach

In this section, we consider the system introduced in Section 2.1 with the Feshbach method. Such a system is described by the model called the single resonance approach, where P space (Q space) is given by the set of the free scattering states (as only one discrete bare state). We first introduce the Hamiltonian and eigenstates of the single resonance approach (Section 3.2.1). In the next Section 3.2.2, we then calculate the on-shell t-matrix using the relation for operators derived in the previous Section 3.1.3, and show that the single resonance approach is equivalent to the formulation in Section 2.1.

3.2.1 Hamiltonian and eigenstates

We start with defining the eigenstates of the free Hamiltonian in the P and Q spaces such that they satisfy the following Schrödinger equations:

$$\hat{H}_{PP}^0 |\boldsymbol{p}\rangle = E_p |\boldsymbol{p}\rangle, \quad E_p = \frac{\boldsymbol{p}^2}{2\mu}, \tag{3.44}$$

$$\hat{H}_{QQ}^0 |\phi\rangle = \nu_0 |\phi\rangle. \tag{3.45}$$

Here E_p is the eigenenergy written by the momentum $\boldsymbol{p}$ of the free scattering states $|\boldsymbol{p}\rangle$ (P space) and ν_0 is the energy of the discrete bare state $|\phi\rangle$ (Q space). Namely, we consider $N_c^{\mathrm{P}} = 1$, $N_d^{\mathrm{P}} = 0$, $N_c^{\mathrm{Q}} = 0$, and $N_d^{\mathrm{P}} = 1$ in Eqs. (3.2) and (3.3). This means that the single resonance approach is equivalent to the formulation in Section 2.1 [see Eqs. (2.17) and (2.18)]. Using the following matrix form of the free Hamiltonian $\hat{H}_0$,

$$\hat{H}_0 = \begin{pmatrix} \hat{H}_{PP}^0 & 0 \\ 0 & \hat{H}_{QQ}^0 \end{pmatrix}, \tag{3.46}$$

the Schrödinger equations (3.44) and (3.45) are summarized as

$$\hat{H}_0 \begin{pmatrix} |\boldsymbol{p}\rangle \\ |\phi\rangle \end{pmatrix} = \begin{pmatrix} E_p & 0 \\ 0 & \nu_0 \end{pmatrix} \begin{pmatrix} |\boldsymbol{p}\rangle \\ |\phi\rangle \end{pmatrix}. \tag{3.47}$$

In this case, the full Hamiltonian $\hat{H}$ is given as

$$\hat{H} = \hat{H}_0 + \hat{V}, \tag{3.48}$$

with the matrix form of the interaction $\hat{V}$

$$\hat{V} = \begin{pmatrix} \hat{V}_{PP} & \hat{V}_{PQ} \\ \hat{V}_{QP} & 0 \end{pmatrix}. \tag{3.49}$$

Here we set $\hat{V}_{QQ} = 0$ because the matrix element of $\hat{V}_{QQ}$, $\langle\phi|\hat{V}_{QQ}|\phi\rangle = c$ can be absorbed by the redefinition of the bare energy $\nu_0' = \nu_0 + c$. The Schödinger equation of the full Hamiltonian is given by

$$\begin{pmatrix} \hat{H}^0_{PP} + \hat{V}_{PP} & \hat{V}_{PQ} \\ \hat{V}_{QP} & \hat{H}^0_{QQ} \end{pmatrix} |\Psi\rangle = E_h \, |\Psi\rangle \,, \tag{3.50}$$

with the two-component eigenstates:

$$|\Psi\rangle = \begin{pmatrix} \int d\boldsymbol{p} \, \langle \boldsymbol{p}|\Psi\rangle \, |\boldsymbol{p}\rangle \\ \langle\phi|\Psi\rangle \, |\phi\rangle \end{pmatrix}. \tag{3.51}$$

In the formulation in Section 2.1, the Hamiltonian (3.48) can also be written as the following form:

$$\hat{H}_0 = \int d\boldsymbol{p} \;\; |\boldsymbol{p}\rangle \, \frac{\boldsymbol{p}^2}{2\mu} \, \langle \boldsymbol{p}| + |\phi\rangle \, \nu_0 \, \langle\phi| \,, \tag{3.52}$$

$$\hat{V} = \int d\boldsymbol{p} d\boldsymbol{p}' \;\; |\boldsymbol{p}\rangle \, \langle \boldsymbol{p}|\hat{V}|\boldsymbol{p}'\rangle \, \langle \boldsymbol{p}'| + \int d\boldsymbol{p} \;\; |\phi\rangle \, \langle\phi|\hat{V}|\boldsymbol{p}\rangle \, \langle \boldsymbol{p}| + \int d\boldsymbol{p} \;\; |\boldsymbol{p}\rangle \, \langle \boldsymbol{p}|\hat{V}|\phi\rangle \, \langle\phi| \,. \tag{3.53}$$

In the single resonance approach, the projection operators $\hat{P}$ and $\hat{Q}$ are written by

$$\hat{P} = \int d\boldsymbol{p} \, |\boldsymbol{p}\rangle \, \langle \boldsymbol{p}| \,, \tag{3.54}$$

$$\hat{Q} = |\phi\rangle \, \langle\phi| \,. \tag{3.55}$$

From Eq. (**??**), the completeness relation is written as

$$1 = \hat{P} + \hat{Q} = \int d\boldsymbol{p} \, |\boldsymbol{p}\rangle \, \langle \boldsymbol{p}| + |\phi\rangle \, \langle\phi| \,. \tag{3.56}$$

Comparing Eq. (3.56) with the completeness relations in the previous formulation (2.19), we see that the model space of the single resonance approach is equivalent to that in the system introduced in Section 2.1. As shown in the completeness relation (3.56), only one discrete eigenstate is introduced in the model space. This is why this model is called the single resonance approach. The system of the single resonance approach is realized if $\hat{H}_{PP}$ has only one scattering channel, and $\hat{H}_{QQ}$ is the confinement potential generating only one discrete state. In other words, the single resonance model is an approximation for the system having more scattering or discrete channels, but the approximation is justified if the additional channels exist sufficiently far away from the energy region considered.

By comparing the eigenstates in the single resonance approach (3.51) with the general ones (3.19), and (3.20), we find that $|P_{\rm base}\rangle$ and $|Q_{\rm base}\rangle$ in the single resonance approach can be schematically expressed as follows:

$$|P_{\rm base}\rangle = \begin{pmatrix} |\boldsymbol{p}_1\rangle \\ |\boldsymbol{p}_2\rangle \\ \vdots \end{pmatrix}, \tag{3.57}$$

$$|Q_{\rm base}\rangle = |\phi\rangle\,. \tag{3.58}$$

Here Eq. (3.57) represents the set of the infinite number of continuum eigenstates. In this case, the eigenstate $|\Psi\rangle$ is regarded as the superposition of the continuum scattering states and the discrete state:

$$\begin{aligned}|\Psi\rangle &= (\langle \boldsymbol{p}_1|\Psi\rangle\,|\boldsymbol{p}_1\rangle + \langle \boldsymbol{p}_2|\Psi\rangle\,|\boldsymbol{p}_2\rangle + \cdots) + \langle\phi|\Psi\rangle\,|\phi\rangle \\ &= \int d\boldsymbol{p}\,\langle \boldsymbol{p}|\Psi\rangle\,|\boldsymbol{p}\rangle + \langle\phi|\Psi\rangle\,|\phi\rangle\,.\end{aligned} \tag{3.59}$$

As shown in Chapter 5, the single resonance approach is useful for introducing the compositeness of the bound state in quantum mechanics.

3.2.2 On-shell t-matrix

t-matrix from L-S equation

Finally, we derive the on-shell t-matrix and self energy. When the effective interaction $V_{\rm eff}$ is separable, the on-shell t-matrix is easily obtained from the expression of the T-operator from the L-S equation (3.35) [see also the discussion around Eq. (2.41)]:

$$t(E_p) = \{[V_{PP} + V_{PQP}(E_p)]^{-1} - G_P^0(E_p)\}^{-1}, \tag{3.60}$$

with the matrix elements of the interactions

$$V_{PP} = \langle \boldsymbol{p}'|\hat{V}_{PP}|\boldsymbol{p}\rangle\,|_{E_p=E_{p'}}, \tag{3.61}$$

$$V_{PQP}(E_p) = \langle \boldsymbol{p}'|\hat{V}_{PQP}(E_p)|\boldsymbol{p}\rangle\,|_{E_p=E_{p'}} = \frac{\langle \boldsymbol{p}'|\hat{V}_{PQ}|\phi\rangle\,\langle\phi|\hat{V}_{QP}|\boldsymbol{p}\rangle}{E_p - \nu_0}, \tag{3.62}$$

and the regularized Green's function in the momentum expression:

$$G_P^0(z) = \int d\boldsymbol{q}\;\frac{|F(\boldsymbol{q})|^2}{z - E_q + i0^+}, \tag{3.63}$$

with the form factor $F(\boldsymbol{q})$. Equation (3.62) indecates that $V_{PQP}(E_p)$ is always separable, while the separability of V_{PP} depends on the interaction considered.

t-matrix from decomposed T-operator

Here we also show the expression of the on-shell t-matrix using Eq. (3.37). By definition of the t-operator (2.36), the on-shell t-matrix within the P channel t_P is obtained from Eq. (3.38) as

$$t_P(E_p) = \langle \boldsymbol{p}'|[\hat{V}_{PP}^{-1} - \hat{G}_P^0(E_p)]^{-1}|\boldsymbol{p}\rangle\Big|_{E_p=E_{p'}}. \tag{3.64}$$

If the interaction $\hat{V}_{PP}$ is separable, t_P is obtained as the algebraic form:

$$t_P(E_p) = \frac{1}{V_{PP}^{-1} - G_P^0(E_p)}, \tag{3.65}$$

The matrix element of $\hat{T}_{PQP}(E)$ (3.39) $[t_{PQP}(E_p)]$ is also defined as

$$t_{PQP}(E_p) = \langle \boldsymbol{p}'|\hat{T}_P\hat{V}_{PP}^{-1}(\hat{V}_{PQP}^{-1} - \hat{G}_P)^{-1}\hat{V}_{PP}^{-1}\hat{T}_P|\boldsymbol{p}\rangle\Big|_{E_p=E_{p'}}. \tag{3.66}$$

Using the relation between interacting ($|\boldsymbol{p},\pm\rangle$) and free ($|\boldsymbol{p}\rangle$) scattering states (2.50), we find that $t_{PQP}(E_p)$ (3.66) is also expressed as a similar form with $t_P(E_p)$ but with the full scattering states $|\boldsymbol{p},\pm\rangle$ [116]:

$$t_{PQP}(z;\boldsymbol{p}',\boldsymbol{p}) = \langle \boldsymbol{p}', -|[\hat{V}^{-1}_{PQP}(z) - \hat{G}_P(z)]^{-1}|\boldsymbol{p},+\rangle\,. \tag{3.67}$$

If the interaction V_{PP} is separable, $t_{PQP}(E_p)$ in this complicated form reduces to an algebraic form:

$$\begin{aligned} t_{PQP}(E_p) &= t_P(E_p)V^{-1}_{PP}\frac{1}{V^{-1}_{PQP}(E_p) - G_P(E_p)}V^{-1}_{PP}t_P(E_p) \\ &= \frac{V^{-2}_{PP}[V^{-1}_{PP} - G^0_P(E)]^2}{V^{-1}_{PQP}(E_p) - G_P(E_p)}, \end{aligned} \tag{3.68}$$

where we use the completeness relation (3.56). In the second line, we use the expression of $t_P(E_p)$ in Eq. (3.65).

If the interaction V_{PP} is separable, the whole on-shell t-matrix $t(E_p)$ is obtained by summing up $t_P(E_p)$ (3.65) and $t_{PQP}(E_p)$ (3.68):

$$t(E_p) = \frac{1}{V^{-1}_{PP} - G^0_P(E_p)} + \frac{V^{-2}_{PP}[V^{-1}_{PP} - G^0_P(E_p)]^2}{V^{-1}_{PQP}(E_p) - G_P(E_p)}. \tag{3.69}$$

This form of $t(E_p)$ is shown to be equivalent to $t(E_p)$ obtained from L-S equation (3.60):

$$\begin{aligned} t &= t_P + t_P V^{-1}_{PP}\frac{1}{V^{-1}_{PQP} - V^{-1}_{PP}t_P G^0_P}(1 + t_P G^0_P) \\ &= t_P\left(1 + \frac{V^{-1}_{PP}(1 + t_P G^0_P)}{V^{-1}_{PQP} - V^{-1}_{PP}t_P G^0_P}\right) \\ &= t_P\frac{V^{-1}_{PQP} + V^{-1}_{PP}}{V^{-1}_{PQP} - V^{-1}_{PP}t_P G^0_P} \\ &= t_P\frac{(V^{-1}_{PQP} + V^{-1}_{PP})V_{PP}V_{PQP}}{(V^{-1}_{PQP} - V^{-1}_{PP}t_P G^0_P)V_{PP}V_{PQP}} \\ &= \frac{V_{PP} + V_{PQP}}{V_{PP}t^{-1}_P - V_{PQP}G^0_P} \\ &= \frac{V_{PP} + V_{PQP}}{V_{PP}(V^{-1}_{PP} - G^0_P) - V_{PQP}G^0_P} \\ &= \frac{V_{PP} + V_{PQP}}{1 - (V_{PP} + V_{PQP})G^0_P} \\ &= \frac{1}{(V_{PP} + V_{PQP})^{-1} - G^0_P}. \end{aligned} \tag{3.70}$$

In the first line, we use the relation (2.32) for the P channel:

$$V_{PP}G_P = t_P G^0_P. \tag{3.71}$$

This explains that the T-operator (3.37) is consistent with the expression in Eq. (3.34) by the L-S equation are consistent with each other.

Bound state condition with self energy

The bound state condition is obtained by taking the matrix element of Eq. (3.43) as

$$\langle\phi|E - \hat{H}_{QQ} - \hat{\Sigma}(E)|\phi\rangle = E - \nu_0 - \Sigma(E) = 0. \tag{3.72}$$

Here $\Sigma(E) = \langle\phi|\hat{\Sigma}(E)|\phi\rangle$ is called the self energy calculated as

$$\Sigma(E) = \int d\boldsymbol{q}d\boldsymbol{q'}\ V_{QP}(\boldsymbol{q'})\,\langle\boldsymbol{q'}|\hat{G}_P(E)|\boldsymbol{q}\rangle\,V_{PQ}(\boldsymbol{q}), \tag{3.73}$$

where we denote the transition form factors as $V_{QP}(\boldsymbol{p}) = \langle\boldsymbol{p}|\hat{V}_{QP}|\phi\rangle$ and $V_{PQ}(\boldsymbol{p}) = \langle\phi|\hat{V}_{PQ}|\boldsymbol{p}\rangle$. It is worth mentioning that the bound state condition (3.73) holds even if the interaction $\hat{V}_{PP}$ is not separable. The bound state condition (3.72) shows that the eigenenergy E is obtained as the modification of the bear state energy ν_0 by the contribution of the self energy Σ with the finite couplings $\hat{V}_{PQ}$ and $\hat{V}_{QP}$. This form of the bound state condition is useful to obtain the eignenergy without calculating the whole part of the on-shell t-matrix.

Chapter 4

Effective field theory

In this chapter, we introduce a model (the resonance model) based on the non-relativistic effective field theory (EFT) which effectively describes phenomena in the sufficiently low-energy region. Here we regard the energy as small when the momentum p is much smaller than the applicable scale of the model, the cutoff Λ. The EFT has been successful in explaining low-energy phenomena in $p \ll \Lambda$, for instance, the Euler-Heisenberg theory for the quantum electro dynamics [124], and the chiral perturbation theory for the quantum chromodynamics [125]. Furthermore, the EFT has been widely applied to study the low-energy universality, not only to the two-body systems but also to the three-body systems such as hypertriton [126], the Efimov effect and halo nuclei (the halo EFT) [127, 128, 129, 130].

The resonance model is one of the EFTs for a two-body scattering system [104]. In this model, we consider the couplings between the bare state to the s-wave scattering states with arbitrary inner degrees of freedom. This picture is equivalent to the model introduced in Chapter 2 and the single resonance approach in the Feshbach method in Chapter 3, and therefore, the resonance model is suitable to introduce the compositeness in the EFT framework [93, 94, 95].

We introduce the single-channel resonance model in Section 4.1. We first define the Hamiltonian and its eigenstates and derive the effective Hamiltonian by the channel elimination. The loop function is calculated by considering the regularization of the momentum integration. From the L-S equation, the on-shell t-matrix and scattering amplitude are obtained. We show the equivalence of the resonance model in the EFT and the single resonance approach in the Feshbach method (Section 3.2). In the next Section 4.2, we extend the resonance model to the system with decay and coupled channels to discuss the physical hadron systems.

4.1 Resonance model

As one of the models in the EFT, here we introduce the resonance model [104, 94] which corresponds to the single resonance approach in the Feshbach method. In the resonance model, the eigenstates of the full Hamiltonian are described by the couplings of the single channel scattering to one discrete bare state. The Hamiltonian and its eigenstates are presented in Section 4.1.1. Then the effective interaction is derived by the channel elimination in Section 4.1.2. To deal with the divergence of the momentum integration, we discuss the regularization of the loop function in Section 4.1.3, and then

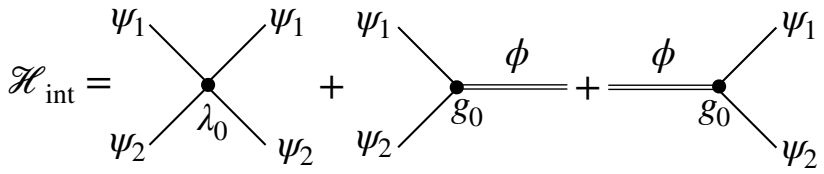

Figure 4.1: The diagrams of the interaction Hamiltonian $\mathcal{H}_{\text{int}}$ (4.3).

the on-shell t-matrix and scattering amplitude are obtained in Section 4.1.4. In Section 4.1.5, we also discuss the renormalization to understand the resonance model with the finite interaction range. Finally, we show the correspondence of the resonance model to the single resonance approach in the Feshbach method (section 4.1.6). In Sections 4.1.1 and 4.1.2, we follow the formulation Ref. [94].

4.1.1 Hamiltonian and eigenstates

Let us start with introducing the Hamiltonian of the single channel scattering where the two scattering fields $\psi_{1,2}$ couple to the single bare field ϕ [104, 94, 71]:

$$\hat{H} = \hat{H}_{\text{free}} + \hat{H}_{\text{int}} = \int d\boldsymbol{r}(\mathcal{H}_{\text{free}} + \mathcal{H}_{\text{int}}), \tag{4.1}$$

$$\mathcal{H}_{\text{free}} = \frac{1}{2m_1}\nabla\psi_1^\dagger \cdot \nabla\psi_1 + \frac{1}{2m_2}\nabla\psi_2^\dagger \cdot \nabla\psi_2 + \frac{1}{2M}\nabla\phi^\dagger \cdot \nabla\phi + \nu_0\phi^\dagger\phi, \tag{4.2}$$

$$\mathcal{H}_{\text{int}} = \lambda_0(\psi_1^\dagger\psi_2^\dagger\psi_1\psi_2) + g_0(\phi^\dagger\psi_1\psi_2 + \psi_1^\dagger\psi_2^\dagger\phi). \tag{4.3}$$

Here $m_{1,2}$, M correspond to the mass of $\psi_{1,2}$ and ϕ, respectively. ν_0 is the energy of ϕ measured from the threshold of $\psi_{1,2}$ scattering. λ_0 and g_0 are the coupling constants of the four-point contact interaction and three-point contact interactions. In non-relativistic EFTs, the ϕ exchange only occurs through the s-channel interaction. However, the contribution of the t-channel interaction in relativistic EFTs is also introduced as the four-point contact interaction of $\psi_{1,2}$ corresponds. We show the vertexes in the interaction Hamiltonian $\hat{H}_{\text{int}}$ (4.3) in Fig. 4.1.

In field theory, eigenstates can be constructed from the vacuum $|0\rangle$ defined as

$$\tilde{\psi}_1(\boldsymbol{p})\,|0\rangle = \tilde{\psi}_2(\boldsymbol{p})\,|0\rangle = \tilde{\phi}(\boldsymbol{p})\,|0\rangle = 0, \tag{4.4}$$

$$\langle 0|0\rangle = 0, \tag{4.5}$$

where $\tilde{\alpha}(\boldsymbol{p})$ is the annihilation operator, and $\tilde{\alpha}(\boldsymbol{p})$ stands for the momentum representation of Fourier transformation:

$$\tilde{\alpha}(\boldsymbol{p}) = \int d\boldsymbol{r}\ e^{-i\boldsymbol{p}\cdot\boldsymbol{r}}\alpha(\boldsymbol{r}). \tag{4.6}$$

By operating the creation operators to vacuum, we can construct the eigenstates of Hamiltonian (4.1) under the following particle number conservation [94]:

$$N_{\psi_1} + N_\phi = \text{constant}, \quad N_{\psi_2} + N_\phi = \text{constant}, \tag{4.7}$$

where N_α corresponds to the particle number of α:

$$N_\alpha = \int d\boldsymbol{r}\alpha(\boldsymbol{r})^\dagger\alpha(\boldsymbol{r}). \tag{4.8}$$

To consider the $\psi_{1,2}$ scattering, here we focus on the sector where $N_{\psi_1} = 1, N_{\psi_2} = 1, N_\phi = 0$ or $N_{\psi_1} = 0, N_{\psi_2} = 0, N_\phi = 1$. Furthermore, we use the barycentric coordinate system. In this case, the eigenstates of the free Hamiltonian are constructed from the vacuum $|0\rangle$ using the creation operators:

$$|\boldsymbol{p}\rangle = \frac{1}{\sqrt{V_{\rm vol}}}\tilde{\psi}_1^\dagger(-\boldsymbol{p})\tilde{\psi}_2^\dagger(\boldsymbol{p})\,|0\rangle\,, \tag{4.9}$$

$$|\phi\rangle = \frac{1}{\sqrt{V_{\rm vol}}}\tilde{\phi}^\dagger(\boldsymbol{0})\,|0\rangle\,. \tag{4.10}$$

Here the phase space of the system $V_{\rm vol}$ are defined as

$$\tilde{\alpha}(\boldsymbol{p}) = \int d\boldsymbol{r}\ e^{-i\boldsymbol{p}\cdot\boldsymbol{r}}\alpha(\boldsymbol{r}), \tag{4.11}$$

$$V_{\rm vol} = (2\pi)^3\delta(\boldsymbol{0}). \tag{4.12}$$

We use the convention widely used in field theory, where the commutation relations for operators α are written as

$$[\alpha(\boldsymbol{r}), \alpha^\dagger(\boldsymbol{r}')] = \delta(\boldsymbol{r}' - \boldsymbol{r}), \tag{4.13}$$

$$[\tilde{\alpha}(\boldsymbol{p}), \tilde{\alpha}^\dagger(\boldsymbol{p}')] = (2\pi)^3\delta(\boldsymbol{p}' - \boldsymbol{p}). \tag{4.14}$$

Using these relations, we can confirm that these eigenstates satisfy the following Schrödinger equation

$$\hat{H}_{\rm free}\,|\boldsymbol{p}\rangle = E_p\,|\boldsymbol{p}\rangle\,, \quad E_p = \frac{\boldsymbol{p}^2}{2\mu}, \tag{4.15}$$

$$\hat{H}_{\rm free}\,|\phi\rangle = \nu_0\,|\phi\rangle\,, \tag{4.16}$$

where $\mu = (1/m_1 + 1/m_2)^{-1}$ is the reduced mass of $\psi_{1,2}$. From these equations, we see that the resonance model describes the same system introduced in Chapter 2 [see Eqs. (2.17) and (2.18)] and single resonance approach in Section 3.2 [see Eqs. (3.44) and (3.45)].

From the particle-number conservation (4.7), the completeness relation in this model is written as [94]

$$1 = \int \frac{d\boldsymbol{p}}{(2\pi)^3}\ |\boldsymbol{p}\rangle\langle\boldsymbol{p}| + |\phi\rangle\langle\phi|\,. \tag{4.17}$$

The normalization and orthogonalization of states are given as

$$\langle\boldsymbol{p}'|\boldsymbol{p}\rangle = (2\pi)^3\delta(\boldsymbol{p}' - \boldsymbol{p}), \tag{4.18}$$

$$\langle\phi|\phi\rangle = 1, \tag{4.19}$$

$$\langle\phi|\boldsymbol{p}\rangle = \langle\boldsymbol{p}|\phi\rangle = 0. \tag{4.20}$$

We note that the normalization (4.18) is different from that in the previous sections in quantum mechanics because we adopt another convention.

The matrix elements of the interaction Hamiltonian are calculated as

$$\langle\boldsymbol{p}'|\hat{H}_{\rm int}|\boldsymbol{p}\rangle = \lambda_0, \tag{4.21}$$

$$\langle\boldsymbol{p}|\hat{H}_{\rm int}|\phi\rangle = \langle\phi|\hat{H}_{\rm int}|\boldsymbol{p}\rangle = g_0. \tag{4.22}$$

From Eq. (4.21), $\langle\boldsymbol{p}'|H_{\rm int}|\boldsymbol{p}\rangle$ is separable since it does not depend on the momentum. This shows that these interactions are constant in the momentum space, namely, point-like in the coordinate space.

4.1.2 Effective interaction

To focus on the $\psi_{1,2}$ scatterings, here we perform the ϕ channel elimination. Let us start from considering the Schrödinger equation of the full Hamiltonian $\hat{H} = \int d\boldsymbol{r}(\mathcal{H}_{\rm free} + \mathcal{H}_{\rm int})$:

$$H\,|\Psi\rangle = E\,|\Psi\rangle\,. \tag{4.23}$$

Using the completeness relation (4.17), $|\Psi\rangle$ is written by the linear combination of the free scattering and discrete states:

$$|\Psi\rangle = \int \frac{d\boldsymbol{p}}{(2\pi)^3}\ \chi(\boldsymbol{p})\,|\boldsymbol{p}\rangle + c\,|\phi\rangle\,, \tag{4.24}$$

where we denote the momentum space wavefunction $\chi(\boldsymbol{p})$ and overlap constant c as

$$\chi(\boldsymbol{p}) = \langle \boldsymbol{p}|\Psi\rangle\,, \tag{4.25}$$

$$c = \langle \phi|\Psi\rangle\,. \tag{4.26}$$

By substituting Eq. (4.24) into the Schrödinger equation (4.23) and multiplying $\langle \boldsymbol{p}|$ and $\langle\phi|$ from the left, we obtain

$$\langle \boldsymbol{p}|H|\Psi\rangle = \chi(\boldsymbol{p})E = \frac{\boldsymbol{p}^2}{2\mu}\chi(\boldsymbol{p}) + \lambda_0 \int \frac{d\boldsymbol{q}}{(2\pi)^3}\ \chi(\boldsymbol{q}) + cg_0, \tag{4.27}$$

$$\langle \phi|H|\Psi\rangle = cE = g_0 \int \frac{d\boldsymbol{q}}{(2\pi)^3}\chi(\boldsymbol{q}) + c\nu_0. \tag{4.28}$$

By eliminating c from Eq. (4.27) using Eq. (4.28), we obtain the following equation with $\chi(\boldsymbol{p})$:

$$E\chi(\boldsymbol{p}) = \frac{\boldsymbol{p}^2}{2\mu}\chi(\boldsymbol{p}) + \left(\lambda_0 + \frac{g_0^2}{E-\nu_0}\right)\int \frac{d\boldsymbol{q}}{(2\pi)^3}\ \chi(\boldsymbol{q}) \tag{4.29}$$

This equation can be rewritten as the following Schrödinger equation [94]

$$\left[\frac{\boldsymbol{p}^2}{2\mu} + \hat{V}_{\rm eff}(E)\right]|\Psi\rangle = E\,|\Psi\rangle\,, \tag{4.30}$$

with the effective interaction $\hat{V}_{\rm eff}$ whose matrix element is

$$\langle \boldsymbol{p}|\hat{V}_{\rm eff}(E)|\boldsymbol{q}\rangle = V_{\rm eff}(E) = \lambda_0 + \frac{g_0^2}{E-\nu_0}. \tag{4.31}$$

By multiplying $\langle \boldsymbol{p}|$ from the left-hand side and using the completeness relation (4.17), Eq. (4.30) can be transformed into Eq. (4.29). This corresponds to the channel elimination of the ϕ degree of freedom, which is equivalent to the Q channel elimination in the single resonance approach in the Feshbach method (see Chapter 3). As mentioned in Section 2.2.2, the effective interaction depends on the energy E. Furthermore, $V_{\rm eff}(E)$ is separable because it only depends on $E = p^2/(2\mu)$, and we can use the algebraic L-S equation (2.46).

4.1.3 Regularization of the loop function

In the field theory, the two-body scattering amplitude is obtained from the four-point function. In the non-relativistic field theory, this is equivalent to calculating the t-matrix from the L-S equation [104].

To obtain t-matrix from the L-S equation (2.46), we also calculate the loop function $G^0(E)$. In field theory, $G^0(E)$ is equivalent to the Green's function up to $(2\pi)^3$ factor (2.42), but called the loop function. This difference arises from the convention of the state normalization (4.18). The loop function on the first Riemann sheet $G^0(E)$ is written as the momentum integral of the propagator of the full Hamiltonian[1]:

$$G^0(E) = \int d\Omega \int_0^\infty \frac{dq}{(2\pi)^3} q^2 \frac{1}{E - E_q + i0^+}. \tag{4.33}$$

In the energy region below the threshold $E < 0$, the poles of the integrand exist on the imaginary axis of the complex momentum plane. In this case, we can straightforwardly perform the integration without $i0^+$ term, and $G^0(E)$ has only a real part. On the other hand, in the region above the threshold $E > 0$, $G^0(E)$ has real poles, and we need the $i0^+$ term for the integration. Therefore, the loop function becomes a complex function in the $E > 0$ region. When the Hamiltonian is Hermitian, the imaginary part of the loop function is determined by the optical theorem [74].

Because the integrand in Eq. (4.33) is proportional to q^0 in the $q \to \infty$ limit, the integral $G^0(E)$ linearly diverges. To avoid this problem, we introduce the form factor $F(p, \Lambda)$:

$$G^0(E, \Lambda) = \int d\Omega \int_0^\infty \frac{dq}{(2\pi)^3} q^2 \frac{|F(p, \Lambda)|^2}{E - E_q + i0^+}. \tag{4.34}$$

The form factor $F(p, \Lambda)$ is a function of momentum p and cutoff Λ, where Λ is regarded as the applicable momentum limit of the EFT. In other words, microscopic phenomena in the momentum scale above Λ cannot be described with the EFT. In this way, the cutoff Λ serves as the typical momentum scale in the model, and other characteristic scales are estimated by the cutoff. For example, the inverse of the cutoff is regarded as the interaction range $R_{\rm int} \sim 1/\Lambda$ in the model. We can choose an arbitrary function as the form factor such that $F(p, \Lambda) \to 0$ at large p. This prescription is called the regularization.

Let us consider some examples of the form factor $F(p, \Lambda)$ with which the interaction becomes separable. Here we present the step function:

$$F(p, \Lambda) = \Theta(\Lambda - p), \tag{4.35}$$

which is consistent with introducing the sharp cutoff. In this case, the cutoff Λ corresponds to the upper limit of the momentum integral. The loop function (4.34) is analytically calculated as

$$\begin{aligned} G^0(E, \Lambda) &= \int \frac{d\boldsymbol{q}}{(2\pi)^3} \frac{\Theta(\Lambda - q)}{E - E_q + i0^+} \\ &= \frac{\mu}{\pi^2} \left[\Lambda + i\sqrt{2\mu E + i0^+} \arctan\left(-\frac{\Lambda}{i\sqrt{2\mu E + i0^+}} \right) \right]. \end{aligned} \tag{4.36}$$

The sharp cutoff is utilized because of its simplicity [93, 94, 95, 71]. In this work, we employ the sharp cutoff to calculate the loop function.

[1]The loop function on the second Riemann sheet $G^0_{II}(E)$ is written as

$$G^0_{II}(E) = \int d\Omega \int_0^\infty \frac{dq}{(2\pi)^3} q^2 \frac{1}{E - E_q - i0^+}, \tag{4.32}$$

where the sign of the $i0^+$ term is opposite to the loop function of the first Riemann sheet. Due to this difference, the imaginary part of $G^0_{II}(E)$ is positive while that of $G^0(E)$ is negative. This induces the difference of the property between bound state poles in the first Riemann sheet and virtual state poles in the second Riemann sheet.

As another example of the form factor, we also show the monopole (Yamaguchi type) form factor [131, 132][2]:

$$F(p,\Lambda) = \frac{\Lambda^2}{p^2+\Lambda^2}. \tag{4.37}$$

By introducing this form factor (4.37), the loop function $G(E)$ becomes finite

$$\begin{aligned} G^0(E,\Lambda) &= \int d\Omega \int_0^\infty \frac{dq}{(2\pi)^3} q^2 \left(\frac{\Lambda^2}{p^2+\Lambda^2}\right)^2 \frac{1}{E-E_q+i0^+}, \\ &= \frac{\mu\Lambda}{4\pi} \frac{-8\mu^2E^2+10\Lambda^2\mu E-2i\Lambda^3\sqrt{2\mu E+i0^+}-\Lambda^4}{(\Lambda^2-2\mu E)^2}. \end{aligned} \tag{4.38}$$

In this way, the loop function $G(E)$ with the monopole form factor can be analytically calculated. It is shown that the Fourier transformation of monopole form factor $\tilde{F}(r,\Lambda)$ is the Yukawa type potential regarded as a typical short-range interaction:

$$\tilde{F}(r,\Lambda) \sim \frac{e^{-r\Lambda}}{r}. \tag{4.39}$$

From these natures, the dipole form factor is adopted to study hadrons for example in Ref. [133, 134, 135].

4.1.4 On-shell t-matrix and scattering amplitude

Thanks to the separable nature of the effective interaction (4.31), we can obtain the on-shell t-matrix from the algebraic L-S equation (2.46). By substituting the effective interaction (4.31) and loop function (4.36) into the L-S equation (2.46), the on-shell t-matrix is derived as

$$t(E) = \left[\left(\lambda_0 + \frac{g_0^2}{E-\nu_0}\right)^{-1} + \frac{\mu}{\pi^2}\left\{\Lambda + i\sqrt{2\mu E+0^+}\arctan\left(-\frac{\Lambda}{i\sqrt{2\mu E+0^+}}\right)\right\}\right]^{-1}. \tag{4.40}$$

From the relation between the on-shell t-matrix and scattering amplitude (2.62), the scattering amplitude $f(p)$ is obtained as

$$f(p) = -\frac{\mu}{2\pi}\left[\left(\lambda_0 + \frac{g_0^2}{\frac{p^2}{2\mu}-\nu_0}\right)^{-1} + \frac{\mu}{\pi^2}\left\{\Lambda + ip\arctan\left(-\frac{\Lambda}{ip}\right)\right\}\right]^{-1}. \tag{4.41}$$

The eignenergy is obtained as the pole of the scattering amplitude:

$$V_{\text{eff}}(E)^{-1} - G^0(E) = \left(\lambda_0 + \frac{g_0^2}{E-\nu_0}\right)^{-1} + \frac{\mu}{\pi^2}\left\{\Lambda + i\sqrt{2\mu E+0^+}\arctan\left(-\frac{\Lambda}{i\sqrt{2\mu E+0^+}}\right)\right\} = 0. \tag{4.42}$$

By comparing Eq. (4.41) to the effective range expansion (2.65), the scattering length a_0 and effective range r_e are obtained as

$$a_0 = \left[\frac{2\pi}{\mu}\left(\lambda_0 - \frac{g_0^2}{\nu_0}\right)^{-1} + \frac{2}{\pi}\Lambda\right]^{-1}, \tag{4.43}$$

[2]This is called monopole type form factor because Eq. (4.37) has single pole with respect to the energy $E \sim p^2$, while it seems to be dipole in terms of p.

$$r_e = -\frac{2\pi g_0^2}{\nu_0^2 \mu^2}\left(\lambda_0 - \frac{g_0^2}{\nu_0}\right)^{-2} + \frac{4}{\pi\Lambda}. \tag{4.44}$$

When the Hamiltonian is Hermitian with the real coupling constant (i.e., $g_0^2 > 0$), the first term of r_e (4.44) is always negative for any coupling constants. This indecates that r_e have an upper limit $4/(\pi\Lambda)$, called the Wigner bound [136, 137, 138]. In contrast, a_0 (4.43) can be arbitrary value, from $-\infty$ to ∞.

4.1.5 Renormalization

While we keep the cutoff Λ finite in this study, it is instructive to discuss the renormalization of the resonance model. To avoid the divergence of the momentum integral (4.33), we performed the regularization in Section 4.1.3. The choice of the regulator (monopole form factor, sharp cutoff etc.) is arbitral, and the result depends on the choice of the form factor $F(p,\Lambda)$ and the value of the cutoff Λ as seen in Eqs. (4.38) and (4.36).

The cutoff dependence should disappear for consistent field theories such as QED and QCD. It is known that the cutoff dependence can be absorbed if the theory is renormalizable. In the renormalization procedure, we let the bare parameters be functions of the cutoff Λ so that the physical quantities (observables) are kept finite in the formal limit of $\Lambda \to \infty$. The resonance model is shown to be renormalizable [77]. After the renormalization, the scattering amplitude $f(p)$ of the resonance model reduces the ERE truncated at $\mathcal{O}(p^2)$:

$$f(p) = \left[-\frac{1}{a_0} + \frac{r_e}{2}p^2 - ip\right]^{-1}. \tag{4.45}$$

Because the inverse of the cutoff $1/\Lambda$ is regarded as the interaction range $R_{\rm int}$, the $\Lambda \to \infty$ limit corresponds to the $R_{\rm int} \to 0$ limit, called the zero-range limit. In this limit, the EFTs correspond to the zero-range theory which describes the system in the low-energy scale with the point-like interactions. Therefore, the zero-range theory has been adapted to consider low-energy phenomena [77, 80].

Although the resonance model is formally renormalizable as discussed above, in this study, we keep the cutoff Λ finite to consider the finite interaction range $R_{\rm int} \sim 1/\Lambda$. The resonance model with finite interaction range is constructed with the Hamiltonian where the form factor in coordinate space $\tilde{F}(\boldsymbol{r}_1, \boldsymbol{r}_2)$ is originally included [139]:

$$\begin{aligned} H_{\rm int} = \lambda_0 \int d\boldsymbol{r}_1 d\boldsymbol{r}_2 d\boldsymbol{r}_1' d\boldsymbol{r}_2' \; \psi_1^\dagger(\boldsymbol{r}_1)\psi_2^\dagger(\boldsymbol{r}_2)\tilde{F}(|\boldsymbol{r}_1 - \boldsymbol{r}_2|,\Lambda)\tilde{F}(|\boldsymbol{r}_1' - \boldsymbol{r}_2'|,\Lambda)\psi_1(\boldsymbol{r}_1')\psi_2(\boldsymbol{r}_2') \\ + g_0 \int d\boldsymbol{x} d\boldsymbol{y} \; [\phi^\dagger(\boldsymbol{x})\tilde{F}\left(|\boldsymbol{y}|,\Lambda\right)\psi_1\left(\boldsymbol{x} + \frac{\boldsymbol{y}}{2}\right)\psi_2\left(\boldsymbol{x} - \frac{\boldsymbol{y}}{2}\right) + \text{h. c. }. \end{aligned} \tag{4.46}$$

From this Hamiltonian, the interaction is calculated as

$$\langle \boldsymbol{p}'|H_{\rm int}|\boldsymbol{p}\rangle = \lambda_0 F(p_1,\Lambda)F(p_2,\Lambda), \tag{4.47}$$

$$\langle \boldsymbol{p}|H_{\rm int}|\phi\rangle = \langle \phi|H_{\rm int}|\boldsymbol{p}\rangle = g_0 F(\boldsymbol{p},\Lambda). \tag{4.48}$$

We note that if we choose the form factor as $\tilde{F}(\boldsymbol{r}_1 - \boldsymbol{r}_2) = \delta(\boldsymbol{r}_1 - \boldsymbol{r}_2)$, Eqs. (4.47) and (4.48) become the contact interaction. The effective interaction $V_{\rm eff}$ is obtained with explicitly including the form factor:

$$V_{\rm eff}(E,\Lambda) = \left(\lambda_0 + \frac{g_0^2}{E - \nu_0}\right)|F(p,\Lambda)|^2. \tag{4.49}$$

With this effective interaction, the momentum integral in the t-matrix appears as the product of form factor (4.49) and loop function (4.33). Thanks to the form factor, the momentum integral converges without artificially introducing an additional cutoff.

4.1.6 Correspondence to Feshbach method

In this subsection, we discuss the relation between the resonance model in the EFT and the single resonance approach in the Feshbach method in Sec. 3.2. By comparing the completeness relations (3.56) to (4.17), it is seen that both models have the same model space whose basis is the free scattering states $|\boldsymbol{p}\rangle$ and single discrete bare state $|\phi\rangle$. Therefore, both formulations equivalently describe the system (2.19) in Section 2.1. We can choose both models appropriately based on the purpose. In the Feshbach method, the Hamiltonian is written as a matrix form (3.48). Thanks to this property, the Feshbach method is suitable for the visual understanding of the Hamiltonian of the system. In contrast, using the EFT, we can explicitly identify the origin of the eigenstates of the free Hamiltonian $|\boldsymbol{p}\rangle$ and $|\phi\rangle$ which are defined by the creation operators and vacuum $|0\rangle$ in Eqs. (4.9) and (4.10).

By comparing the t-matrix in the single resonance approach (3.60) with that in the resonance model (4.40), we find that

$$V_{PP} + V_{PQP}(E) = \lambda_0 + \frac{g_0^2}{E - \nu_0}, \tag{4.50}$$

$$G_P^0(E_p)\big|_{\text{single resonance approach}} = (2\pi)^3 G^0(E,\Lambda)\big|_{\text{resonance model}}. \tag{4.51}$$

Here we denote the Green's function in the single resonance approach as $G_P^0(E_p)\big|_{\text{single resonance approach}}$, and the loop function in the resonance model as $G^0(E,\Lambda)\big|_{\text{resonance model}}$. From this observation, the single resonance approach reduces to the resonance model, if we determine the interactions in the Hamiltonian (3.48) as

$$V_{PP} = \lambda_0, \tag{4.52}$$

$$\langle \boldsymbol{p}|\hat{V}_{PQ}|\phi\rangle = \langle\phi|\hat{V}_{QP}|\boldsymbol{p}\rangle = g_0, \tag{4.53}$$

with the following correspondence of the form factors:

$$F(\boldsymbol{p})|_{\text{single resonance approach}} = (2\pi)^{3/2} F(p,\Lambda)\Big|_{\text{resonance model}}. \tag{4.54}$$

Here $F(\boldsymbol{p})|_{\text{single resonance approach}}$ is the form factor in the single resonance approach and $|_{\text{resonance model}}$ is that of the resonance model. From Eq. (4.53), the self energy Σ (3.73) in the resonance model is given as

$$\Sigma(E) = g_0^2\{[G^0(E)]^{-1} - \lambda_0\}^{-1}. \tag{4.55}$$

In this way, the system single-channel scattering system in Chapter 2.1 can be formulated in both the single resonance approach and resonance model. These frameworks are utilized to introduce the compositeness [72, 140, 91, 92], as will be shown in the next chapter. Furthermore, in Chapter 6, we discuss the compositeness of shallow bound states using the resonance model, as the main topic of this thesis.

4.2 Resonance model with decay width and coupled channel

In the previous section, we have considered the model with the single-channel scatterings. In the present section, for more practical applications to exotic hadrons, we construct the model with the decay channel (lower channels than the eigenstate) and coupled channel (a higher channel than the eigenstate), as an expansion of the resonance model [71]. We show how to introduce the decay contribution in Section 4.2.1 and coupled-channel contribution in Section 4.2.2.

4.2.1 Decay contribution

Here we show a simple way to effectively introduce the contribution of the decay channel to the resonance model. It is using the complex coupling constant $\lambda_0, g_0 \in \mathbb{C}$ instead of the real λ_0, g_0.[3] In the single-channel elastic scattering in Section 4.1, the Hamiltonian (4.2) and (4.3) are Hermitian $\hat{H}^\dagger = \hat{H}$ due to the real coupling constants. However, the Hamiltonian with the complex λ_0 and g_0 becomes non-Hermitian because $\lambda_0^* \neq \lambda_0$ and $g_0^* \neq g_0$. This non-Hermitian nature allows to have complex eigenenergy and unstable eigenstates as shown in the following. With the complex coupling constant, the eigenstate is obtained as the state below the threshold, but with the decay width. Such a state is called a quasi-bound state.

In the energy region below the threshold, while the loop function $G(E)$ is real, the effective interaction $V_{\text{eff}}(E)$ 4.31 becomes the complex function due to the complex coupling constants. Therefore, the eigenenergy from the pole condition (4.42) is obtained as a complex value. This is consistent with the fact that the eigenenergy of unstable states is expressed as the complex value (2.83). Here we denote the complex eigenenergy of quasi-bound states as

$$E = -B - i\frac{\Gamma}{2}, \tag{4.56}$$

with the quasi-binding energy $B > 0$ and decay width $\Gamma > 0$. In this way, we effectively introduce the decay channel.

The physical quantities such as the scattering amplitude, scattering length, and effective range are also written as the same formula in Section 4.1.4 but with the complex coupling constants. This model is utilized to discuss the contribution of decay to the near-threshold states in Chapter 6.

4.2.2 Coupled channel resonance model

Let us consider the two-channel resonance model for coupled-channel systems. For this purpose, we introduce another tow-body scattering of Ψ_1, Ψ_2 (channel 2) in addition to that of ψ_1, ψ_2 (channel 1) in the free Hamiltonian (4.2) [94]:

$$\begin{aligned}\mathcal{H}_{\text{free}} = &\frac{1}{2m_1}\nabla\psi_1^\dagger \cdot \nabla\psi_1 + \frac{1}{2m_2}\nabla\psi_2^\dagger \cdot \nabla\psi_2 + \frac{1}{2M_1}\nabla\psi_1^\dagger \cdot \nabla\Psi_1 + \frac{1}{2M_2}\nabla\Psi_2^\dagger \cdot \nabla\psi_2 + \frac{1}{2M}\nabla\phi^\dagger \cdot \nabla\phi \\ &+ \omega_1\Psi_1^\dagger\Psi_1 + \omega_2\Psi_2^\dagger\Psi_2 + \nu_0\phi^\dagger\phi,\end{aligned} \tag{4.57}$$

[3] As another procedure, we can also construct the model by explicitly introducing the decay channel as in the higher coupled channel case (Section 4.2). However, we need a complicated calculation in this case, because the three-body decay should be considered to apply the model to exotic hadrons. In contrast, we can effectively consider the decay contribution by letting g_0 be complex, even if the system has many-body decays.

where $M_{1,2}$ are the masses of $\Psi_{1,2}$, and $\omega_{1,2}$ are the energy of $\Psi_{1,2}$ measured from the $\psi_1\psi_2$ threshold. We denote the threshold energy difference as $\Delta\omega = \omega_1 + \omega_2 > 0$. The interaction Hamiltonian is defined as

$$\begin{aligned}\mathcal{H}_{\rm int} = &\lambda_{11}(\psi_1^\dagger\psi_2^\dagger\psi_1\psi_2) + \lambda_{12}(\psi_1^\dagger\psi_2^\dagger\Psi_1\Psi_2) + \lambda_{21}(\Psi_1^\dagger\Psi_2^\dagger\psi_1\psi_2) + \lambda_{22}(\Psi_1^\dagger\Psi_2^\dagger\Psi_1\Psi_2)\\ &+ g_{0,1}(\phi^\dagger\psi_1\psi_2 + \psi_1^\dagger\psi_2^\dagger\phi) + g_{0,2}(\phi^\dagger\Psi_1\Psi_2 + \Psi_1^\dagger\Psi_2^\dagger\phi).\end{aligned} \tag{4.58}$$

The terms with λ_{12} and λ_{21} represent the direct transition between channel 1 and channel 2, and terms with $g_{0,1}$ and $g_{0,2}$ correspond to the transition through the bare state ϕ. In this model, the completeness relation is written as

$$\int \frac{d\boldsymbol{p}_1}{(2\pi)^3}\,|\boldsymbol{p}_1\rangle\,\langle\boldsymbol{p}_1| + \int \frac{d\boldsymbol{p}_2}{(2\pi)^3}\,|\boldsymbol{p}_2\rangle\,\langle\boldsymbol{p}_2| + |\phi\rangle\,\langle\phi| = 1, \tag{4.59}$$

where $|\boldsymbol{p}_i\rangle$ is the free scattering states in the i-th channel.

In the multi-channel case, the on-shell t-matrix $t(p_1)$ is written as the 2×2 array by the matrix interaction $V(p_i)$ and loop function $G^0(p_i)$ [94]:

$$t(p_1) = V(p_1) + V(p_1)G^0(p_1)t(p_1), \tag{4.60}$$

$$V(p_1) = \begin{pmatrix} V_{11} & V_{12} \\ V_{21} & V_{22}\end{pmatrix} = \begin{pmatrix} \lambda_{11} + \frac{g_{0,1}^2}{p_1^2/(2\mu_1)-\nu_0} & \lambda_{12} + \frac{g_{0,1}g_{0,2}}{p_1^2/(2\mu_1)-\nu_0} \\ \lambda_{21} + \frac{g_{0,1}g_{0,2}}{p_1^2/(2\mu_1)-\nu_0} & \lambda_{22} + \frac{g_{0,2}^2}{p_1^2/(2\mu_1)-\nu_0}\end{pmatrix}, \tag{4.61}$$

$$G^0(p_1) = \begin{pmatrix} G_1^0(p_1) & 0 \\ 0 & G_2^0(p_2(p_1))\end{pmatrix}, \quad G_i^0(p_i) = -\frac{\mu_i}{\pi^2}\left[\Lambda - ip_i\arctan\left(-\frac{\Lambda}{ip_i}\right)\right]. \tag{4.62}$$

Here $p_{1,2}$ are the momenta of the channel 1 and 2, respectively:

$$p_1 = \sqrt{2\mu_1 E}, \tag{4.63}$$

$$p_2(p_1) = \sqrt{2\mu_2(E-\Delta\omega)} = \sqrt{\frac{\mu_2}{\mu_1}p_1^2 - 2\mu_2\Delta\omega}, \tag{4.64}$$

with the reduced masses of each channel $\mu_{1,2}$. As in the single-channel cases, the eigenenergy is obtained by the pole condition of the on-shell t-matrix (4.60). In the coupled-channel cases, it is shown that the pole condition is written as [141]

$$\det[1 - G^0(E)V(E)] = 0. \tag{4.65}$$

To calculate the compositeness in a later discussion, we derive the effective interaction in this model. In the two-channel case, the effective interaction $V_{\rm eff}(p_1)$ is obtained by eliminating the channels other than the $\psi_{1,2}$ scattering which is not only the bare state ϕ but also $\Psi_{1,2}$ scattering [94]:

$$V_{\rm eff}(p_1) = V_{11}(p_1) + \frac{[V_{12}(p_1)]^2}{[G_2^0(p_1)]^{-1} - V_{22}(p_1)}. \tag{4.66}$$

Using the effective interaction $V_{\rm eff}(p_1)$, the bound state condition is also written as

$$t_{11}^{-1}(E) = 1 - G_1^0(E)V_{\rm eff}(E) = 0. \tag{4.67}$$

This condition is confirmed to be equivalent to Eq. (4.65) by using the relation $V_{12} = V_{21}$. We will use this model to consider the coupled channel system in Chapter 6.

Chapter 5

Compositeness

In this chapter, we review the compositeness, a useful measure for analyzing the internal structure of states. We start with an introduction of the wavefunction renormalization factor which provides the foundation for the idea of the compositeness (Section 5.1). We then define the compositeness of bound states in Section 5.2. For bound states, the compositeness is straightforwardly regarded as the probability of finding the molecular component in the wavefunction. For later calculations, we also show some useful expressions of the compositeness in Section 5.3. To discuss the universal nature of the compositeness of shallow bound states, we present the weak-binding relation in Section 5.5. Since actual exotic hadrons appear as unstable states in multi-channel scatterings, we define the compositeness for coupled-channel systems in Section 5.4, and we extend the notion of the compositeness to generalized eigenstates (virtual states and resonances) in Section 5.6. As shown in Section 5.6, however, the compositeness of virtual states and resonances cannot be regarded as the probability. To address this issue, we discuss a prescription of the probabilistic interpretation of the compositeness of generalized eigenstates by considering the nature of unstable states in Section 5.7. Finally, in Section 5.8, we present various applications of the compositeness not only to exotic hadrons but also to nuclei and atomic systems. This demonstrates the universal applicability of the compositeness.

5.1 Wavefunction renormalization factor

Before the introduction of the compositeness, we discuss an essentially equivalent quantity called "the renormalization factor of the wavefunction" in quantum mechanics or "field renormalization constant" in field theory. The renormalization factor is defined as the coefficient of the perturbed eigenstate [142, 143]. Let us consider the perturbative expansion of an eigenstate of the full Hamiltonian $|n\rangle_p$:

$$|n\rangle_p = |n\rangle_0 + |n\rangle_1 + ..., \tag{5.1}$$

where $|n\rangle_i$ represents the i-th perturbation of the wavefunction. Here we define $|n\rangle_0$ as the eigenstate of the free Hamiltonian which is normalized and orthogonal to $|n\rangle_{i\neq 0}$:

$${}_0\langle n|n\rangle_0 = 1, \quad {}_0\langle n|n\rangle_{i\neq 0} = 0 \tag{5.2}$$

Therefore, the norm of $|n\rangle_p$ deviates from unity:

$$ {}_p\langle n|n\rangle_p = 1/Z \neq 1. \tag{5.3}$$

To "re"-normalize perturbed eigenstate of the full Hamiltonian $|n\rangle_p$, we define the normalized eigenstate $|n\rangle_N$:

$$ |n\rangle_N = \sqrt{Z}\,|n\rangle_p\,, \tag{5.4}$$

$$ {}_N\langle n|n\rangle_N = Z \cdot {}_p\langle n|n\rangle_p = 1 \tag{5.5}$$

By substituting Eq. (5.1), the perturbative expansion of the normalized eigenstate is written as

$$ |n\rangle_N = \sqrt{Z}\,|n\rangle_0 + \sqrt{Z}\,|n\rangle_1 + ... \tag{5.6}$$

From Eq. (5.2), we see Z is written as the overlap of $|n\rangle_N$ and $|n\rangle_0$:

$$ {}_0\langle n|n\rangle_N = \sqrt{Z} \cdot {}_0\langle n|n\rangle_0 = \sqrt{Z}, \tag{5.7}$$

$$ Z = |\,{}_0\langle n|n\rangle_N\,|^2. \tag{5.8}$$

From this equation, Z is regarded as the probability of finding the eigenstate of the free Hamiltonian $|n\rangle_0$ in that of the full Hamiltonian $|n\rangle_N$. In this sense, the renormalization constant Z is essentially equivalent to the elementarity Z as shown in the next section.

Around 1960, the field renormalization constant Z was applied to particle physics to distinguish the elementary and composite particles [144, 145, 98]. A summary of studies in this era is given by the review article [146]. The remarkable application of the field renormalization constant is performed by S. Weinberg in a series of four works [75, 76, 147, 72]. It is epoch-making that he develops the model-independent approach to calculate the field renormalization constant from the observables. This method is now known as the weak-binding relation, which is shown in Section 5.5. Using the weak-binding relation, it is shown that the deuteron is not an elementary particle, namely, the composite particle of two nucleons [72].

Since 2003, motivated by observations of exotic hadrons (see Section 1.1), Weinberg's works have been revisited as a framework for investigating the internal structure of hadrons [140]. The extension of Weinberg's idea has developed into the method for analyzing the internal structure of hadrons using the compositeness and is now being widely applied. The representative studies and applications of the compositeness are summarized in Section 5.8.

5.2 Definition of compositeness

In this section, we define the compositeness X and elementality Z. Here we consider the system introduced in Section 2.1.2 where the bound state $|B\rangle$ (2.7) is written as the linear combination of the free scattering states $|\boldsymbol{p}\rangle$ (2.17) and bare discrete state $|\phi\rangle$ (2.18). The compositeness X (elementarity Z) is defined as the overlap of the bound state $|B\rangle$ and the free scattering states $|\boldsymbol{p}\rangle$ (the bare discrete state $|\phi\rangle$):

$$ X = \int d\boldsymbol{p}\;|\,\langle \boldsymbol{p}|B\rangle\,|^2, \tag{5.9}$$

$$Z = |\langle \phi | B \rangle|^2. \tag{5.10}$$

From the completeness relation (2.19), the sum of X and Z is normalized:

$$X + Z = 1. \tag{5.11}$$

In the effective field theory in Section 4.1, the definition of X and Z can be written by the momentum space wavefunction $\chi(\boldsymbol{p}) = \langle \boldsymbol{p} | B \rangle$ (4.25) and overlap constant $c = \langle \phi | B \rangle$ (5.32):

$$X = \int \frac{d\boldsymbol{p}}{(2\pi)^3} |\chi(\boldsymbol{p})|^2, \tag{5.12}$$

$$Z = |c|^2. \tag{5.13}$$

Furthermore, X and Z can also be regarded as the weights which are obtained by the projection of $|B\rangle$ to the P and Q spaces in the single resonance approach in the Feshbach method in Section 3.2 [148, 74]:

$$X = \langle B | \hat{P} | B \rangle, \tag{5.14}$$

$$Z = \langle B | \hat{Q} | B \rangle. \tag{5.15}$$

To regard the compositeness X and elementarity Z as probabilities, the following two conditions should be satisfied;

(i) X and Z are real and positive value; and

(ii) $X + Z$ is normalized.

In this case, the compositeness X and elementarity Z are

$$0 \leq X \leq 1, \quad 0 \leq Z \leq 1. \tag{5.16}$$

For bound states, the absolute value square of the overlaps in Eqs. (5.9) and (5.10) is real and positive, which guarantees the condition (i). The condition (ii) is satisfied by the sum rule (5.11). In this way, the compositeness X (elementarity Z) can be regarded as the probability of finding the composite component (elementary component) in the bound state $|B\rangle$. In fact, this consideration is confirmed by the following expansion of $|B\rangle$ by the completeness relation (4.17):

$$|B\rangle = \int d\boldsymbol{p} \, \langle \boldsymbol{p} | B \rangle \, |\boldsymbol{p}\rangle + \langle \phi | B \rangle \, |\phi\rangle. \tag{5.17}$$

Due to the probabilistic nature of the compositeness, we can perform the quantitative analysis of the internal structure of bound states. For example, if the compositeness X is larger than 50 % ($X > 0.5$), we can see the composite component is dominant in the wavefunction, and therefore the state is concluded as composite dominant. In contrast, the state is non-composite or elementary dominant when $X < 0.5$. We emphasize that the notion of the compositeness can be used to characterize any bound state in the two-body sector as long as the free scattering states $|\boldsymbol{p}\rangle$ can be defined. In hadron physics, the compositeness represents the weight of the hadronic molecular component when $|\boldsymbol{p}\rangle$ corresponds to the hadron scatterings. However, the compositeness cannot be defined for the quark degrees of freedom, because there are no free scattering states $|\boldsymbol{p}\rangle$ due to the color confinement.

Finally, we emphasize that the compositeness X and elementarity Z are the model-dependent quantities. We recall that the free Hamiltonian $\hat{H}_0$ can be arbitrarily chosen for a given full Hamiltonian

$\hat{H}$, as mentioned in Section 2.1.2. Therefore, the eigenstates $|\boldsymbol{p}\rangle$ of $\hat{H}_0$ also depend on the choice. As shown in the definition (5.9), the compositeness contains the overlap of the free scattering states $|\boldsymbol{p}\rangle$ and the bound state. Therefore, the compositeness X can also be changed depending on the choice of $\hat{H}_0$. This arbitrariness induces the model dependence of the compositeness.

5.3 Expressions of compositeness

In this section, let us review some useful expressions of the compositeness X and elementarity Z [17, 74].

5.3.1 Compositeness with t-matrix

We first derive the expression of the compositeness X by the form factor $g_{\rm th}^2 F(E)$ in Chapter 2. By multiplying the free scattering state $\langle \boldsymbol{p}|$ to the Schrödinger equation of the full Hamiltonian (2.7), we obtain

$$\begin{aligned} -B\langle \boldsymbol{p}|B\rangle &= \langle \boldsymbol{p}|\hat{H}|B\rangle\,, \\ &= \langle \boldsymbol{p}|(\hat{H}_0+\hat{V})|B\rangle\,, \\ &= E_p\langle \boldsymbol{p}|B\rangle + \langle \boldsymbol{p}|\hat{V}|B\rangle\,, \\ \Rightarrow \langle \boldsymbol{p}|B\rangle &= -\frac{\langle \boldsymbol{p}|\hat{V}|B\rangle}{E_p+B}. \end{aligned} \tag{5.18}$$

By substituting this $\langle \boldsymbol{p}|B\rangle$ into the definition (5.9), X is written by the binding energy B and form factor $g_{\rm th}^2 F(E)$:

$$X = \int d\boldsymbol{p}\frac{|\langle \boldsymbol{p}|\hat{V}|B\rangle|^2}{(E_p+B)^2}, \tag{5.19}$$

$$= 4\pi\sqrt{2\mu^3}g_{\rm th}^2\int_0^\infty dE\frac{\sqrt{E}|F(E)|^2}{(E+B)^2}, \tag{5.20}$$

In the second line, $\langle \boldsymbol{p}|\hat{V}|B\rangle$ is written by Eq. (2.53) for the bound state coupling to the scatterings in the s wave. For general partial waves, see Ref. [74].

We then show Eq. (5.20) can further be rewritten with the on-shell t-matrix obtained by the Low-equation (2.52). Solving Eq. (2.54) for the square of the form factor $|F(E)|^2$, we obtain:

$$X = 4\pi\sqrt{2\mu^3}\int_0^\infty dE\frac{\sqrt{E}}{E+B}\left[t(E) - v - 4\pi\sqrt{2\mu^3}\int_0^\infty dE'\frac{\sqrt{E'}|t(E')|^2}{E-E'+i0^+}\right], \quad v = \langle \boldsymbol{p}|\hat{V}|\boldsymbol{p}\rangle\,. \tag{5.21}$$

We note that the compositeness X in Eq. (5.21) is obtained as real because the imaginary part of t-matrix cancels with that of the third term [17] as shown in the following. From the optical theorem (2.66) and (2.67), the imaginary part of the scattering amplitude $f(E)$ is expressed by the magnitude of $f(E)$:

$$\mathrm{Im}\, f(E) = p|f(E)|^2. \tag{5.22}$$

Using the relation between $f(E)$ and $t(E)$ (2.59), we then obtain

$$\mathrm{Im}\, t(E) = -\mu(2\pi)^2 p|t(E)|^2. \tag{5.23}$$

In fact, this exactly cancels with the imaginary part of the third term in Eq. (5.21) which is calculated as

$$\mathrm{Im}\left(\int_0^\infty dE' \frac{\sqrt{E'}|t(E')|^2}{E-E'+i0}\right) = -\pi\sqrt{E}|t(E)|^2. \tag{5.24}$$

Here the following integral formula with the principal value $\mathcal{P}$ is utilized

$$\frac{1}{x \pm i0} = \mathcal{P}\left(\frac{1}{x}\right) \mp i\pi\delta(x). \tag{5.25}$$

Using $p = \sqrt{2\mu E}$, we see that the imaginary part of X in Eq. (5.21) is canceled.

5.3.2 Compositeness with effective interaction

The elementarity Z is also expressed by the derivative of the effective interaction $\hat{V}_{\rm eff}(E)$ [148]. From the property of the projection operator $\hat{Q} = \hat{Q}\hat{Q}$ and Eq. (3.27), Z (5.15) is written as

$$\begin{aligned} Z &= \langle\Psi|\hat{Q}\hat{Q}|\Psi\rangle\,, && (5.26)\\ &= \langle Q|Q\rangle\,, && (5.27)\\ &= \langle P|\hat{H}_{PQ}(E-\hat{H}_{QQ})^{-2}\hat{H}_{QP}|P\rangle\,, && (5.28)\\ &= \langle P|\left(-\frac{d\hat{V}_{\rm eff}(E)}{dE}\right)|P\rangle\,. && (5.29) \end{aligned}$$

In the third line, we use Eq. (3.33). Using the sum rule $X = 1-Z$, the compositeness X is also written by

$$X = \langle P|\left(1+\frac{d\hat{V}_{\rm eff}(E)}{dE}\right)|P\rangle\,. \tag{5.30}$$

From this expression, we see that $X = 1$ and $Z = 0$ for an energy-independent interaction. In other words, the energy dependence of the interaction induces the finite elementarity. Note that to obtain reasonable X and Z, some conditions are imposed for the energy derivative. For $Z > 0$ ($X > 0$), the energy derivative of the effective interaction should be negative (have a lower limit) [149, 150].

5.3.3 Compositeness for separable interaction

If the interaction is separable, it is possible to express the compositeness X and elementality Z with the effective interaction and the loop function (Green's function). We demonstrate this using the single-channel resonance model with $\lambda_0 = 0$ in the EFT (Section 4.1). From Eqs. (4.29) and (4.28), $\chi(\boldsymbol{p})$ and c are obtained as

$$\chi(\boldsymbol{p}) = \frac{V_{\rm eff}(-B)}{-B-E_p}\int\frac{d\boldsymbol{q}}{(2\pi)^3}\,\chi(\boldsymbol{q}), \tag{5.31}$$

$$c = \frac{g_0}{-B-\nu_0}\int\frac{d\boldsymbol{q}}{(2\pi)^3}\,\chi(\boldsymbol{q}). \tag{5.32}$$

By substituting Eq. (5.31) into the definition of X (5.12), we obtain

$$X = -G^{0\prime}(-B)[V_{\rm eff}(-B)]^2\left|\int\frac{d\boldsymbol{p}}{(2\pi)^3}\chi(\boldsymbol{p})\right|^2, \tag{5.33}$$

where we denote

$$\alpha'(E) = \frac{d\alpha(E)}{dE}. \tag{5.34}$$

In the same way, by substituting Eq. (5.32) into the definition (5.13), Z is also written as

$$Z = -V'_{\rm eff}(-B) \left| \int \frac{d\boldsymbol{p}}{(2\pi)^3} \chi(\boldsymbol{p}) \right|^2, \tag{5.35}$$

By eliminating $\left|\int d\boldsymbol{p}/(2\pi)^3 \chi(\boldsymbol{p})\right|^2$ using the sum rule (5.11) the following formulas of X and Z can be derived [94]:

$$X = \left. \frac{G^{0\prime}(E)}{G^{0\prime}(E) - [1/V_{\rm eff}(E)]'} \right|_{E=-B}, \tag{5.36}$$

$$Z = \left. \frac{-[1/V_{\rm eff}(E)]'}{G^{0\prime}(E) - [1/V_{\rm eff}(E)]'} \right|_{E=-B}. \tag{5.37}$$

These formulas are used to calculate X and Z in Chapter 6.

We also show that the compositeness is expressed by the residue g^2 of the t-matrix. By substituting the Lippmann-Schwinger equation (2.46) into the square of the residue g^2 (2.55), we obtain

$$g^2 = \lim_{E \to -B} (E+B)[1/V_{\rm eff}(E) - G^0(E)]^{-1}. \tag{5.38}$$

By expanding $1/V_{\rm eff}(E)$ and $G^0(E)$ around $E = -B$, and using the bound state condition

$$\frac{1}{t(-B)} = 1/V_{\rm eff}(-B) - G^0(-B) = 0, \tag{5.39}$$

the residue can be rewritten as

$$g^2 = - \left. \frac{1}{G^{0\prime}(E) - [1/V_{\rm eff}(E)]'} \right|_{E=-B}. \tag{5.40}$$

Because this equation corresponds to the denominator of Eq. (5.36), the compositeness X and elementarity are also expressed by the residue and derivative of the loop function:

$$X = -g^2 G^{0\prime}(E)|_{E=-B}, \tag{5.41}$$

$$Z = g^2 [1/V_{\rm eff}(E)]'|_{E=-B}. \tag{5.42}$$

We note that the same expressions of X and Z can be used in quantum mechanics for the general separable interaction (2.46) using the appropriate convention (see Section 2.3.2). For example, the loop function in the field theory (2.63) should be replaced by that in quantum mechanics (2.42).

5.3.4 Compositeness with self energy

Finally, we show the expression of X by the self energy $\Sigma(E)$:

$$X = \left. \frac{-\Sigma'(E)}{1 - \Sigma'(E)} \right|_{E=-B}, \tag{5.43}$$

$$Z = \left. \frac{1}{1 - \Sigma'(E)} \right|_{E=-B}. \tag{5.44}$$

In the following, we show that Z in this expression is equivalent to that in Eq. (5.37) in the resonance model.

We first tranceform the operator $\hat{\Sigma}$ to calculate the energy derivative of the self energy $\Sigma(E) = \langle\phi|\hat{\Sigma}(E)|\phi\rangle$. From the relation between full Green's function in P channel space $\hat{G}_P(E)$ (3.40) and free Green's function $\hat{G}^0_P(E)$ (3.36), we obtain [97]

$$\begin{aligned}\hat{G}_P(E) &= [1 - \hat{G}^0_P(E)\hat{V}_{PP}]^{-1}\hat{G}^0_P(E) \\ &= \{[\hat{G}^0_P(E)]^{-1} - \hat{V}_{PP}\}^{-1}. \end{aligned} \tag{5.45}$$

We then substitute this relation into the operator $\hat{\Sigma}(E)$ (3.42) and calculate the energy derivative of $\hat{\Sigma}(E)$ at $E = -B$:

$$\begin{aligned}\frac{d}{dE}\hat{\Sigma}(-B) &= \frac{d}{dE}\hat{H}_{QP}\{[\hat{G}^0_P(-B)]^{-1} - \hat{V}_{PP}\}^{-1}\hat{H}_{PQ} \\ &= -\hat{H}_{QP}\{[\hat{G}^0_P(-B)]^{-1} - \hat{V}_{PP}\}^{-1}\frac{d}{dE}[\hat{G}^0_P(-B)]^{-1}\{[\hat{G}^0_P(-B)]^{-1} - \hat{V}_{PP}\}^{-1}\hat{H}_{PQ} \\ &= -\hat{H}_{QP}[\hat{V}_{\rm eff}(-B) - \hat{V}_{PP}]^{-1}\frac{d}{dE}[\hat{G}^0_P(-B)]^{-1}[\hat{V}_{\rm eff}(-B) - \hat{V}_{PP}]^{-1}\hat{H}_{PQ} \\ &= \hat{H}_{QP}[\hat{H}_{PQ}\hat{G}_Q(-B)\hat{H}_{QP}]^{-1}[\hat{G}^0_P(-B)]^{-1}\frac{d}{dE}[\hat{G}^0_P(-B)][\hat{G}^0_P(-B)]^{-1}[\hat{H}_{PQ}\hat{G}_Q(-B)\hat{H}_{QP}]^{-1}\hat{H}_{PQ} \\ &= [\hat{H}_{PQ}\hat{G}_Q(-B)]^{-1}[\hat{G}^0_P(-B)]^{-1}\frac{d}{dE}[\hat{G}^0_P(-B)][\hat{G}^0_P(-B)]^{-1}[\hat{G}_Q(-B)\hat{H}_{QP}]^{-1}. \end{aligned} \tag{5.46}$$

Here we define

$$\hat{G}_Q(E) = (E - \hat{H}_{QQ})^{-1}. \tag{5.47}$$

In the third line, we use the bound state condition for operators:

$$\hat{V}^{-1}_{\rm eff}(E) - \hat{G}^0_P(E) = 0 \Big|_{E=-B}. \tag{5.48}$$

Furthermore, we use the formulas of the derivative of the inverse of the operators:

$$\frac{d}{dE}[\hat{\alpha}(E)]^{-1} = -[\hat{\alpha}(E)]^{-1}\frac{d}{dE}\hat{\alpha}(E)[\hat{\alpha}(E)]^{-1}, \tag{5.49}$$

$$\frac{d}{dE}[1 - \hat{\alpha}(E)]^{-1} = [1 - \hat{\alpha}(E)]^{-1}\frac{d}{dE}\hat{\alpha}(E)[1 - \hat{\alpha}(E)]^{-1} \tag{5.50}$$

By calculating the matrix element of Eq. (5.46) in the resonance model, we obtain

$$\begin{aligned}\langle\phi|\frac{d}{dE}\hat{\Sigma}(-B)|\phi\rangle &= \langle\phi|\,[\hat{H}_{PQ}\hat{G}_Q(-B)]^{-1}[\hat{G}^0_P(E)]^{-1}\frac{d}{dE}[\hat{G}^0_P(E)][\hat{G}^0_P(E)]^{-1}[\hat{G}_Q(-B)\hat{H}_{QP}]^{-1}\,|\phi\rangle \\ &= \langle\phi|\,[\hat{G}_Q(-B)]^{-1}\hat{H}^{-1}_{PQ}\hat{V}_{\rm eff}(-B)\frac{d}{dE}[\hat{G}^0_P(E)]\hat{V}_{\rm eff}(-B)\hat{H}^{-1}_{QP}[\hat{G}_Q(-B)]^{-1}\,|\phi\rangle \\ &= \int\frac{d\boldsymbol{p}}{(2\pi)^3}\,\langle\phi|\,[\hat{G}_Q(-B)]^{-1}\hat{H}^{-1}_{PQ}\hat{V}_{\rm eff}(-B)\,|\boldsymbol{p}\rangle\,\langle\boldsymbol{p}|\,\frac{d}{dE}[\hat{G}^0_P(E)]\hat{V}_{\rm eff}(-B)\hat{H}^{-1}_{QP}[\hat{G}_Q(-B)]^{-1}\,|\phi\rangle \\ &= \int\frac{d\boldsymbol{p}}{(2\pi)^3}(-B-\nu_0)^{-1}\,\langle\phi|\hat{H}^{-1}_{PQ}|\boldsymbol{p}\rangle\,V_{\rm eff}(-B)\frac{-1}{(-B-E_p)^2}V_{\rm eff}(-B)\,\langle\boldsymbol{p}|\hat{H}^{-1}_{QP}|\phi\rangle\,(-B-\nu_0)^{-1} \\ &= \int\frac{d\boldsymbol{p}}{(2\pi)^3}(-B-\nu_0)^{-1}g_0^{-1}V_{\rm eff}(-B)\frac{-1}{(-B-E_p)^2}V_{\rm eff}(-B)g_0^{-1}(-B-\nu_0)^{-1} \\ &= \int\frac{d\boldsymbol{p}}{(2\pi)^3}\frac{-1}{(-B-E_p)^2}\frac{1}{(-B-\nu_0)^2}g_0^{-2}V_{\rm eff}(-B)^2 \end{aligned}$$

$$= G_P^{0\prime}(-B)\frac{1}{\{[V_{\rm eff}(-B)]^{-1}\}'}. \tag{5.51}$$

In the third line, we multiply the completeness relation (4.17). By substituting this result into Eq. (5.44), we find that the expression with energy derivative of $\Sigma(E)$ is equivalent to the expression (5.37) by appropriately taking into account the $(2\pi)^3$ factor.

$$\begin{aligned} Z &= \frac{1}{1-\frac{[G_P^0(-B)]'}{[1/V_{\rm eff}(-B)]'}} \\ &= \frac{[1/V_{\rm eff}(-B)]'}{[1/V_{\rm eff}(-B)]' - [G_P^0(-B)]'}. \end{aligned} \tag{5.52}$$

Equation (5.44) shows that the elementarity Z can be written by the same expression as the field renormalization constant [151].

5.4 Compositeness for coupled channels

To consider exotic hadrons observed in the multi-channel scatterings, we extend the notion of the compositeness for the coupled-channel systems. Different from the single-channel scatterings discussed in the previous sections, let us consider the multi-channel system where several channels couple to the bound state. Here we call the lowest-energy channel "the threshold channel" and all other higher-energy channels "the coupled channels". To define the compositeness in the multi-channel system, we first need to fix the model space. Let us pick up the N scattering channels out of all possible coupled channels. In this case, the compositeness of the threshold channel X_1 (coupled channels X_i) is schematically defined as the weight of the threshold channel component $|\text{ch. } 1\rangle$ (the coupled channel component $|\text{ch. } i\rangle$) in the bound state $|B\rangle$:

$$|B\rangle = \sqrt{X_1}\,|\text{ch. } 1\rangle + \sqrt{X_2}\,|\text{ch. } 2\rangle + ... + \sqrt{X_i}\,|\text{ch. } i\rangle + ... + \sqrt{X_N}\,|\text{ch. } N\rangle + \sqrt{Z}\,|\text{others}\rangle\,. \tag{5.53}$$

Here we emphasize that the elementarity Z is defined due to the existence of channels not explicitly considered in this model space, $|\text{others}\rangle$. The components contained in $|\text{others}\rangle$ depend on the choice of the model space. Therefore, the elementarity Z is not uniquely given in multi-channel systems. For example, with the channel elimination, the coupled channels become implicitly contained in $|\text{others}\rangle$, and X_i of the eliminated channel is redefined as a part of Z.

The compositeness for the multi-channel system is defined as in the single-channel case in Section 5.2. Let us consider the system with N scattering channels $|\boldsymbol{p}, \pm, i\rangle$ and one bound state $|B\rangle$:

$$\hat{H}\,|\boldsymbol{p}, \pm, i\rangle = E_{p,i}\,|\boldsymbol{p}, \pm, i\rangle\,, \quad E_{p,i} = \frac{\boldsymbol{p}^2}{2\mu_i} + E_{{\rm th},i}, \tag{5.54}$$

$$\hat{H}\,|B\rangle = -B\,|B\rangle\,, \tag{5.55}$$

with $i = 1, 2, ..., N$. The energy of the i-th threshold is denoted as $E_{{\rm th},i}$, where the lowest threshold energy is setted as $E_{{\rm th},1} = 0$, and the index i is assigned in ascending order $E_{{\rm th},i+1} > E_{\rm th,i}$. Here we introduce the free Hamiltonian whose eigenstates are N free scattering states $|\boldsymbol{p}, i\rangle$ and one discrete bare state $|\phi\rangle$:

$$\hat{H}_0\,|\boldsymbol{p}, i\rangle = E_{p,i}\,|\boldsymbol{p}, i\rangle\,, \tag{5.56}$$

$$\hat{H}_0 \left|\phi\right\rangle = \nu_0 \left|\phi\right\rangle . \tag{5.57}$$

We note that the free scattering states $|\boldsymbol{p}, i\rangle$ consist of the same set of channels as the interacting scattering states $|\boldsymbol{p}, \pm, i\rangle$ to span the same Hilbert space.[1] The free scattering states and discrete bare state are normalized and orthogonal to each other:

$$\langle \boldsymbol{p}', i|\boldsymbol{p}, j\rangle = \delta(\boldsymbol{p}' - \boldsymbol{p})\delta_{ij}, \tag{5.58}$$

$$\langle \phi|\phi\rangle = 1, \tag{5.59}$$

$$\langle \boldsymbol{p}, i|\phi\rangle = \langle \phi|\boldsymbol{p}, i\rangle = 0. \tag{5.60}$$

The completeness relation for the multi-channel case is given by

$$1 = \sum_{1\le i\le N} \int d\boldsymbol{p} \ \left|\boldsymbol{p}, i\right\rangle \left\langle \boldsymbol{p}, i\right| + \left|\phi\right\rangle \left\langle \phi\right| . \tag{5.61}$$

The compositeness of i-th channel X_i and the elementarity Z are defined

$$X_i = \int d\boldsymbol{p} \ |\left\langle \boldsymbol{p}, i|B\right\rangle|^2, \tag{5.62}$$

$$Z = |\left\langle \phi|B\right\rangle|^2. \tag{5.63}$$

Using the completeness relation (5.61), the bound state $|B\rangle$ can be expanded as

$$\left|B\right\rangle = \sum_{1\le i\le N} \int d\boldsymbol{p} \left\langle \boldsymbol{p}, i|B\right\rangle \left|\boldsymbol{p}, i\right\rangle + \left\langle \phi|B\right\rangle \left|\phi\right\rangle . \tag{5.64}$$

This relation shows that X_i represents the probability of finding the i-th scattering channel in the bound state $|B\rangle$. Thanks to Eq. (5.61), a sum rule holds for X_i and Z:

$$\sum_{1\le i\le N} X_i + Z = 1. \tag{5.65}$$

The practical calculation of the compositeness X_i can be performed as in the single-channel case in Section 5.3. Let us show the expression of X_i in the coupled-channel resonance model introduced in Section 4.2.2. The compositeness of threshold channel X_1 is obtained by the components of the loop function G_1^0 (4.62), and the effective interaction $V_{\rm eff}$ (4.66) [94]:

$$X_1 = \left. \frac{G_1^{0\prime}(E)}{G_1^{0\prime}(E) - [V_{\rm eff}^{-1}(E)]'} \right|_{E=-B}, \tag{5.66}$$

We will use this expression in Chapter 6.

5.5 Weak-binding relation

In this section, we introduce the method to estimate the compositeness of shallow bound states from observables, called the weak-binding relation. In the single-channel case, the compositeness of the

[1] In general, multiple discrete states can be introduced, independently from the scattering states. In this case, the elementarity can be defined for each bare state [74].

shallow bound state X is related to the observables, the scattering length a_0 and the radius of the bound state $R = 1/\sqrt{2\mu B}$ through the weak-binding relation [72, 17, 94]:

$$a_0 = R\left\{\frac{2X}{1+X} + \mathcal{O}\left(\frac{R_{\rm typ}}{R}\right)\right\}. \tag{5.67}$$

Here $R_{\rm typ}$ corresponds to the interaction range, which characterizes the uncertainty $\mathcal{O}(R_{\rm typ}/R)$ of the compositeness in the weak-binding relation. For example, the interaction range of the nuclear force is characterized by the mass of the pion as $1/m_\pi$, because the long-range part of the nuclear force can be described by the π exchange. In this case, the interaction range is estimated as $R_{\rm typ} \sim 1/m_\pi$. By solving Eq. (5.67) for X, the compositeness is written as

$$X = \frac{a_0/R + \mathcal{O}\left(R_{\rm typ}/R\right)}{2 - a_0/R - \mathcal{O}\left(R_{\rm typ}/R\right)}. \tag{5.68}$$

This relation shows that when the binding energy B is sufficiently small, the radius of the bound state R becomes much larger than $R_{\rm typ}$ so that the uncertainty $\mathcal{O}(R_{\rm typ}/R)$ is negligible. In this case, the compositeness X can be estimated only by observables, the scattering length a_0 and the radius R. Although the compositeness is a model-dependent quantity in general, the compositeness of the shallow bound states can be obtained in a model-independent manner by the weak-binding relation. The weak-binding relation was developed by S. Weinberg to discuss the internal structure of the deuteron, and he succeeded in showing that the deuteron is not an elementary particle [72]. After his work, the weak-binding relation has been widely used as the model-independent method to estimate the compositeness of the near-threshold exotic hadrons [140, 94].

In the following, we review the details of the weal-binding relation. In Section 5.5.1, we derive the weak-binding relation following the original paper [72]. We then discuss the quantitative estimation of the uncertainty $\mathcal{O}(R_{\rm typ}/R)$ in Section 5.5.2 [93, 94]. To enlarge the applicable region of the weak-binding relation, we introduce the range correction in Section 5.5.3 [95].

5.5.1 Derivation of weak-binding relation

Let us discuss the nature of the compositeness of the shallow bound state to derive the weak-binding relaiton [72, 17, 74]. In quantum mechanics, the weak-binding relation can be obtained from the expression of the compositeness X with the coupling constant $g_{\rm th}$ and the form factor $F(E)$ (5.20). For the derivation, we focus on the shallow bound state with a small binding energy B, where B is much smaller than the typical energy scale of the system $E_{\rm typ}$. We first expand the square of the form factor $|F(E)|^2$ in terms of the energy E around $E = 0$:

$$\begin{aligned} |F(E)|^2 &= |F(0)|^2 + E\,\frac{d}{dE}|F(E)|^2\bigg|_{E=0} + \mathcal{O}(E^2) \\ &= 1 + E\frac{d}{dE}|F(0)|^2 + \mathcal{O}(E^2), \end{aligned} \tag{5.69}$$

where we denote $\frac{d}{dE}|F(E)|^2\big|_{E=0} = \frac{d}{dE}|F(0)|^2$ for simplicity. When B is much smaller than $E_{\rm typ}$, the integrand in Eq. (5.20) is dominated by the near-threshold region $E \lesssim E_{\rm typ}$. Therefore, the integration range of Eq. (5.20) can be restricted within $0 \le E \le E_{\rm typ}$. By substituting the expansion (5.69) into Eq. (5.20), compositeness is given by

$$X = 4\pi\sqrt{2\mu^3}g_{\rm th}^2\left[\int_0^{E_{\rm typ}} dE\frac{\sqrt{E}}{(E+B)^2} + \frac{d}{dE}|F(0)|^2\int_0^{E_{\rm typ}} dE\frac{E\sqrt{E}}{(E+B)^2} + ...\right]. \tag{5.70}$$

The first term in the parentheses is integrated as

$$\int_0^{E_{\rm typ}} dE \frac{\sqrt{E}}{(E+B)^2} = -\frac{\sqrt{E_{\rm typ}}}{B+E_{\rm typ}} + \frac{1}{\sqrt{B}} \arctan\sqrt{\frac{E_{\rm typ}}{B}}. \tag{5.71}$$

For small $B/E_{\rm typ}$, the leading contribution is $\pi/(2\sqrt{B})$. The other terms in Eq. (5.70) are in higher orders of $B/E_{\rm typ}$. For example, the second integral is calculated as

$$\int_0^{E_{\rm typ}} dE \frac{E\sqrt{E}}{(E+B)^2} = \frac{B\sqrt{E_{\rm typ}}}{B+E_{\rm typ}} + 2\sqrt{E_{\rm typ}} - 3\sqrt{B} \arctan\sqrt{\frac{E_{\rm typ}}{B}}, \tag{5.72}$$

where all terms are finite in the $B \to 0$ limit. Therefore, the compositeness of shallow bound states is written as

$$X = 2\pi^2 \sqrt{2\mu^3} g_{\rm th}^2 \frac{1}{\sqrt{B}} \left[1 + \mathcal{O}\left(\sqrt{\frac{B}{E_{\rm typ}}} \right) \right]. \tag{5.73}$$

This relation indicates that the square of the coupling constant $g_{\rm th}^2$ should have the $\mu^{-3/2}\sqrt{B}$ dependence in the weak-binding limit ($B \to 0$) so that the compositeness X is finite. In the weak-binding limit, the square of the form factor $|F(E)|^2$ behaves as constant at $E \sim -B$

$$|F(-B)|^2 = 1 + \mathcal{O}\left(\frac{B}{E_{\rm typ}} \right). \tag{5.74}$$

From this equation and Eq. (2.56), the residue of the bound state g^2 is approximated as $g_{\rm th}^2$. Therefore, the compositeness can also be expressed as

$$X = 2\pi^2 \sqrt{2\mu^3} g^2 \frac{1}{\sqrt{B}} \left[1 + \mathcal{O}\left(\sqrt{\frac{B}{E_{\rm typ}}} \right) \right]. \tag{5.75}$$

Because the residue of the bound state g is determined model-independently [74], we find that the compositeness is model-independent in the weak-binding limit ($B \to 0$). In other words, the model dependence of the compositeness disappears in the $B \to 0$ limit.

We then consider the low-energy behavior of the t-matrix using the Low equation (2.54) for $E \ll E_{\rm typ}$. From Eq. (5.73), the square of the coupling constant $g_{\rm th}^2$ is proportional to $\sqrt{B}$. Therefore, the first term $\langle \boldsymbol{p}|\hat{V}|\boldsymbol{p}\rangle$ is negligible compared with the second term $\propto g_{\rm th}^2/(E+B)$ in the Low equation (2.54) for small B. This corresponds to setting $\hat{V}_{PP} = 0$ in the Feshbach method [see Section (3.1.1)] or $\lambda_0 = 0$ in the resonance model [see Section 4.1]. While the third term has no explicit B dependence[2], this term cannot be neglected to guarantee the unitarity of the t-matrix [72]. Therefore, the Low-equation is approximated in the low-energy region as

$$t(E_p) = \left[\frac{g_{\rm th}^2}{E_p + B} + 4\pi\sqrt{2\mu^3} \int_0^\infty dE_q \, \frac{\sqrt{E_q}|t(E_q)|^2}{E_p - E_q + i0^+} \right] \left[1 + \mathcal{O}\left(\sqrt{\frac{B}{E_{\rm typ}}} \right) \right]. \tag{5.76}$$

If we neglect the higher-order terms $\mathcal{O}(\sqrt{B/E_{\rm typ}})$, this integral equation can be analytically solved in terms of $t(E_p)$ [72]. This is because after neglecting $\langle \boldsymbol{p}|\hat{V}|\boldsymbol{p}\rangle$, the remaining interaction is separable

[2]Note that this term implicitly contains B dependence through $t(E_p)$ in the integrand.

in the low-energy region, as shown in Eq (3.62). The scattering amplitude $f(p)$ is then obtained as [72, 17, 74]

$$f(p) = \left[-\frac{B}{4\pi^2 \mu g_{\rm th}^2} - \frac{\sqrt{2\mu B}}{2} + \frac{1}{2}\left(-\frac{1}{4\pi^2 \mu^2 g_{\rm th}^2} + \frac{1}{\sqrt{2\mu B}} \right) p^2 - ip \right]^{-1}. \tag{5.77}$$

By comparing this equation and the effective range expansion (ERE) (2.65) and using Eq. (5.75), we find that the scattering length a_0 and the effective range r_e can be written by the compositeness X as

$$a_0 = \frac{2X}{X+1} R + \mathcal{O}(R_{\rm typ}), \tag{5.78}$$

$$r_e = \frac{X-1}{X} R + \mathcal{O}(R_{\rm typ}). \tag{5.79}$$

These equations are the weak-binding relations.

The weak-binding relation can also be reserved with the EFT framework [93, 94]. In this derivation, Eq. (5.78) with a_0 is found to be more fundamental than Eq. (5.79) with r_e. From the t-matrix (2.46) and the relation (2.62), the scattering length $a_0 = -1/f(0)$ is written by the effective interaction $V_{\rm eff}$ and loop function $G^0(E)$:

$$a_0 = -\frac{\mu}{2\pi} \frac{1}{V_{\rm eff}^{-1}(0) - G^0(0)}. \tag{5.80}$$

By expanding a_0 by $R_{\rm typ}/R$, we obtain Eq. (5.78) [93, 94]. Equation (5.79) is then obtained using the bound state condition in the ERE by assuming that the bound state pole exists within the convergence radius of the ERE.

Finally, we discuss the weak-binding relation in the zero-range limit ($R_{\rm typ} \to 0$). In this case, the uncertainty becomes exactly zero, and the weak-binding relation is written as

$$a_0 = R \frac{2X}{1+X} \quad (R_{\rm typ} \to 0). \tag{5.81}$$

In this limit, the compositeness X can be completely determined by the observables. We will return to this topic in Section 6.1.

5.5.2 Uncertainty estimation

Let us quantitatively estimate the uncertainty of the compositeness $\mathcal{O}(R_{\rm typ}/R)$ in the weak-binding relation (5.67). If we neglect the uncertainty in Eq. (5.68), the central value of the compositeness X_c is obtained as

$$X_c = \frac{a_0/R}{2 - a_0/R}. \tag{5.82}$$

For example, X_c of the deuteron is obtained as $X_c = 1.68$ which cannot be regarded as a probability. In general, the compositeness exceeds unity if the scattering length a_0 is larger than the radius R. In fact, the scattering length ($a_0 = 5.42$ fm) is larger than the radius ($R = 4.32$ fm). It is therefore important to consider the uncertainty to obtain the meaningful compositeness $0 < X < 1$ [95].

To quantitatively estimate the uncertainty, we introduce ξ [94]:

$$\xi = \frac{R_{\rm typ}}{R}, \tag{5.83}$$

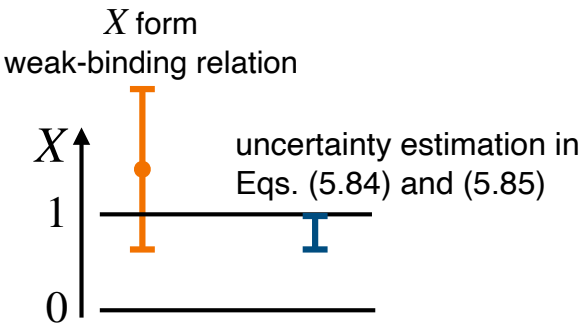

Figure 5.1: The schematic illustration of the uncertainty estimation of the weak-binding relation. The bars correspond to the range of the compositeness X estimated by Eq. (5.84) and by Eqs. (5.85) and (5.86).

Using ξ, the uncertainty of the compositeness is estimated as [94]

$$\frac{a_0/R - \xi}{2 - a_0/R + \xi} \leq X \leq \frac{a_0/R + \xi}{2 - a_0/R - \xi}. \tag{5.84}$$

By considering $0 \leq X \leq 1$ in Eq. (5.16), we define the upper and lower boundaries of the compositeness X_u and X_l (see Fig. 5.1) [95]:

$$X_u = \min\left\{1,\ \frac{a_0/R + \xi}{2 - a_0/R - \xi}\right\}, \tag{5.85}$$

$$X_l = \max\left\{0,\ \frac{a_0/R - \xi}{2 - a_0/R + \xi}\right\}, \tag{5.86}$$

We exclude the regions $X < 0$ and $1 < X$ where the exact value of the compositeness does not exist. We note that when the binding energy B is large, $X_u - X_l$ can be too large to estimate the compositeness from the weak-binding relation. In other words, the weak-binding relation is useful as long as $X_u - X_l$ is sufficiently small [95].

5.5.3 Finite range correction

To extend the applicability of the weak-binding relation, we finally introduce the contribution of the higher order term of the ERE, which is called the finite range correction. It is known that some hadron systems have a sizable effective range r_e by comparing to other length scales. In this case, the effective range plays an important role in characterizing the low-energy phenomena in the system. For example, the effective range of the deuteron $r_e = 1.75$ fm is larger than the interaction range $R_{\rm typ} = 1.43$ fm, and this suggests that the range correction is necessary to consider the deuteron, as mentioned in the introduction.

In Ref. [95], we show that the weak-binding relation does not correctly work for the system with a large effective range $r_e > R_{\rm typ}$. To apply the weak-binding relation to such systems, we introduce the finite range correction to the weak-binding relation by redefining $R_{\rm typ}$ as the maximum length scale between the interaction range $R_{\rm int}$ and the magnitude of the effective range $|r_e|$ [152, 153, 95, 154]:

$$R_{\rm typ} = \max\{R_{\rm int}, |r_e|\}. \tag{5.87}$$

With this range correction, we show the applicable region of the weak-binding relation to the system with $|r_e| > R_{\rm int}$, such as the deuteron system. The range correction is also discussed in Refs. [100, 155, 156, 157, 158].

5.6 Compositeness of virtual states and resonances

In the previous sections, we consider the compositeness of bound states. Strictly speaking, the compositeness in Section 5.2 can be defined only for bound states, which are normalizable $\langle B|B\rangle = 1$, in contrast to virtual states and resonances whose norms diverge. However, the notion of the compositeness can be extended for virtual states and resonances, using the expression of the compositeness in Section 5.3 and using the Gamow vector in Section 2.5, respectively.

Let us first discuss the compositeness of virtual states. For virtual states $|V\rangle$, the compositeness and elementality cannot be calculated by definition using Eqs. (5.9) and (5.15), because of the divergence of the norm $\langle V|V\rangle \to \infty$. However, if the effective interaction $V_{\rm eff}$ is given, the compositeness of virtual states can be obtained by extending Eq. (5.36) with the following replacement;

- the binding energy $-B$ with the virtual state eigenenergy $-E_V$; and
- the loop function in the first Riemann sheet of the energy plane $G(E)$ with that of the second Riemann sheet $G^{II}(E)$.

The eigenmomentum p of virtual states is pure imaginary and its imaginary part is negative ($p = -i\kappa$ with real and positive κ). In this case, it is shown that both the energy derivative of $1/V_{\rm eff}(E)$ and that of $G^{II}(E)$ are positive. From Eq. (5.36), we find that the compositeness of virtual states is always larger than unity $X > 1$ due to $[1/V_{\rm eff}]'/G^{II'} > 0$. Furthermore, the sum rule (5.11) indicates that the elementarity Z is always negative. This is consistent with the fact that virtual states are the negative norm states with the negative residue. In this way, the compositeness of virtual states can be calculated from the expression of X. However, we note that $X > 1$ and $Z < 0$ cannot be interpreted as probability, and the internal structure of virtual states is not discussed straightforwardly by the compositeness.

For unstable resonances, we can define compositeness and elementality using the Gamow vector $\langle\tilde{R}|$ instead of the usual eigenvector $\langle R|$. In this case, the compositeness and elementality are defined as complex:

$$X = \int d\boldsymbol{p}\ \langle\tilde{R}|\boldsymbol{p}\rangle\langle\boldsymbol{p}|R\rangle = \int d\boldsymbol{p}\ \chi(\boldsymbol{p})^2 \in \mathbb{C}, \tag{5.88}$$

$$Z = \langle\tilde{R}|\phi\rangle\langle\phi|R\rangle = c^2 \in \mathbb{C}. \tag{5.89}$$

This is because X and Z of resonances are obtained from the square of complex values $\chi(\boldsymbol{p})$ and c, not from the absolute square of those. This property can also be seen in Eqs. (5.14) and (5.15), because the expectation values with Gamow vector become complex as shown in Sec. 2.5. The expressions of the compositeness in Section 5.3 are also modified by replacing the normal eigenvector $|R\rangle$ with the Gamow vector $|\tilde{R}\rangle$ and the binding energy $-B$ with the complex eigenenergy E_R. Even for resonances, the sum rule is not modified, namely, $X + Z = 1$ holds for complex X and Z. On the other hand, the definitions (5.88) and (5.89) show that the compositeness X and elementality Z of resonances do not satisfy the condition for probability (i). Therefore, the internal structure of resonances cannot be

Table 5.1: The summary of the compositeness X and elementarity Z for bound states, virtual states, and resonances.

States	$X,\ Z$	Probabilistic interpretation
Bound states	$0 \leq X \leq 1,\ 0 \leq Z \leq 1$	Yes
Virtual states	$1 < X,\ Z < 0$	No
Resonances	$X, Z \in \mathbb{C}$	No

probabilistically analyzed by the compositeness, different from the bound state case. However, since exotic hadrons appear as unstable resonances, we need to propose a prescription for a probabilistic interpretation of complex X and Z for the application to the exotic hadrons. We will discuss this topic in Section 5.7.

Finally, we summarize the nature of the compositeness of bound states, virtual states, and resonances in Table 5.1 The compositeness X and elementarity Z are regarded as probabilities only for bound states, and X and Z of virtual states and resonances do not satisfy the conditions for a probability.

5.7 The probabilistic interpretation of complex compositeness

To apply the notion of the compositeness not only to bound states but also to resonances, the probabilistic interpretation of the complex compositeness has been studied. In this section, we review several prescriptions of the probabilistic interpretation of the complex compositeness of unstable resonances in Sections 5.7.1, 5.7.2, and 5.7.3. Finally, in Section 5.7.4, we propose a new interpretation scheme by considering the unstable nature of resonances.

5.7.1 Taking absolute value or real part of X

To extract some probabilistic information about the molecular component from the complex compositeness, it is necessary to define some real quantities based on the compositeness. One of the simplest proposals is taking the absolute value $|X|$ or real part Re X of the compositeness X. In Refs. [159, 17, 160, 150], the authors consider that the absolute value of the complex X is associated with the molecular component of the resonance wavefunction. The real part of the complex X is regarded as the weight of the molecular component of the resonance [112]. However, we note that $|X|$ and Re X can be negative or larger than unity, and such values cannot be regarded as a probability. Therefore, we should take care of the applicability of these schemes.

5.7.2 Using weak-binding relation

For near-threshold states, the compositeness can be estimated by the weak-binding relation, as discussed above. Based on the weak-binding relation, there are some proposals to obtain the probabilistic compositeness of resonances. Reference [161] suggests that the compositeness is calculated as a prob-

abilistic quantity not only for bound states but also resonances by using the following relation:

$$\bar{X} = \sqrt{\frac{1}{\left|1 - \frac{2r_e}{a_0}\right|}}, \tag{5.90}$$

where a_0 is the scattering length and r_e is the effective range. In the later work [138], $\bar{X}_A$ is proposed by imposing the smoothness assumptions with which the compositeness becomes $0 \leq \bar{X}_A \leq 1$ in all momentum region:

$$\bar{X}_A = \sqrt{\frac{1}{1 + \left|\frac{2r_e}{a_0}\right|}}. \tag{5.91}$$

Using $\bar{X}_A$, we can obtain the probabilistic compositeness also for virtual states while $\bar{X}$ provides the negative value as the compositeness of virtual states.

5.7.3 Defining new quantity

As another approach, we can also define a new probabilistic measure from complex compositeness X. Some interpretation schemes are proposed inspired by Ref. [162] where the probabilistic interpretation of the expectation value of resonances is discussed. For example, in Refs. [93, 94], the probabilities $\tilde{X}_{\rm KH}$ and $\tilde{Z}_{\rm KH}$ are defined from the absolute values of X and Z as

$$\tilde{X}_{\rm KH} = \frac{1 - |Z| + |X|}{2}, \tag{5.92}$$

$$\tilde{Z}_{\rm KH} = \frac{1 - |X| + |Z|}{2}, \tag{5.93}$$

with the quantity U:

$$U = |Z| + |X| - 1. \tag{5.94}$$

We can clearly confirm that $\tilde{X}_{\rm KH}$ and $\tilde{Z}_{\rm KH}$ satisfy the conditions for probability: $0 \leq \tilde{X}_{\rm KH}, \tilde{Z}_{\rm KH} \leq 1$, and $\tilde{X}_{\rm KH} + \tilde{Z}_{\rm KH} = 1$. In this scheme, U is defined as the measure of uncertainty of the interpretation which characterizes the reasonability of the interpretation of the internal structure of resonances. If the decay width is large, the nature of resonance is expected to be apart from that of a resonance with narrow width (the narrow resonance), because the pole exists very far from the physical scattering region Re $E > 0$. For resonances with broad decay width (the broad resonances), Im X and Im $Z = -$ Im X are expected to be large. In this case, U becomes large [94], and the interpretation of the internal structure of resonances is regarded to have a large uncertainty. As a criterion for the interpretation, the authors propose that the state with $U > 1$ is considered not to be worth interpreting with X.

For coupled channels, the probability $\tilde{X}$ is proposed using the compositeness of each channels X_j as [163]

$$\tilde{X}_j = \frac{|X_j|}{1 + U}, \tag{5.95}$$

$$\tilde{Z} = \frac{|Z|}{1 + U}, \tag{5.96}$$

with

$$U = \sum_{1 \leq j \leq N} |X_j| + |Z| - 1. \tag{5.97}$$

We use $\tilde{X}_j$ to discuss the compositeness in the multi-channel system in Chapter 6.

5.7.4 $\mathcal{X}, \mathcal{Y}, \mathcal{Z}$

In the interpretation scheme in Section 5.7.3, the degree of the uncertain identification U is defined to distinguish the broad resonance from narrow resonances by focusing on the relation between the decay width and the imaginary part of the compositeness. However, in the previous works, the criterion for U is not based on the physical consideration. Here let us propose another scheme by introducing the physical-based criterion for the states with large uncertain identification [96, 164]. In this scheme, we define the probability of the uncertain identification $\mathcal{Y}$ as an equivalently essential quantity to the compositeness $\mathcal{X}$ and elementarity $\mathcal{Z}$:

$$\mathcal{X} = \frac{(\alpha - 1)|X| - \alpha|Z| + \alpha}{2\alpha - 1}, \tag{5.98}$$

$$\mathcal{Y} = \frac{|X| + |Z| - 1}{2\alpha - 1}, \tag{5.99}$$

$$\mathcal{Z} = \frac{(\alpha - 1)|Z| - \alpha|X| + \alpha}{2\alpha - 1}. \tag{5.100}$$

Here α is an arbitrary real parameter with $\alpha \leq 1/2$. The new quantity $\mathcal{Y}$ reflects the ambiguities arising from the identification of the resonance. This is a significant difference from other prescriptions shown above where all resonance is characterized only by compositeness and elementarity. From the definition of $\mathcal{Y}$ (5.99), the broad resonances with a large magnitude of Im X have large $\mathcal{Y}$. As shown below, based on the large $\mathcal{Y}$, we determine the criterion for the broad resonances whose internal structure is not worth interpreting with compositeness.

Here we explain the foundation of the idea of $\mathcal{X}, \mathcal{Y}, \mathcal{Z}$. Let us consider observing an eigenstate in an experiment. For the bound state case, there arise no ambiguities to distinguish a bound state contribution from other spectra in the experimental data Fig 5.2 (a)]. This is because the bound state below the threshold is observed as a delta function, where any spectra of the continuum scattering backgrounds are not observed. In contrast, if we try to distinguish the resonance above the threshold from a background, the identification of the resonance spectra has some uncertainty arising from the following two factors [Fig. 5.2 (b)] [162];

- the finite decay width (the width of the resonance spectra) induces the ambiguity to identify the eigenenergy of the resonance; and
- the separation from the background is not unique, which depends on the framework of the analysis.

In this way, the identification of resonances is qualitatively different from that of bound states.

We apply this idea to the classification of the internal structure of resonances by focusing on the observation. We consider that the ambiguities also appear in the identification of the internal structure of resonances, in addition to observing the composite or elementary states. It is reasonable

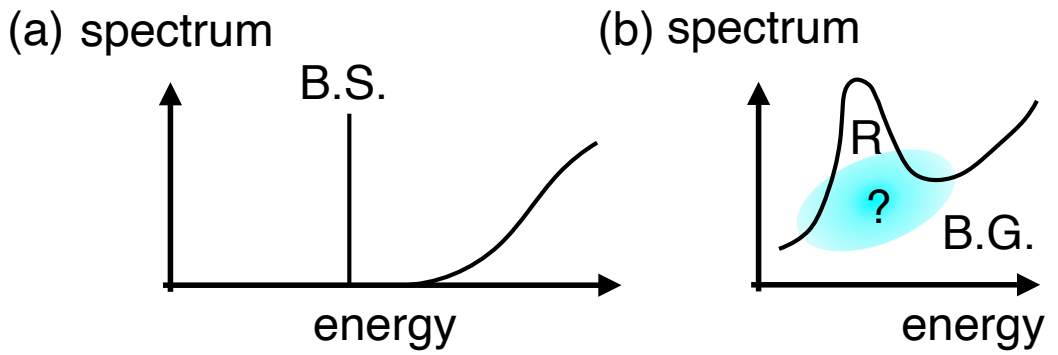

Figure 5.2: The schematic illustration of the experimental spectrum including a bound state [B.S. in panel (a)] and that including a resonance [R in panel (b)]. The spectra in the shaded region in panel (b) represent the ambiguity of resonance spectra, the finite decay width, and the separation from the background (B.G.) contribution.

to regard that the internal structure of bound states is uniquely identified in a single observation, whether composite or elementary. Therefore, after a sufficiently large number of observations, we can conclude that the internal structure of bound states is composite dominant or not. This is because the compositeness X and elementarity Z of bound states are defined as real and probabilistic quantities. On the other hand, X and Z of resonances are complex by definition. We consider that the complex X and Z reflect the ambiguity of the identification of the internal structure of resonances which is induced by the instability of resonances [96]. Based on this consideration, we assume that the internal structure of resonances is characterized by the following three quantities

$\mathcal{X}$: the probability to certainly finding the composite component;

$\mathcal{Z}$: the probability to certainly finding the elementary component; and

$\mathcal{Y}$: the probability of uncertain identification.

In this case, the internal structure of resonances is regarded as the dominant component among $\mathcal{X}$, $\mathcal{Y}$, and $\mathcal{Z}$, as composite dominant, elementary dominant, and uncertain to identify. The large uncertain identification $\mathcal{Y}$ corresponds to the situation that the internal structure cannot be identified whether composite or not, because of a large ambiguity of broad resonances.

To be a natural extension of the compositeness of bound states, $\mathcal{X}, \mathcal{Y}, \mathcal{Z}$ are defined to satisfy that

- normalized as $\mathcal{X} + \mathcal{Y} + \mathcal{Z} = 1$; and
- $\mathcal{X} \to X$, $\mathcal{Z} \to Z$, and $\mathcal{Y} \to 0$ in the bound state limit where the limit where the decay width goes to zero,

In the second condition, $\mathcal{Y}$ should be zero for stable bound states because it characterizes the uncertain nature of resonances. In addition to these conditions, for a probabilistic interpretation, $\mathcal{X}$, $\mathcal{Y}$, and $\mathcal{Z}$ should also be positive and smaller than unity. Because $\alpha > 1/2$, we see $\mathcal{Y}$ (5.99) is always positive from the triangle inequality. However, $\mathcal{X}$ (5.98) and $\mathcal{Z}$ (5.100) can be negative even if $\alpha > 1/2$. In this prescription, we regard that such a state with negative $\mathcal{X}$ or $\mathcal{Z}$ has a non-interpretable structure

with the compositeness. Adopting the category "non-interpretable", we propose the classification of the internal structure of resonances as follows;

- composite dominant, if $\mathcal{X} > 0$, $\mathcal{Z} > 0$, and $\mathcal{X}$ is largest;
- elementary dominant, if $\mathcal{X} > 0$, $\mathcal{Z} > 0$, and $\mathcal{Z}$ is largest;
- uncertain whether composite or elementary, if $\mathcal{X} > 0$, $\mathcal{Z} > 0$, and $\mathcal{Y}$ is largest; and
- non-interpretable with the compositeness, if $\mathcal{X} < 0$ or $\mathcal{Z} < 0$.

In this prescription, the internal structure of resonances is at first classified into interpretable or non-interpretable. Then the interpretable states are categorized into composite dominant, elementary dominant, or uncertain (Fig. 5.3). In summary, the internal structure of resonances can be classified into not only composite or elementary dominant but also uncertain or non-interpretable, which are newly introduced based on the ambiguities of resonances. We note that the category "non-interpretable" is not considered in the previous works in Section 5.7.3 where the internal structure of all resonances is interpreted by the compositeness.

We note that $\mathcal{Y}$ does not have an upper limit and can be larger than unity, while the lower limit is determined as $\mathcal{Y} \geq 0$. If $\mathcal{Y}$ is much large, $\mathcal{X}$ or $\mathcal{Z}$ can be negative because of the sum rule $\mathcal{X}+\mathcal{Y}+\mathcal{Z} = 1$, and the state is regarded as non-interpretable. For example, either $\mathcal{X}$ or $\mathcal{Z}$ must be negative if $\mathcal{Y} > 1$. As discussed above, the broad resonances are considered to have large Im X, and therefore have large $\mathcal{Y}$. In this sense, broad resonances are expected to be automatically distinguished from narrow resonances as a non-interpretable state. By determining the value of α in the next paragraph, we will show this expectation holds.

From Eqs. (5.98), (5.99), and (5.100), $\mathcal{X}, \mathcal{Y}, \mathcal{Z}$ have not only on the eigenenergy dependence through X and Z, but also on the parameter α dependence. This indicates that the classification of the resonance also depends on the value of α. In principle, the choice of α is arbitrary within the region $\alpha > 1/2$. Here we discuss a reasonable value of α based on the physical consideration. For this purpose, we first see the α dependence of the region where the state is interpretable with positive $\mathcal{X}$ and $\mathcal{Z}$ in the complex X plane. If we set $\alpha = 1/2$, the interpretable region is restricted only within real and $0 \leq X \leq 1$. Because the states with X in this region correspond to the bound state, this setup claims that only bound states are meaningful to interpret with the compositeness. In contrast, in the $\alpha \to \infty$ limit, $\mathcal{X}, \mathcal{Y}, \mathcal{Z}$ reduce to the interpretation scheme in the previous work [94]: $\mathcal{X} \to \tilde{X}_{\rm KH}$, $\mathcal{Z} \to \tilde{Z}_{\rm KH}$, and $\mathcal{Y} \to 0$ as seen in Eqs. (5.98), (5.99), and (5.100). In other words, this corresponds to the scheme where all resonances are interpretable with the compositeness.

The limits of α discussed above correspond to excessive cases, and it is not suitable for practical discussion. As a reasonable value of α, let us choose α by relating the non-interpretable states with the broad resonances. Specifically, we determine the value of α with which the broad resonances are classified into the non-interpretable state. As the criterion of the broad resonance, we adopt

$$\text{Re } E < \Gamma \quad \Leftrightarrow \quad \text{Re } E < -2\,\text{Im } E, \tag{5.101}$$

where Γ is the decay width. Based on this criterion, we regard the state satisfying Eq. (5.101) as the broad resonance. By using the weak-binding relation in the zero-range limit (6.5), the corresponding value of α is obtained as [96]

$$\alpha = \frac{\sqrt{5} - 1 + \sqrt{10 - 4\sqrt{5}}}{2} \approx 1.1318. \tag{5.102}$$

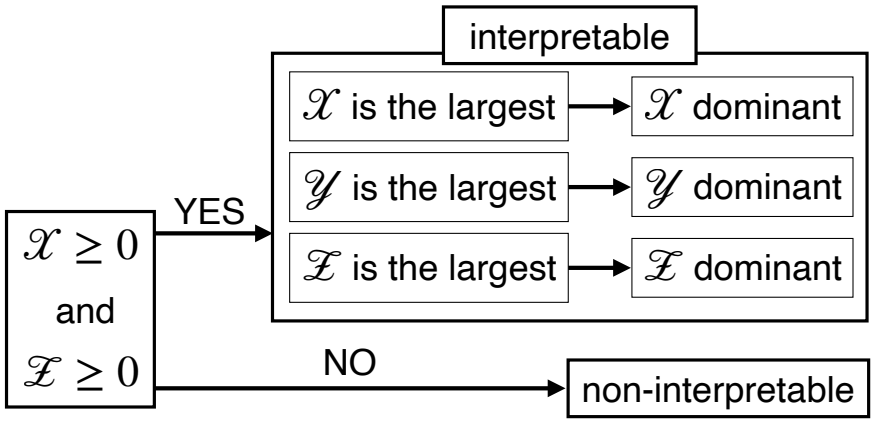

Figure 5.3: The classification of the internal structure of resonances using $\mathcal{X}, \mathcal{Y}, \mathcal{Z}$.

We use this criterion in Chapter 6 to obtain the compositeness of $T_{cc}(3875)^+$ and $X(3872)$.

5.8 Applications of compositeness

In this section, we introduce some applications of the compositeness to various states. We first focus on the application to the quark-model exotics in hadron physics, to baryons in Section 5.8.1 and mesons in Section 5.8.2. We then see the application of the compositeness of the quantum-number exotic and quarkonium-associated exotic hadrons in Section 5.8.3. We also show the compositeness applies to the lattice QCD prediction (Section 5.8.4), the nuclei, and atoms (Section 5.8.5). Here we denote the compositeness of the AB molecular component as X_{AB}.

5.8.1 Application to baryons

deuteron

Let us start with the deuteron as the first applied hadron. Actually, before Weinberg's work, the internal structure of the deuteron was discussed in section 5 in Ref. [146]. However, it is innovative that Weinberg's consideration is based only on three observables, the binding energy, scattering length, and effective range. Since the development of the weak-binding relation, the compositeness of the deuteron has been discussed multiple times. We align the representative works on the compositeness of the deuteron;

- $Z \sim 0$ (the pioneering work of the weak-binding relation) [72];
- $X = 1.68^{+2.15}_{-0.83}$, using the weak-binding relation (5.67) [165];
- $\bar{X}_A = 0.8$, using the extended weak-binding relation (5.91) [138].

The compositeness of the deuteron is considered particularly with consideration of the range correction;

- $X \geq 0.62$ even with a much smaller cutoff [100];
- $X \sim 1$, namely, mostly a pn molecule [156];

- $X \gtrsim 0.7$ is very plausible [157]
- $0.74 \leq X \leq 1$ [95].

In addition to the deuteron in the pn scattering, the virtual state in the nn scattering is also studied using the compositeness in Ref. [157].

N and Δ resonances

Not only the deuteron but also excited N and Δ baryons are investigated using the compositeness [166, 163]. In Ref. [166], the authors calculate the compositeness from the residue and loop function. In Refs. [163], the compositeness of various exotic hadrons is studied using $\tilde{X}$ (5.95). In these studies, the compositeness of N and Δ is calculated as follows.

- $N(1535)$: the non-molecular dominant with $Z = 0.70 - 0.09i$ Ref. [166] and $\tilde{Z} = 0.62$ [163]
- $N(1650)$: the elementarity dominant with $\tilde{Z} = 0.74$ [163].
- $\Delta(1232)$: the πN molecule-dominant with $\tilde{X} = 0.61$ - 0.71 [163];

Λ, Σ, and Ξ resonances

As an application to the exotic hadrons in the strange sector with s quarks, we first focus on $\Lambda(1405)$. There are a lot of approaches to studying the structure of $\Lambda(1405)$, from the viewpoint of the finite-volume effect [167], with the generalized weak-binding relation [93, 94], using the idea of the rank one projection operator [160], and with a unitarized meson-baryon model [168]. The results of these are summarized as follows;

- $X_{\bar{K}N} = 0.99 + 0.05i$ (see Table II in the paper). With the finite volume effect, $X_{\bar{K}N,\mathrm{FV}} = 0.82$ - 1.03 [167];
- $\tilde{X}_{\mathrm{KH}} = 0.6$ - 1.0 [93, 94] (see Table I in Ref. [93] and Table 2, 3, and 4 in Ref. [94]);
- the total compositeness is $X = 0.73^{+0.15}_{-0.10}$.

As a representative study of other strange baryons, a comprehensive examination of the structure of excited decuplet heavy baryons is performed in Ref. [112]. We present some results as follows;

- $\Lambda(1380)$: the total compositeness is $X = 0.14 + 0.40i$ (see Table III in the paper) [167], $X = 0.23 + 0.46i$ [166], and $X = 1.00^{+0.49}_{-0.25}$ [160];
- $\Lambda(1520)$: elementary dominant with the small total compositeness (e.g., $X = 0.21$, see Table III in the paper) [169];
- $\Lambda(1670)$: the total compositeness is $X = 0.47 + 0.06i$ [166];
- $\Sigma(1385)$: $X_{\pi\Lambda} = 0.13$ - 0.24 (depending on the cutoff) [112];
- $\Xi(1535)$: $X_{\pi\Xi} = 0.09$ - 0.15 (depending on the cutoff) [112];
- $\Xi(1690)$: $\bar{K}\Sigma$ molecule-dominant with $X_{\bar{K}\Sigma^-} = 0.86 - 0.50i$ using the coupled-channel unitary approach [170].

- Ω^-: $X_{\bar{K}\Xi} = 0.18$ - 0.53, and $X_{\pi\Sigma} = 0.09$ - 0.12 (depending on the cutoff) [112].

Also for the baryons in the heavy sector, the compositeness is applied mainly to Λ_c baryons. For example, in Ref. [161], the internal structure of the near-threshold s-wave resonance is studied using the effective range expansion, and the framework is applied to $\Lambda_c(2595)$. The compositeness of $\Lambda_c(2595)$ is also studied in Ref. [171] with the SU(6) $\times$ HQSS model. In Ref. [172], the compositeness of $\Lambda_c(2595)$ is calculated based on the result of the pole analysis. In the following, we summarize the compositeness of $\Lambda_c(2595)$;

- not likely a $\pi\Lambda_c$ molecule [161];
- total compositeness is $X = 0.11^{+0.02}_{-0.02}$ [160];
- not a composite dominant with small total compositeness (see Table IV in the paper for more quantitative results) [168];
- $X = 0.14 \pm 0.02$ - 0.17 ± 0.04 for single-channel analysis, and $X = 0.11 \pm 0.02$ - 0.04 ± 0.01 for coupled-channel analysis (depending on the setup) [172];
- they consider $\pi\Sigma_c$ molecular component, and obtain $X_{\pi\Sigma_c} = -0.024 + 0.107i$. For more results with other setups, see table II in Ref. [171].

In addition to $\Lambda_c(2595)$, the compositeness of other Λ_c baryons are considered. In Ref. [168], the compositeness of $\Lambda_c(2625)$ is computed as $X_{\pi\Sigma_c^*} = 0.268$. Other-channel compositeness is shown in Table IV in that paper. Furthermore, Λ_b baryon in the bottom sector is also discussed. In Ref. [168], the authors show the compositeness of $\Lambda_b(5912)$ and $\Lambda_b(5920)$ as $X_{\bar{B}^* N} = 0.539$ and $X_{\pi\Sigma_b^*} = 0.581$, respectively. The compositeness of other components is shown in Table V in that paper.

5.8.2 Application to mesons

Light mesons

From now on, let us present the various studies of the compositeness of exotic mesons. For light mesons, $f_0(980)$ and $a_0(980)$ are actively studied. For example, in Ref. [140], the compositeness of $f_0(980)$ and $a_0(980)$ is calculated with the extended weak-binding relation which is developed based on the spectrum function. In Ref. [173], the $K\bar{K}$ compositeness of $f_0(980)$ and $a_0(980)$ are investigated from the consideration of the $a_0(980)$-$f_0(980)$ mixing density. We first summarize the compositeness of $f_0(980)$;

- $X \gtrsim 0.8$ [140]
- $X_{\pi\pi} = 0.01 + 0.01i$, $X_{K\bar{K}} = 0.74 - 0.11i$. With the finite volume effect, $X_{K\bar{K},\mathrm{FV}} = 0.73$ - 0.97 [167];
- $X_{K\bar{K}} = 0.87 - 0.04i$, $X_{\eta\eta} = 0.06 + 0.01i$ [166];
- $X_{K^+K^-} = 0.35 - 0.05i$, $X_{K^0\bar{K}^0} = 0.35 - 0.05i$, $X_{\pi^+\pi^-} = 0.01 + 0.01i$, and $X_{\pi^0\pi^0} = 0.01 + 0.00i$ [173];
- the compositeness is small $\tilde{X}_{\mathrm{KH}} = 0.3$ - 0.9 (depending on the dataset) [93, 94];

- total compositeness $X = 0.67^{+0.28}_{-0.27}$ [160].

The compositeness of $a_0(980)$ is computed as

- $X = 0.5$ - 0.75 [140];
- the compositeness is small $\tilde{X}_{\rm KH} = 0.1$ - 0.3 for most of all dataset [93, 94];
- $X_{K^+K^-} = 0.17 - 0.15i$, $X_{K^0\bar{K}^0} = 0.17 - 0.15i$, and $X_{\pi^0\eta} = -0.07 + 0.12i$ [173].

Other light mesons, such as $\rho(770)$, $a_0(1450)$, $a_1(1260)$, σ meson (also as known as $f_0(500)$), $f_0(1710)$ are also studied. In Ref. [174], the mixture of the quark and hadronic component in $a_1(1260)$ structure is discussed. We summarize the compositeness of these mesons as follows;

- $\rho(770)$: $X_{\pi\pi} = -0.08 + 0.03i$, and $X_{K\bar{K}} = -0.02 + 0.00i$ [166];
- $\rho(770)$: total compositeness $X = 0.08^{+0.01}_{-0.01}$ [160];
- $a_0(1450)$: total compositeness $X = 0.23^{+0.37}_{-0.18}$ [160];
- $a_1(1260)$: total compositeness $X = 0.46$ [160];
- $a_1(1260)$: $a_{1(1260)}$ has comparable amounts of the elementary component to the $\pi\rho$ composite component [174];
- $\sigma = f_0(500)$: $X_{\pi\pi} = -0.09 + 0.37i$, and $X_{K\bar{K}} = -0.01 - 0.00i$ [166];
- $\sigma = f_0(500)$: total compositeness $X = 0.40^{+0.02}_{-0.02}$ [160];
- $f_0(1710)$: total compositeness $X = 0.25^{+0.10}_{-0.10}$ [160].

Strange mesons

In the strange sector, there are some applications of the compositeness to the excited K mesons (K^*). In Ref. [175], the internal structure of K^* mesons is discussed as the state appearing with p-wave in the πK scatterings. We summarize the studies on strange mesons;

- K^*: $|X| = 0.158$ - 0.192 (depending on the cutoff) [175];
- $K_0^*(800) = \kappa$: $X_{\pi K} = 0.32 + 0.36i$ and $X_{\eta K} = -0.01 - 0.00i$ [166];
- $K_0^*(800) = \kappa$: total compositeness $X = 0.94^{+0.39}_{-0.52}$ [160];
- $K^*(892)$: $X_{\pi K} = -0.03 + 0.04i$ and $X_{\eta K} = -0.03 + 0.00i$ [166];
- $K^*(892)$: total compositeness $X = 0.05^{+0.01}_{-0.01}$ [160].

Charmed mesons

In the charm sector, the compositeness is often applied to $X(3872)$. In Ref [155], the authors calculate the compositeness of $X(3872)$ using Eq. (5.91). The compositeness of $X(3872)$ is studied from the analysis of the experimental line shape [176, 177]. We summarize the compositeness of $X(3872)$ as follows;

- $\bar{X}_A \gtrsim 0.9$ [155]
- $Z = 0.19 \pm 0.29$ [176]
- $0.86 < X < 0.948$ [177]
- $0.53 \leq X \leq 1$ [95]

The compositeness of $X(3872)$ is also studied in this thesis, in Chapter 6. Also in Ref. [160], the internal structure of $Y(4260)$ is considered as the non-composite state with the total compositeness $X = 0.21$.

Strange and charmed mesons

The compositeness is also applied to the mesons including both s and c quarks, called D_s mesons. For example, in Ref. [178], the compositeness of $D^*_{s0}(2317)$ and $D^*_{s1}(2460)$ is considered using the result of the lattice QCD. In Ref. [179], the compositeness of $D^*_{s0}(2317)$ is calculated using the chiral unitarity model. We summarize the compositeness of $D^*_{s0}(2317)$;

- $X_{KD} = 72 \pm 13 \pm 5$ % [178];
- $X_{DK} = 0.69$ and $X_{D_s\eta} = 0.09$ [179];
- total compositeness $X = 0.70^{+0.07}_{-0.05}$ [160];
- $X_{KD} \geq 0.6$ [156];
- $X_{KD} \geq 0.5$ [157];
- $0.81 \leq X \leq 1$ [95].

The compositeness of $D^*_{s1}(2460)$ is also calculated as

- $X_{KD^*} = 57 \pm 21 \pm 6$ % [178]
- $0.4 < X_{KD^*} < 0.7$ [156];
- $0.55 \leq X \leq 1$ [95].

5.8.3 Application to the quantum-number and quarkonium-associated exotic hadrons

In the previous subsection, we show the applications for quark-model exotic hadrons, including the candidates of exotic hadrons. In addition to these, the compositeness is used to analyze the internal structure of quantum-number exotic hadrons and the quarkonium-associated exotic hadrons. For example, the compositeness of $T_{cc}(3875)^+$ is calculated with Eq. (5.91) [155, 64], using the weak-binding relation with the range correction [157], from the residue of the pole [64];

- the compositeness is for exmaple obtained as $\bar{X}_A = 0.87^{\pm 0.01}_{\pm 0.07}$. It depends on the scheme, and the quantitative result is almost the same among the schemes [155];
- it is consistent with the molecular picture [157];
- for example, $X_{D^0 D^{*+}} = 0.71^{\pm 0.01}_{\pm 0.02}$, $X_{D^+ D^{*0}} = 0.29^{\pm 0.01}_{\pm 0.02}$ using the residue of the pole (also depending on the scheme) [155].

We also consider the compositeness of the quantum-number exotic hadron, $T_{cc}(3875)^+$ using the EFT model in the later Chapter.

5.8.4 Application to lattice QCD results

The compositeness is applied not only to the experimentally observed states but also to the states predicted by the lattice QCD simulation. For example, the internal structure of $N\Omega$ and $\Omega\Omega$ dibaryons is considered using the weak-binding relation [95];

- $N\Omega$ dibaryon: $0.80 \leq X_{N\Omega} \leq 1$;
- $\Omega\Omega$ dibaryon: $0.79 \leq X_{\Omega\Omega} \leq 1$.

These results suggest that the bound states of $N\Omega$ and $\Omega\Omega$ are suitable to the dybaryon picture.

5.8.5 Application to nuclei and atoms

Because the notion of the compositeness is universal, the compositeness is also applicable to nuclei and atomic systems. In Ref. [95], the compositeness of the hypertriton ${}^3_\Lambda$H and ^{4}He dimer are estimated by the weak-binding relation;

- ${}^3_\Lambda$H: $0.74 \leq X_{d\Lambda} \leq 1$;
- ^{4}He dimer: $0.93 \leq X \leq 1$.

These results show that they are composite dominant. In particular, the result of ^{4}He dimer agrees with the dimer picture from the ab initio calculation. This analysis serves as a demonstration of the validity of the weak-binding relation. Furthermore, the essentially same concept to elementarity Z is discussed to consider the atomic systems [180, 181] and the polaron-molecule [182].

Chapter 6

Structure of near-threshold bound states

In this chapter, we discuss the internal structure of the near-threshold bound states using the compositeness. In Section 6.1, we show that the compositeness is unity in the exact weak-binding limit and discuss the threshold rule for the states with small but finite binding energy. Based on the expectation from the empirical threshold rule, the near-threshold bound states are considered to be composite dominant. In Section 6.2, we establish the theoretical foundation of the threshold rule using the single-channel resonance model introduced in Section 4.1. In anticipation of applications to exotic hadrons, we study the nature of near-threshold states in the presence of the decay width (Section 6.3) and channel couplings (Section 6.4) using the models in Section 4.2. Finally, we apply the present framework to analyze the internal structure of $T_{cc}(3875)^+$ and $X(3872)$ by examining the decay and coupled-channel effects in Section 6.5.

6.1 Low-energy universality and threshold rule

In this section, we discuss the qualitative nature of near-threshold bound states from the viewpoint of the low-energy universality. We first introduce general concepts of the low-energy universality in Section 6.1.1. Then we discuss the compositeness of shallow bound states relation with the threshold rule in Section 6.1.2.

6.1.1 Low-energy universality

Here we examine the consequence of the low-energy universality using the effective range expansion (ERE) (2.65). In the near-threshold energy region with a sufficiently small momentum p, the scattering amplitude $f(p)$ is governed by the scattering length a_0, by neglecting the higher order terms in the ERE:

$$f(p) \sim \frac{1}{-\frac{1}{a_0} - ip}. \tag{6.1}$$

Let us assume that the system has a shallow bound state. From the bound state condition $1/f(p) = 0$ with the near-threshold scattering amplitude (6.1), the eigenmomentum of the shallow bound state is

written as

$$p \sim \frac{i}{a_0}. \tag{6.2}$$

The binding energy B can also be estimated by the scattering length a_0:

$$B = -\frac{p^2}{2\mu} \sim \frac{1}{2\mu a_0^2}. \tag{6.3}$$

This equation indicates that the scattering length a_0 diverges when the bound state exists exactly at the threshold $B = 0$, as mentioned in the introduction. In the same way, near the threshold energy region, all the quantities are scaled only by a_0. This observation leads to the low-energy universality: the near-threshold phenomena is universally described by the theory characterized solely by the scattering length as the relevant scale (the zero-range theory) [77, 104, 80].

6.1.2 Compositeness theorem and threshold rule

Based on the low-energy universality, let us discuss the compositeness of shallow bound states. It is shown in Eqs. (5.43) and (5.44) that the compositeness X and the elementarity Z are expressed by the energy derivative of the self energy $\Sigma(E)$. In the $E \to 0$ limit, $\Sigma(E)$ is proportional to $\sqrt{E}$ as $G^0(E)$ is, and therefore, $\Sigma'(E)$ diverges for $E \to 0$. Namely, we obtain

$$X = 1, \quad Z = 0 \quad (B \to 0) \tag{6.4}$$

Thus, the compositeness is unity when the state exists exactly at the threshold ($B \to 0$) [161, 91, 92]. Therefore, a hadron at the threshold always has a pure hadronic molecular structure. This fact is called the compositeness theorem. We emphasize that this is a model-independent consequence of the low-energy universality.

The result of the compositeness theorem can be confirmed by the weak-binding relation (5.67). As discussed in Section 4.1.5, taking the zero-range limit ($R_{\rm int} \to 0$) corresponds to considering the low-energy limit of the scattering amplitude which is capable of describing the shallow bound state. Thus, the compositeness X of the shallow bound state is estimated by the weak-binding relation in the zero-range limit:

$$a_0 \sim R\frac{2X}{1+X}, \quad R = \frac{1}{\sqrt{2\mu B}}. \tag{6.5}$$

By substituting the result of the compositeness theorem, $X = 1$, we obtain $a_0 \sim R$. This is equivalent to Eq. (6.3) obtained from the low-energy universality.

The $B \to 0$ limit is an idealization, and physical bound states have a small but finite binding energy $B \neq 0$. Naively, shallow bound states are expected to be composite dominant with $X \sim 1$. This expectation aligns with the empirical fact that the near-threshold states are observed as molecule-dominant states, the threshold rule (see Section 1.3). However, strictly speaking, the composite theorem is shown only at the threshold $B = 0$. Therefore, the internal structure of shallow bound states ($B \neq 0$) is not theoretically well established. In fact, for finite binding energy $B \neq 0$, it is shown that non-composite shallow bound states can always be realized with a tuning of the parameters, even if B is small [91, 92]. In other words, by deliberately choosing the parameters, it is always possible to construct a model that does not follow the threshold rule. These facts indicate that the reason why the threshold rule holds is not theoretically clear. Given this background, we study the theoretical foundation of the threshold rule by focusing on the tunings of model parameters.

6.2 Threshold rule in single-channel systems

Here we numerically examine the realization of the threshold rule using the single-channel resonance model in Section 4.1. We first present the setup of the numerical calculation in Section 6.2.1. The results of the analysis of the compositeness are then shown in Section 6.2.2.

6.2.1 Set up

To clarify the theoretical basis of the threshold rule, we examine the model dependence of the compositeness through the comparison of typical and shallow bound states. Here we use the single-channel resonance model introduced in Section 4.1. By setting $\lambda_0 = 0$ for simplicity, this model has three parameters, the coupling constant g_0, bare state energy ν_0, and cutoff Λ (see Section IIIA of Ref.[93] for the effect of finite λ_0). In this case, eigenstates are described by the coupling of a bare state to a single free scattering state. The compositeness X is calculated from the effective interaction $V_{\rm eff}(E)$ (4.31) and loop function G^0 (4.36) using the formula (5.36):

$$X(B,\nu_0,\Lambda) = \left[1 + \frac{\pi^2\kappa}{g_0^2\mu^2}\left(\arctan\left(\frac{\Lambda}{\kappa}\right) - \frac{\frac{\Lambda}{\kappa}}{1+\left(\frac{\Lambda}{\kappa}\right)^2}\right)^{-1}\right]^{-1}, \tag{6.6}$$

with $\kappa = \sqrt{2\mu B}$. Here the ν_0 dependence arises from g_0^2 which is given by the bound state condition (4.42):

$$g_0^2(B;\nu_0,\Lambda) = \frac{\pi^2}{\mu}(B+\nu_0)\left[\Lambda - \kappa\arctan\left(\frac{\Lambda}{\kappa}\right)\right]^{-1}. \tag{6.7}$$

It can be analytically shown in Eq. (6.6) that, in the weak-binding limit $B \to 0$ (i.e., $\kappa \to 0$), the compositeness X becomes unity, in accordance with the compositeness theorem (6.4). However, with the finite binding energy $\kappa \neq 0$, the compositeness X depends on the model parameters, such as the bare energy ν_0 and the cutoff Λ. In fact, for $B \neq 0$, we find $X \to 0$ for $\nu_0 \to -B$ and $X \to 1$ for $\nu_0 \to \infty$. This indicates that the compositeness of bound states with $B \neq 0$ can be varied arbitrarily by adjusting the model parameters.

To set a reference for the energy scale, we define

$$E_{\rm typ} = \frac{\Lambda^2}{2\mu}. \tag{6.8}$$

This energy $E_{\rm typ}$ can be regarded as the typical energy scale in the EFT framework because the cutoff Λ represents the intrinsic momentum scale in the microscopic theory. Based on the argument of naturalness [183, 184, 185, 186], we expect that a typical bound state in this system has the binding energy of the order of $E_{\rm typ}$ if the system has a bound state. Because Λ is the upper limit of the EFT, we assume $B \leq E_{\rm typ}$ so that the bound state appears in the applicable region of the model.

In this work, we study the model dependence of the compositeness by considering two representative cases: a typical bound state with $B = E_{\rm typ}$, and a shallow bound state with $B = 0.01E_{\rm typ}$. In this model, there are three model parameters: the coupling constant g_0, bare state energy ν_0, and cutoff Λ. For a given binding energy B, one degree of freedom of the model parameters can be reduced by the bound state condition as shown in Eq. (6.7). Furthermore, we use the dimensionless quantities with the cutoff Λ so that the Λ dependence in the results is absorbed. For example, the dimensionless

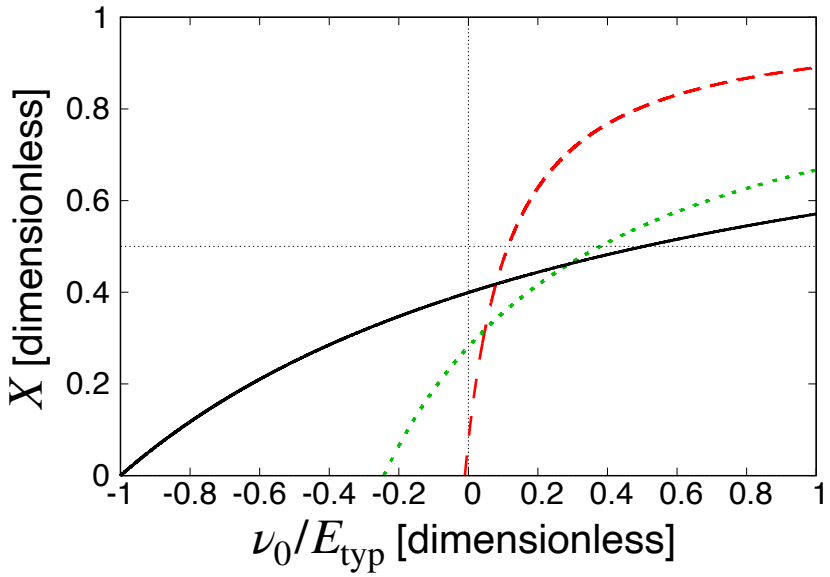

Figure 6.1: The compositeness X as a function of the bare state energy ν_0 in the parameter region (6.9). The solid line corresponds to X of the typical bound state $B = E_{\rm typ}$, the dashed line to the shallow bound state $B = 0.01E_{\rm typ}$, and the dotted line to the bound state with the critical binding energy $B = B_{\rm cr} = 0.243E_{\rm typ}$. This figure is adapted from Ref. [71].

binding energy $B/E_{\rm typ}$ is used instead of B. Because this procedure also reduces one more degree of freedom of the model parameters, the bare state energy ν_0 is the only remaining parameter in this setup. The determination of ν_0 requires the knowledge of the microscopic theory because it cannot be given within the framework of the EFT. For hadron systems, ν_0 may be calculated by the constituent quark model, where the bare state $|\phi\rangle$ corresponds to the multiquark state. In this work, we take a different approach; we vary ν_0 in the allowed region in the resonance model, and regard the ν_0 dependence as the model dependence of X (6.6). The allowed parameter region of ν_0 is given as

$$-\frac{B}{E_{\rm typ}} \leq \frac{\nu_0}{E_{\rm typ}} \leq 1. \tag{6.9}$$

The lower limit is determined to have the real coupling constant $g_0^2 > 0$ from Eq. (6.7). The upper limit $\nu_0/E_{\rm typ} = E_{\rm typ}/E_{\rm typ} = 1$ is given as the maximum energy scale in the EFT.

6.2.2 Structure of near-threshold bound states

We numerically calculate the compositeness X (6.6) by varying the bare state energy ν_0 within the model-allowed region (6.9). In Fig. 6.1, we plot the compositeness X of the typical bound state $B/E_{\rm typ} = 1$ (solid line) and shallow bound state $B/E_{\rm typ} = 0.01$ (dashed line). Note that the ν_0 regions are different in each plot of X since the lower limit of the region is determined by the binding energy (6.9).

At $\nu_0/E_{\rm typ} = -B/E_{\rm typ}$, the compositeness becomes zero for all cases. This can be analytically shown by substituting $g_0^2 = 0$ into Eq. (6.6), where g_0^2 becomes zero when $\nu_0 = -B$ in Eq. (6.7). When the couplings vanish $g_0 = 0$, the state becomes the pure elementary bare state whose compositeness is

exactly zero $X = 0$. When ν_0 increases, we find that X becomes larger. This is because the couplings g_0^2 of the bare state to the scattering state increase with ν_0 as shown in Eq. (6.7), and the scattering states contribute to enhancing the compositeness X. This heavier of the compositeness is discussed also in Refs. [187, 92]. We note that the degree of the increase of X depends on the binding energy, while the qualitative behavior of X is common among the bound states with different binding energies. In the following, we discuss the compositeness of typical, shallow, and critical bound states individually.

Typical bound state

We first focus on the typical bound state with $B = E_{\rm typ}$. In this case, the compositeness X is $X < 0.5$ for most parameter region $-1 \leq \nu_0/E_{\rm typ} \leq 1$. This means that, when we randomly choose the model to determine ν_0, it is usual to obtain the non-composite state for the typical binding energy. We can understand this result from the feature of the resonance model; the origin of the bound state is the bare state $|\phi\rangle$ which contributes to the elementary component.

Shallow bound state

In contrast to the typical bound case, the compositeness of the shallow bound state $B = 0.01E_{\rm typ}$ is larger than 0.5 in a large proportion of the $-0.01 \leq \nu_0/E_{\rm typ} \leq 1$ region. This shows that the shallow bound state is usually composite dominant while a bound state in this model is constructed from the pure elementary bare state with $X = 0$. However, at the same time, we also find that the elementary dominant state ($X < 0.5$) is realized if we tune the value of ν_0 within the small parameter region. This is the demonstration of the results in Refs. [91, 92].

Let us further consider the fine tuning of the parameter from the viewpoint of naturalness. As discussed above, if the system has a bound state, it is usual to obtain the order of the typical energy scale as the binding energy $B \sim E_{\rm typ}$. On the other hand, to obtain a shallow bound state, we have to tune the binding energy so that $B \ll E_{\rm typ}$. In addition, we need one more fine-tuning of ν_0 discussed above to obtain the shallow non-composite bound state. This situation corresponds to double fine tuning, which is very unlikely from the viewpoint of naturalness. In Ref. [188], the same feature of the shallow bound state is observed using the dynamical quark model.

Bound state with critical binding energy

We search for the critical binding energy $B_{\rm cr}$ with which the fraction of the model parameter region of $X < 0.5$ and $X > 0.5$ becomes half and half. The critical binding energy is numerically found to be $B_{\rm cr} = 0.243E_{\rm typ}$. The behavior of X with $B = B_{\rm cr}$ is shown in Fig. 6.1 by the dotted line. The definition of $B_{\rm cr}$ indicates that the fraction of the ν_0 region of the composite dominant state is larger (smaller) if $B < B_{\rm cr}$ ($B > B_{\rm cr}$). In other words, the exception of the threshold rule becomes less and less frequent when the binding energy decreases from $B_{\rm cr}$. This suggests that $B_{\rm cr}$ can become a criterion of the applicability of the threshold rule. We note that the value of $B_{\rm cr}$ depends on the model because the result of the compositeness X (6.6) is affected, for instance, by the choice of the Hamiltonian (the effective interaction) and that of the regularization (the loop function).

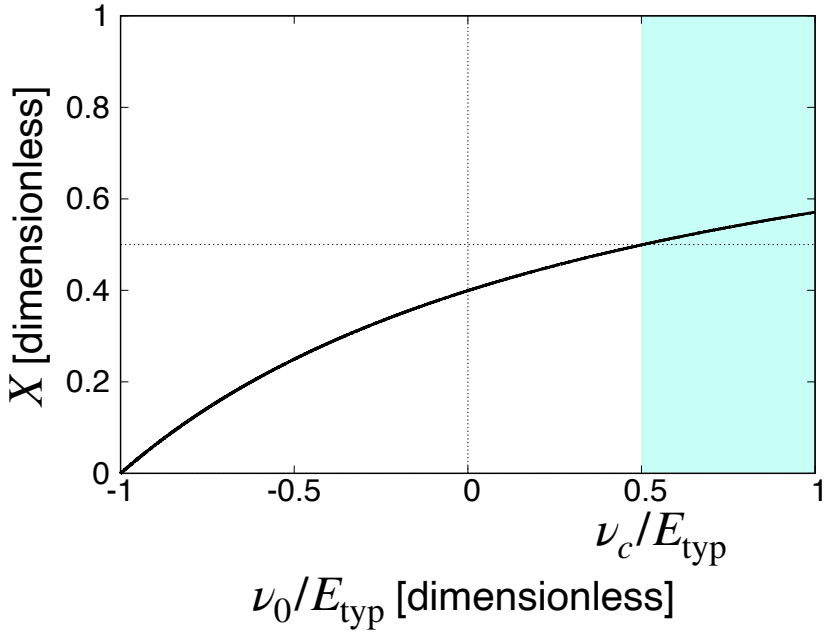

Figure 6.2: The schematic figure of the definition of $P_{\rm comp}$ in the $B = E_{\rm typ}$ case. $P_{\rm comp}$ corresponds to the fraction of the shaded region $\nu_c/E_{\rm typ} < \nu_0/E_{\rm typ} < 1$ to the whole parameter region (6.9). This figure is adapted from Ref. [71].

Probability of obtaining composite dominant model ($P_{\rm comp}$)

In order to quantitatively examine the fine tuning of a parameter for various binding energy, we define $P_{\rm comp}$ as the probability of obtaining the model with the composite dominant bound state:

$$P_{\rm comp}(B) = \frac{1 - \nu_c(B)/E_{\rm typ}}{1 + B/E_{\rm typ}}, \tag{6.10}$$

where ν_c is the value of ν_0 with which $X(B;\nu_c) = 0.5$. In other words, we can quantitatively examine the validity of the threshold rule through $P_{\rm comp}$. The definition of $P_{\rm comp}$ is schematically shown in Fig. 6.2. The fraction of the entire parameter region (horizontal axis) corresponds to the denominator in Eq. (6.10), and the shaded region to the numerator. In this way, with a given binding energy B, $P_{\rm comp}$ (6.2) corresponds to the fraction of the model (ν_0) with the composite dominant state to all models (whole ν_0 region). By definition of $B_{\rm cr}$, it is clear that $P_{\rm comp}(B_{\rm cr}) = 0.5$. In Fig. 6.1, the typical bound state is found to be $P_{\rm comp}(E_{\rm typ}) = 0.25$, and shallow bound state to be $P_{\rm comp}(0.01E_{\rm typ}) = 0.88$.

In Fig. 6.3, we show the binding energy $B/E_{\rm typ}$ dependence of $P_{\rm comp}$. We see $P_{\rm comp}$ monotonically increases with the decrease of the binding energy B. Finally, at $B = 0$, we find $P_{\rm comp} = 1$, which indicates that the bound state with $B = 0$ is always composite dominant regardless of the choice of the model (the value of ν_0), which is consistent with the compositeness theorem (6.4). Moreover, in the small B region, we also see $P_{\rm comp}$ is smaller but still close to unity. Therefore, it is natural to expect that the bound state retains the composite nature, namely, the threshold rule is valid, even when the binding energy deviates slightly from the $B \to 0$ limit. More quantitatively, the threshold rule holds for shallow bound states whose $P_{\rm comp}$ is sufficiently large.

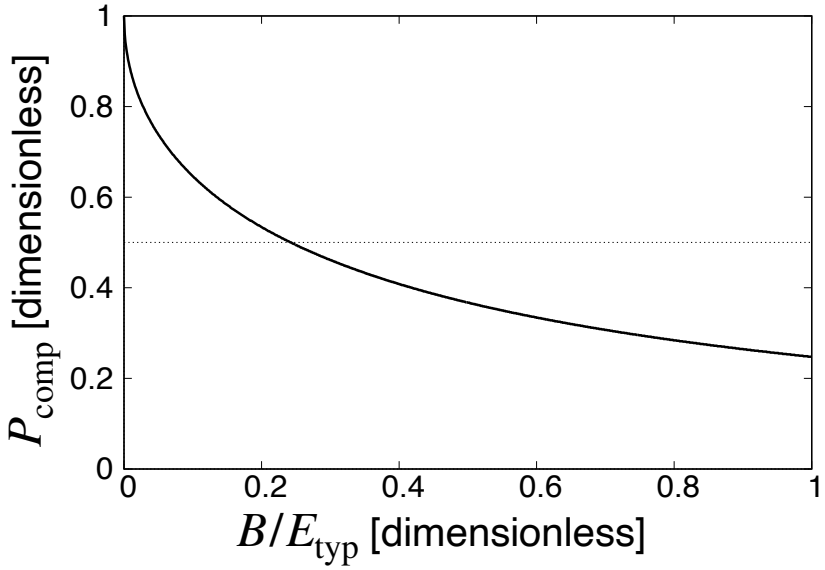

Figure 6.3: The probability of finding the model with the composite dominant bound state $P_{\rm comp}$ as a function of the binding energy $B/E_{\rm typ}$. This figure is adapted from Ref. [71].

6.3 Decay contribution to compositeness

As shown in the introduction (Fig. 1.7), exotic hadron systems have the decay width and channel couplings. To apply to the exotic hadrons, we first consider the decay contribution in this section. Here we adopt the resonance model with the complex coupling constant $g_0 \in \mathbb{C}$ in Section 4.2.2, where the unstable quasi-bound state with the finite decay width $\Gamma \neq 0$ can be described. For comparison with the single-channel case, we set $\lambda_0 = 0$ also in this section. To see the model dependence of the compositeness, we fix the binding energy and vary the model parameter as was done in the previous section. From the pole condition (4.42), the relation between g_0^2 and model parameters are obtained as almost same as Eq. (6.11) but with decay width Γ:

$$g_0^2\left(B+i\frac{\Gamma}{2};\nu_0,\Lambda\right)=\frac{\pi^2}{\mu}\left(B+i\frac{\Gamma}{2}+\nu_0\right)\left[\Lambda-\kappa\arctan\left(\frac{\Lambda}{\kappa}\right)\right]^{-1},\quad \kappa=\sqrt{2\mu\left(B+i\frac{\Gamma}{2}\right)}. \tag{6.11}$$

We can confirm the coupling constant is complex with $\Gamma \neq 0$, and g_0^2 becomes real in the $\Gamma \to 0$ limit. Even in this case, we adopt the same ν_0 region as Eq. (6.9) as the allowed parameter region to be compared with the $\Gamma = 0$ case.

In this study, we investigate the contribution of the decay to the typical and shallow quasi-bound states by fixing the eigenenergy $-B-i\Gamma/2$. The compositeness X is calculated by the same expression as Eq. (6.6), but with the complex g_0^2. As discussed in Section 5.6, the compositeness of an unstable state becomes complex. To discuss the internal structure, we adopt the prescription in Ref. [163] with the $N = 1$ in Eqs. (5.95), (5.96), and (5.97):

$$\tilde{X}=\frac{|X|}{|X|+|Z|},\quad \tilde{Z}=\frac{|Z|}{|X|+|Z|}. \tag{6.12}$$

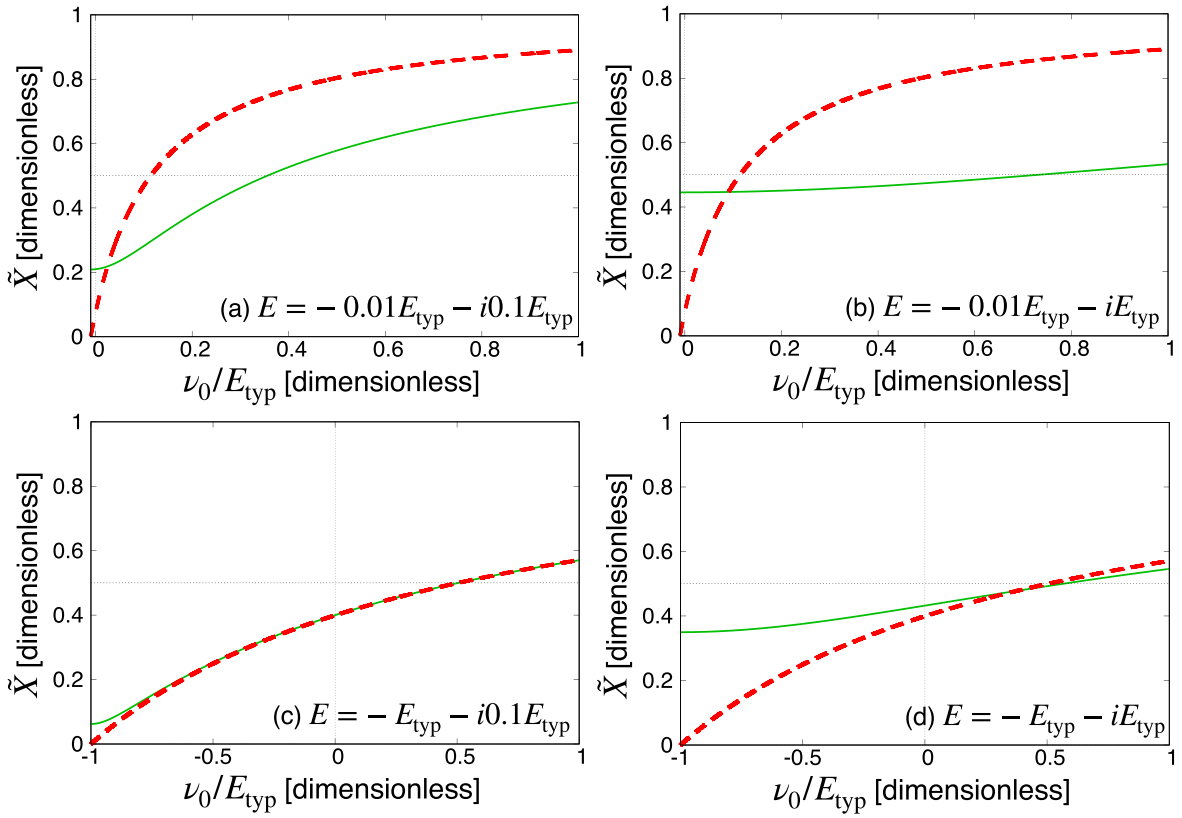

Figure 6.4: The compositeness $\tilde{X}$ with $\Gamma \neq 0$ (solid lines) and $\tilde{X}$ with $\Gamma = 0$ (dashed lines) as functions of the bare state energy $\nu_0/E_{\rm typ}$ with the typical and shallow binding energy and decay width. The panel (a) shows $\tilde{X}$ with $(B, \Gamma/2) = (0.01E_{\rm typ}, 0.1E_{\rm typ})$, (b) with $(B, \Gamma/2) = (0.01E_{\rm typ}, E_{\rm typ})$, (c) with $(B, \Gamma/2) = (E_{\rm typ}, 0.1E_{\rm typ})$, and (d) with $(B, \Gamma/2) = (E_{\rm typ}, E_{\rm typ})$. This figure is adapted from Ref. [71].

Compositeness $\tilde{X}$ of near-threshold quasi-bound states

Here we numerically study the decay contribution to $\tilde{X}$ of the shallow quasi-bound state. In Fig. 6.4, we plot the compositeness $\tilde{X}$ of the quasi-bound states as a function of the normalized bare state energy $\nu_0/E_{\rm typ}$ with $\Gamma \neq 0$ (solid lines) and with $\Gamma = 0$ (dashed lines). We use the same parameter region with the $\Gamma = 0$ case in Eq. (6.9). For the comparison of the shallow and typical bound states, we show the shallow case with the real part of the eigenenergy $B = 0.01E_{\rm typ}$ in panels (a) and (b), and the typical case with $B = E_{\rm typ}$ in panels (c) and (d). Furthermore, to investigate the decay contribution to the compositeness, we show the case with a narrow decay width $\Gamma/2 = 0.1E_{\rm typ}$ in panels (a) and (c), and a broad width $\Gamma/2 = E_{\rm typ}$ in panels (b) and (d). The contribution of the decay is represented by the difference between solid and dashed lines. We note that the dashed lines with $\Gamma = 0$ are the same as the solid and dashed lines in Fig. 6.1.

By comparing the solid and dashed lines in all panels, we find that the compositeness $\tilde{X}$ with decay width Γ (solid lines) is usually smaller than that without Γ (dashed lines). This indicates that the decay contribution reduces the compositeness. In this model, the decay components are implicitly contained in the elementarity as a non-composite component. Thus, with the presence of the decay,

there exists a larger fraction of the non-composite components than that in the $\Gamma = 0$ system. As a consequence, the elementarity increases with the decay contribution, which is equivalent to the decrease of the compositeness due to $\tilde{X} + \tilde{Z} = 1$.

However, in the small $\nu_0/E_{\rm typ}$ region, $\tilde{X}$ with $\Gamma \neq 0$ becomes lager than that with $\Gamma = 0$. This is because at $\nu_0 = -B$, $\tilde{X}$ is finite with $\Gamma \neq 0$, in contrast to that with $\Gamma = 0$. It is analytically shown from Eq. (6.11), that $g_0^2 \neq 0$ with finite Γ at $\nu_0 = -B$:

$$g_0^2\left(B + i\frac{\Gamma}{2}; \nu_0 = -B, \Lambda\right) = \frac{\pi^2}{\mu} \times i\frac{\Gamma}{2} \times \left[\Lambda - \kappa \arctan\left(\frac{\Lambda}{\kappa}\right)\right]^{-1} \neq 0. \tag{6.13}$$

The finite g_0^2 at $\nu_0 = -B$ leads to the finite value of the complex X (6.6) and $\tilde{X}$ (6.12), which explains the irregular behavior of $\tilde{X}$ at $B/E_{\rm typ} \sim -\nu_0/E_{\rm typ}$.

Furthermore, by comparing panels (a), (c) and (b), (d), we find that the ν_0 dependence of $\tilde{X}$ becomes smaller for larger decay width Γ. The reason is shown by Eq. (6.11) where ν_0 dependence of g_0^2 is suppressed with large $|B + i\Gamma/2| \gg \nu_0$. In the formal limit $\Gamma \to \infty$, it is shown that the compositeness finally becomes constant[1] [71]:

$$\tilde{X} = \frac{1}{2} + \dots , \tag{6.14}$$

From this observation, we find that $\tilde{X}$ in panels (b) and (d) is the appearance of the feature of $\tilde{X}$ in the $\Gamma \to \infty$ limit.

To see the contribution of the decay width, we compare panels (a) with (c), which have the same $\Gamma/2$ but different binding energy B. We find that the difference between solid and dashed lines is sizable in panel (a), while that is too small to distinguish in panel (c). In other words, the decay contribution to $\tilde{X}$ is much smaller in panel (c) than in panel (a), while both have the same $\Gamma/2$. By focusing on the ratio, $\Gamma/2$ is 10 times larger than B in panel (a), and 10 times smaller in panel (c). This indicates that the suppression of $\tilde{X}$ is determined by the ratio of B and Γ, not by the magnitude of Γ.

Probability of obtaining composite dominant model $P_{\rm comp}$

In order to observe the nature of the shallow quasi-bound states, we show the probability of finding the composite dominant model $P_{\rm comp}(B, \Gamma)$ (Fig 6.5). We note that $P_{\rm comp}(B, \Gamma)$ is the function of not only the binding energy B but also the decay width Γ in this case. In this observation, we fix the decay width Γ. The definition of $P_{\rm comp}(B, \Gamma)$ is essentially same as Eq. (6.10) with the replacement of B with $B + i\Gamma/2$, but ν_c is defined with $\tilde{X} = 0.5$. The solid, dashed, and dotted lines stand for the case with $\Gamma/2 = 0$ (the same plot with the Fig. 6.3), $\Gamma/2 = 0.1E_{\rm typ}$, and $\Gamma/2 = E_{\rm typ}$, respectively.

To discuss the decay contribution to $P_{\rm comp}(B, \Gamma)$, we compare the solid, dashed, and dotted lines. We see that $P_{\rm comp}(B, \Gamma)$ becomes smaller with the larger decay width Γ. This is explained by the comparison of the solid lines in panels (a) with (b) or (c), (d), which shows that ν_c becomes larger when the Γ is increasing. Furthermore, the difference of ν_c becomes smaller in panels (c) and (d) than that in (a) and (b). This explains the fact that the difference between dashed and dotted lines is smaller in the large B region while that is prominent in the small B region.

[1]The $\Lambda \to \infty$ limit exceeds the applicable energy scale of the EFT $\Gamma \gg \Lambda$, as shown below. Therefore, this consideration should only be utilized to understand the behavior of $\tilde{X}$ with the increase of Γ.

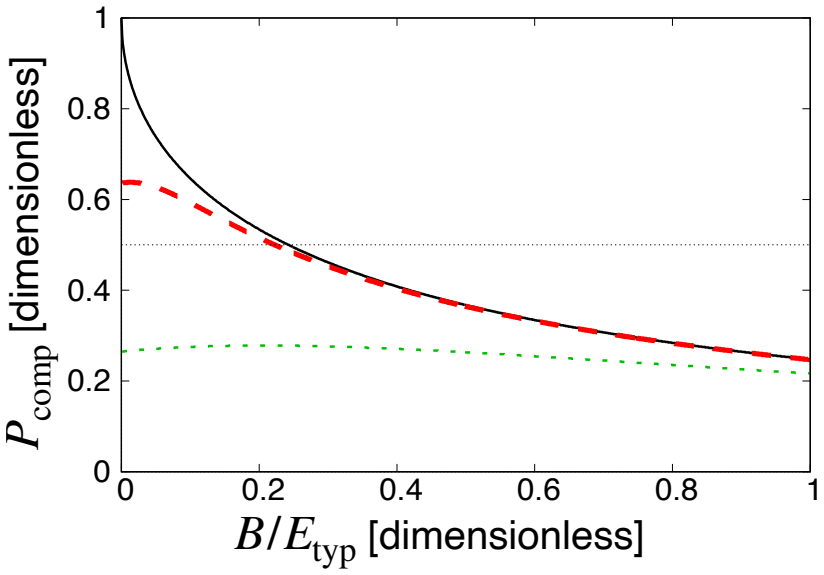

Figure 6.5: The probability of obtaining the composite dominant model $P_{\rm comp}(B,\Gamma)$ as a function of the binding energy $B/E_{\rm typ}$. The solid line corresponds to $P_{\rm comp}$ with $\Gamma/2 = 0$, the dashed with $\Gamma/2 = 0.1E_{\rm typ}$, and the dotted with $\Gamma/2 = E_{\rm typ}$. This figure is adapted from Ref. [71].

We then compare $P_{\rm comp}$ with and without decay width Γ. By decreasing B from $B/E_{\rm typ} = 1$, we see that the deviation of dashed and dotted lines ($\Gamma \neq 0$) from the solid line ($\Gamma = 0$) becomes larger. This is expressed by the nature of the decay contribution to the compositeness discussed above; the suppression of $\tilde{X}$ by Γ is determined by the ratio of B to Γ. Because the ratio of B to Γ becomes smaller when we decrease B with the fixed Γ, the decay more contributes to suppressing $\tilde{X}$ for the smaller B region.

We finally focus on the small B region $B \sim 0$. We find that $P_{\rm comp}$ does not become unity at $B = 0$ with the finite $\Gamma \neq 0$ (dashed and dotted lines). With the presence of Γ, the states do not go to the threshold $B = \Gamma = 0$ even in the $B \to 0$ limit. In this case, the coupling constant g_0^2 (6.11) and κ are finite in Eq. (6.6), and $\tilde{X}$ cannot become unity even in $B \to 0$ limit, as long as Γ is finite. This is the reason why $P_{\rm comp}(B,\Gamma) < 1$ at $B = 0$ with finite decay width. Furthermore, the dotted line never exceeds $P_{\rm comp} = 0.5$ even with small B. This shows that the state with $\Gamma/2 = E_{\rm typ}$ is usually elementary dominant. From these observations, we find that the quasi-bound states are not always composite dominant even if B is small, and their internal structure is characterized by the ratio of B to Γ is large. We note that even when we decrease B, the state remains in the far-threshold region unless Γ is sufficiently small (see Fig. 6.6). From the viewpoint of the low-energy universality, the finite scattering length induces the fact that $P_{\rm comp} < 1$ at $B = 0$ with finite Γ.

6.4 Coupled channel contributions to compositeness

In addition to the previous discussion with the decay channel, here we consider the coupled channel higher than the threshold channel. For this purpose, we use the coupled-channel EFT model in Section 4.2.2. To focus on the situation that a bound state couples to the two higher-energy channels,

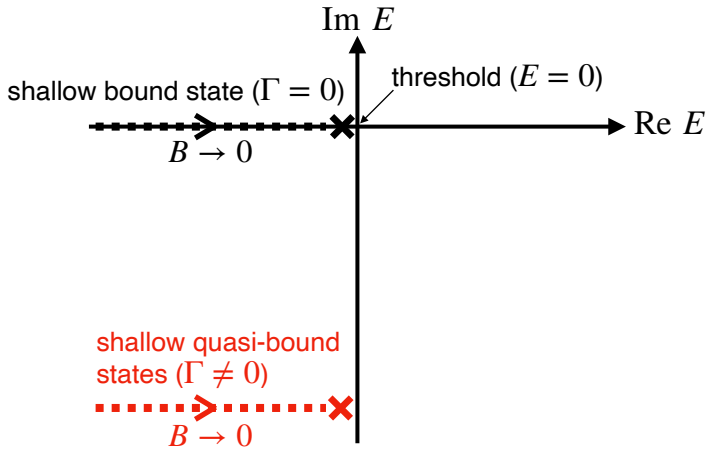

Figure 6.6: The schematic illustration of the position of shallow bound state with $\Gamma \neq 0$ and shallow quasi-bound state with $\Gamma \neq 0$ in the complex energy plane.

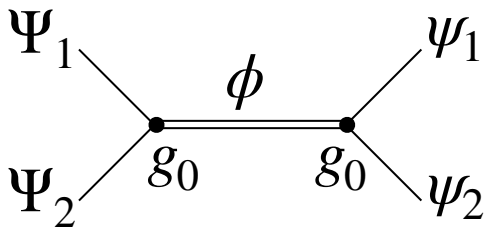

Figure 6.7: The diagram of the transition between $\psi_1\psi_2$ scattering (channel 1) and $\Psi_1\Psi_2$ scattering (channel 2) where these two channels couples to the bare state ψ with the common coupling constant g_0.

we assume that a bound state exists below the threshold of the lowest energy channel. For the calculation of the compositeness in this case, we should determine the threshold energy difference $\Delta\omega$ in addition to the model parameters, the coupling constants $g_{0,1}$, $g_{0,2}$, λ_{11}, λ_{12}, λ_{21}, λ_{22}, bare state energy ν_0, cutoff Λ. We set $\lambda_{11} = \lambda_{12} = \lambda_{21} = \lambda_{22} = 0$ also in this section. Furthermore, to focus on the contribution of the channel coupling, we assume that the channels coupled to the bound state with the same coupling constants $g_{0,1} = g_{0,2} = g_0$. In this case, the transition between channels 1 and 2 occurs through the bare field ϕ with the coupling constant g_0 (Fig. 6.7). We note that the coupling constant g_0 is real, in contrast to the previous section on decay contribution.

In the coupled channel case, we define the compositeness of the threshold channel X_1 and that of the coupled channel X_2 from the completeness relation (4.59) as discussed in Section 5.4. The compositeness X_1, X_2, and elementarity Z are written by the loop functions (4.62) as [94, 71]

$$X_i(B, \Delta\omega, \nu_0, g_0, \Lambda) = \frac{G_i^{0\prime}(i\kappa_i)}{G_1^{0\prime}(i\kappa_1) + G_2^{0\prime}(i\kappa_2) - [v^{-1}(i\kappa_1)]'}, \tag{6.15}$$

$$Z(B, \Delta\omega, \nu_0, g_0, \Lambda) = -\frac{[v^{-1}(i\kappa_1)]'}{G_1^{0\prime}(i\kappa_1) + G_2^{0\prime}(i\kappa_2) - [v^{-1}(i\kappa_1)]'}, \tag{6.16}$$

with $i = 1, 2$. $\kappa_{1,2}$ and v are given as

$$\kappa_1 = \sqrt{2\mu_1 B}, \quad \kappa_2 = \sqrt{2\mu_2(B + \Delta\omega)}, \tag{6.17}$$

$$v(k) = \frac{g_0^2}{\frac{k}{2\mu_i} - \nu_0}. \tag{6.18}$$

$X_{1,2}$ are real because the loop functions are real with positive B. From Eqs. (6.15) and (6.16), we see that $X_1 + X_2 + Z = 1$. The energy derivative of $v^{-1}(i\kappa_1)$ and loop functions are negative. Therefore, $0 \leq X_1 \leq 1$, $0 \leq X_2 \leq 1$, and $0 \leq Z \leq 1$. In this way, we can confirm that X_1, X_2, and Z can be regarded as the probability.

From Eq. (6.15), the compositeness in this model depends not only on the binding energy B and the model parameters ν_0, g_0, Λ, but also on the threshold energy difference $\Delta\omega$. In this study, we fix B and $\Delta\omega$ to investigate the model dependence of the compositeness. As was the same in the previous Section 6.2, we can reduce the one degree of the model parameters from the bound state condition, and further reduce Λ dependence by using the dimensionless quantities. In this case, the result depends on the reduced mass ratio μ_1/μ_2. To focus on the $\Delta\omega$ dependence, we assume $\mu_1/\mu_2 = 1$ in the numerical calculation.

Compositeness X_1 and X_2 of near-threshold bound states

To observe the coupled-channel contributions to the compositeness, we show the compositeness of the threshold channel X_1 and that of the coupled-channel X_2 of the typical and shallow bound states as functions of the normalized model parameter $\nu_0/E_{\rm typ}$. For the comparison with the single-channel case, we adopt the same parameter region (6.9). In Fig. 6.8, X_1 is plotted as the dotted lines, and the total compositeness $X_1 + X_2$ as the solid line. Therefore, the difference between solid and dotted lines corresponds to X_2. To see the coupled-channel contributions, we also show the compositeness of the single-channel case as the dashed line, which is calculated by the single-channel resonance model (6.6). The panels (a) and (b) correspond to the shallow bound states with $B = 0.01E_{\rm typ}$, and (c) and (d) to the typical bound states with $B = E_{\rm typ}$. The states with small threshold energy difference $\Delta\omega$ are shown in panels (a) and (c), and large $\Delta\omega$ is in panels (b) and (d).

We first focus on how the threshold energy differences $\Delta\omega$ affect to the threshold channel compositeness X_1, which is quantified by the difference between the threshold channel compositeness with channel couplings (dotted lines) and that without channel couplings (dashed lines). By comparing the dashed and dotted lines in all panels, we first find that the threshold channel compositeness decreases with the presence of the coupled channel. This is because the probability is shared also by the coupled channel component, not only by the threshold channel and elementary components. In other words, the channel couplings induce the reduction of the threshold channel compositeness. This is understood by the quantitatively same reason as the decay contribution.

We then compare the panels (a) with (b) and (c) with (d), where the binding energy is the same but $\Delta\omega$ is different. From the difference between the dashed and dotted lines, we find that the degree of the reduction of X_1 is smaller when the threshold energy difference $\Delta\omega$ is larger. Because channel 1 and 2 have the same coupling constant g_0, the contribution of the channel coupling to the bound state is determined only by the threshold energy difference $\Delta\omega$. Therefore, the coupled channel does not affect very much the compositeness with the larger $\Delta\omega$. Furthermore, for comparison panels (b) with (d), we find that the difference between dashed and dotted lines is smaller in panel (b), even though

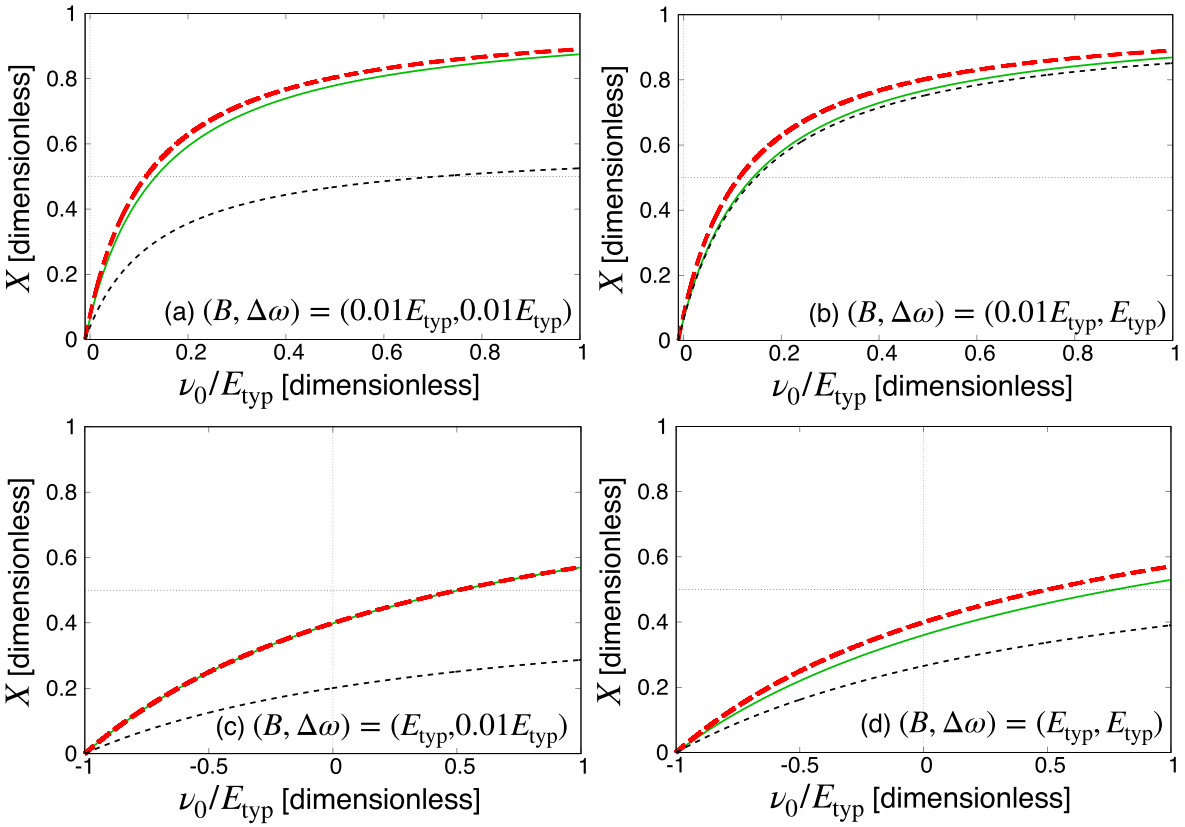

Figure 6.8: The compositeness X_1 (dotted lines), total compositeness $X_1 + X_2$ (solid lines) and X in the single channel case (dashed lines) as functions of the bare state energy $\nu_0/E_{\rm typ}$. The panel (a) shows the case with $(B, \Delta\omega) = (0.01E_{\rm typ}, 0.1E_{\rm typ})$, (b) with $(B, \Delta\omega) = (0.01E_{\rm typ}, E_{\rm typ})$, (c) with $(B, \Delta\omega) = (E_{\rm typ}, 0.1E_{\rm typ})$, and (d) with $(B, \Delta\omega) = (E_{\rm typ}, E_{\rm typ})$. This figure is adapted from Ref. [71].

the $\Delta\omega$ is common in these two panels. This indicates that the coupled channel contribution X_2 is determined by the ratio of B to $\Delta\omega$, not by the magnitude of $\Delta\omega$.

We then compare the total compositeness $X_1 + X_2$ (solid lines) with that in the single channel case (dashed lines). As discussed above, the dashed lines correspond to the case with $\Delta\omega \to \infty$. We find that the solid and dashed lines do not differ very much in all panels. This is considered as the appearance of the feature of the model, where the bound state is constructed by the dressing of the bare state through the couplings to the scattering states. The couplings to each scattering channel contribute to the increase of X_1 and X_2. In both the single and coupled channel models, the bare state needs almost the same amount of the dressing so that the bound state appears at $E = -B$ with the same bare state energy ν_0. Therefore, the amount of the dressing in the coupled-channel model is produced by the cooperation of channels 1 and 2, while that in the single-channel model is provided only by the threshold channel. This is the reason why the total compositeness $X_1 + X_2$ is close to the X in the single channel case.

By comparing panels (a) with (b) and (c) with (d), the coupled channel compositeness X_2 is smaller with larger $\Delta\omega/B$. This relation between X_2 and $\Delta\omega$ is analytically observed from Eq. (6.15). In the

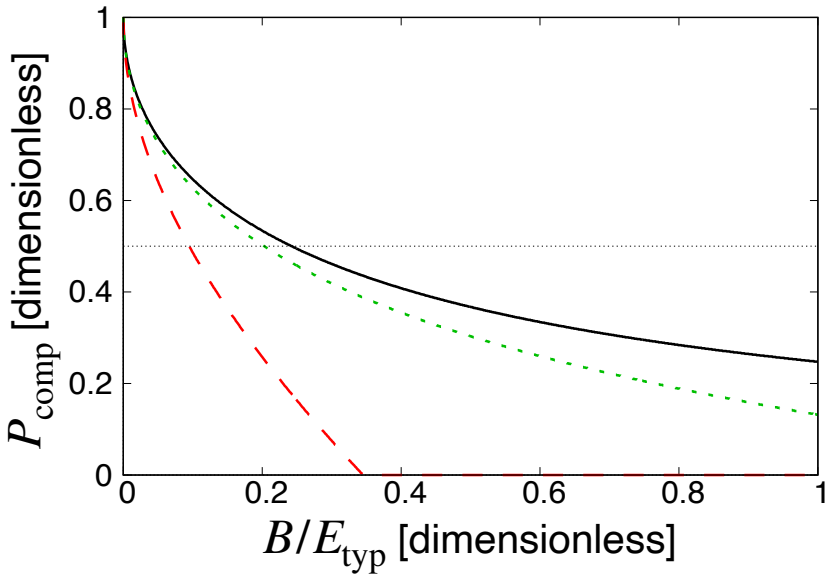

Figure 6.9: The probability of obtaining the composite dominant model $P_{\rm comp}(B, \Delta\omega)$ as a function of the binding energy $B/E_{\rm typ}$. The solid line stands for $P_{\rm comp}$ in the single-channel model with $\Delta\omega \to \infty$, the dashed line for $\Delta\omega = E_{\rm typ}$, and dotted line for $\Delta\omega = 10E_{\rm typ}$. This figure is adapted from Ref. [71].

formal limit $\Delta\omega \to \infty$, the momentum of the coupled channel κ_2 also goes to infinity. In this case, the loop function becomes zero and $X_2 \propto G_2^{0\prime}(i\kappa_2) \to 0$. This is intuitively regarded as the contribution of the channel coupling vanishes when the coupled channel goes infinitely far away from the bound state. In this case, the system reduces to the single channel case and X_1 to X in the single channel resonance model.

We finally consider the opposite limit $\Delta\omega \to 0$. From Eq. (6.15), we analytically see $\kappa_1 = \kappa_2$ and $G_1^0 = G_2^0$. Because we assume $\mu_1 = \mu_2$, the compositeness becomes $X_1 = X_2$ in this limit. This is because the bound state couples to both channels 1 and 2 with an equal weight, through the common g_0. In Fig. 6.8, we see this feature is reflected in panel (c), where the threshold energy difference is too small than the binding energy to be negligible as $\Delta\omega \sim 0$.

Probability of obtaining composite dominant model $P_{\rm comp}$

To quantitatively discuss the nature of the near-threshold states in a coupled-channel system, we define the probability of finding the composite dominant model $P_{\rm comp}(B, \Delta\omega)$. In the presence of the channel coupling, $P_{\rm comp}(B, \Delta\omega)$ also depends on the threshold energy difference $\Delta\omega$ in addition to the binding energy B. In this case, we define ν_c in $P_{\rm comp}(B, \Delta\omega)$ (6.10) as $X_1(\nu_c) = 0.5$, in order to focus on the threshold channel. We plot the probability of finding the composite dominant model $P_{\rm comp}(B, \Delta\omega)$ as functions of the normalized binding energy $B/E_{\rm typ}$ in Fig. 6.9. The solid line represents $P_{\rm comp}(B, \Delta\omega)$ in the single channel case with $\Delta\omega \to \infty$ (the same plot with the Fig. 6.3), dashed line in the coupled channel case with $\Delta\omega = E_{\rm typ}$, and dotted line with $\Delta\omega = 10E_{\rm typ}$.

In the $B \to 0$ limit, we find that $P_{\rm comp}(B, \Delta\omega)$ goes to unity in all cases, which means that $X_1 \to 1$, $X_2 \to 0$, and $Z \to 0$ at $B = 0$. When the binding energy B is sufficiently small, the threshold

energy difference $\Delta\omega$ becomes relatively much larger than B, and we can neglect the higher coupled channel as shown in the discussion of $\Delta\omega \to \infty$ limit. This is consistent with the compositeness theorem (6.4), where the coupled channel component is included in the non-threshold-channel one with the elementarity Z.

When we deviate from the point at $B = 0$, we see the gradient of $P_{\rm comp}(B, \Delta\omega)$ becomes larger when $\Delta\omega$ is smaller. The reason is explained by the behavior of X_1 in Fig. 6.8, where ν_c becomes larger with decreasing $\Delta\omega$ by comparing panels (a) with (b). On the other hand, in panels (c) and (d), X_1 never goes beyond 0.5 in the whole ν_0 region. The behavior of the dashed line reflects this property of X_1, where $P_{\rm comp}(B, \Delta\omega)$ becomes zero in the large $B/E_{\rm typ}$ region.

6.5 Application to $T_{cc}(3875)^+$ and $X(3872)$

Set up

In the last section, we discuss the internal structure of the near-threshold exotic hadrons by calculating the compositeness. As well-known examples of the near-threshold exotic hadrons, we consider $T_{cc}(3875)^+$ and $X(3872)$. The detail of the system of $T_{cc}(3875)^+$ and $X(3872)$ are shown in Fig. 1.7 in the introduction. As mentioned there, $T_{cc}(3875)^+$ and $X(3872)$ are observed as the quasi-bound states just below the D^0D^{*+} and $D^0\bar{D}^{*0}$ thresholds, respectively. The binding energies and decay width of $T_{cc}(3875)^+$ and $X(3872)$ are observed by the experiments as in Ref. [29] and PDG [1], respectively:

$$T_{cc}(3875)^+ : E = -0.36^{+0.044}_{-0.040} - i0.024^{+0.001}_{-0.007}\ \text{MeV}, \tag{6.19}$$

$$X(3872) : E = -0.04 \pm 0.06 - i0.595 \pm 0.105\ \text{MeV}. \tag{6.20}$$

As shown in the data above, their binding energies are much smaller than the typical energy scale of the binding energy of hadrons [$\lesssim \mathcal{O}(10)$ MeV]. In this sense, $T_{cc}(3875)^+$ and $X(3872)$ are regarded as the near-threshold quasi-bound states. $T_{cc}(3875)^+$ and $X(3872)$ have a decay width with 0.048 MeV and 1.19 MeV, respectively. We note that the binding energy of $X(3872)$ is much smaller than the decay width, even though Γ is already smaller than the typical decay width $\mathcal{O}(10)$ MeV - $\mathcal{O}(100)$ MeV. Furthermore, in addition to the threshold channels, there are higher coupled channels $D^{*0}D^+$ ($D^{*-}D^+$) in the $T_{cc}(3875)^+$ ($X(3872)$) system, which exists 1.41 MeV (8.23 MeV) above the D^0D^{*+} ($D^0\bar{D}^{*0}$) threshold. The deviation between threshold and coupled channels is induced by isospin symmetry breaking. Thus, these coupled channels might affect the structure of $T_{cc}(3875)^+$ and $X(3872)$ as the isospin partner of the threshold channel. In this way, both the decay width and channel coupling should be considered to study $T_{cc}(3875)^+$ and $X(3872)$.

To calculate the compositeness, we construct the EFT model combining the resonance models with decay width (Section 4.2.1) and channel couplings (Section 4.2.2), so that both of these contributions are included in the model. In the model with decay width in Section 4.2.1, we effectively introduced the decay contribution. In contrast, we explicitly considered the channel coupling to the higher channel in the coupled channel resonance model in Section 4.2.2. Based on these, in the model considered here, we let the coupling constant in the coupled channel model be the complex value. For simplicity, we again set $\lambda_0 = 0$. Furthermore, we assume $g_{0,1} = g_{0,2} = g_0$ as in the previous Section 6.4.

For numerical calculation, we take the mass of D mesons from PDG [1]. Based on these values, the reduced masses μ_1 and μ_2 of the $T_{cc}(3875)^+$ and $X(3872)$ system are determined, while we assumed $\mu_1 = \mu_2$ in the previous section.

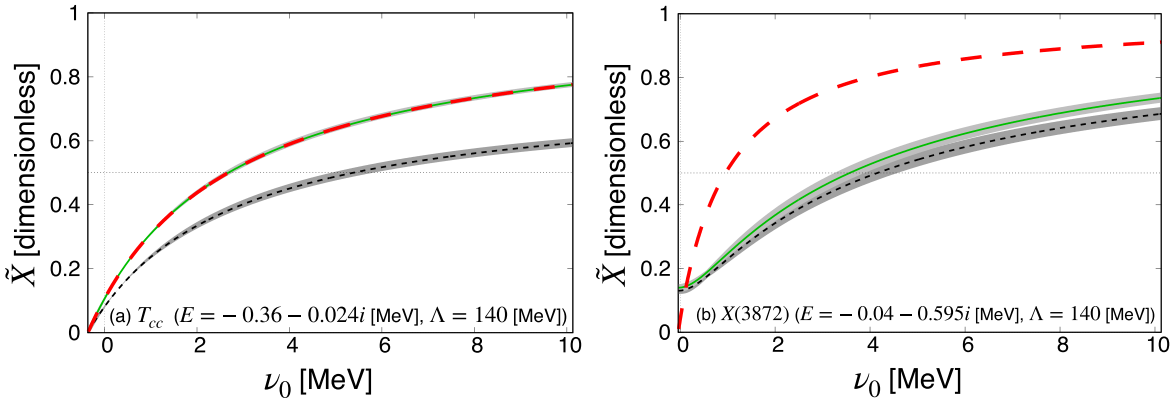

Figure 6.10: The compositeness of $T_{cc}(3875)^+$ [panel (a)] and $X(3872)$ [panel (b)] as functions of the bare state energy ν_0. The compositeness of the threshold channel $\tilde{X}_1$ is plotted as the dashed lines, and the total compositeness with $\Gamma \neq 0$ is as the solid line. The dashed lines correspond to the total compositeness without decay contribution $\Gamma = 0$. The gray bands show the compositeness by considering the experimental error. We use the cutoff $\Lambda = 140$ MeV. This figure is adapted from Ref. [71].

With this setup, the compositeness of the threshold channel X_1 and coupled channel X_2 are calculated from Eq. (6.15) but with the complex coupling constant $g_0 \in \mathbb{C}$. In this case, X_1 and X_2 are obtained as the complex values. For the probabilistic interpretation, we use the prescription Eqs. (5.95) and (5.96) in Ref. [163], where $\tilde{X}_1$ ($\tilde{X}_2$) is regarded as the compositeness of the threshold channel (the coupled channel).

In the previous sections, we use the dimensionless quantities with the cutoff Λ. However, to consider the actual hadron system of $T_{cc}(3875)^+$ and $X(3872)$, here we use the fixed cutoff $\Lambda = 140$ MeV $\sim m_\pi$ because the interaction between D mesons can occur through the π exchange. In this case, the typical energy scale $E_{\rm typ}$ becomes

$$T_{cc}(3875)^+ : E_{\rm typ} = 10.13 \text{ MeV}, \tag{6.21}$$

$$X(3872) : E_{\rm typ} = 10.14 \text{ MeV}. \tag{6.22}$$

Compositeness of $T_{cc}(3875)^+$ and $X(3872)$

In Fig 6.10, we plot the compositeness of $T_{cc}(3875)^+$ [panel (a)] and $X(3872)$ [panel (b)] by varying the bare state energy ν_0. The dotted lines stand for the compositeness of the threshold channel $\tilde{X}_1$. To see the decay contribution, we plot the total compositeness $\tilde{X}_1 + \tilde{X}_2$ with finite decay width $\Gamma \neq 0$ (the solid line), and that without decay contribution $\Gamma = 0$ (the dashed lines). The shaded bands represent the error from the experimental uncertainty of the binding energy in Eqs. 6.19 and (6.20).

At first, we discuss the decay contribution to the compositeness by comparing the total compositeness with $\Gamma \neq 0$ (the solid lines) and that with $\Gamma = 0$ (the dashed lines). In the $T_{cc}(3875)^+$ case in the left panel, we see the solid and dashed lines overlap, which means that the difference between the two lines is too small to distinguish. This is because the decay width of $T_{cc}(3875)^+$ ($\Gamma = 0.048$ MeV) is about ten times smaller than the binding energy ($B = 0.36$ MeV). This nature of the compositeness

was observed in Section 4.2.1; the decay contribution to the compositeness becomes smaller with the small ratio of Γ to B. On the other hand, we find that the decay contributes very much to the compositeness of $X(3872)$ because the difference between dashed and solid lines is sizable. This is explained by the much larger decay width $\Gamma = 1.19$ MeV of $X(3872)$ than its binding energy $B = 0.04$ MeV.

We then focus on the coupled channel contribution to the compositeness. By comparing the dashed with dotted lines, we find that the degree of the reduction of the threshold channel compositeness of $T_{cc}(3875)^+$ is larger than that of $X(3872)$. This indicates that the coupled channel contributes more to the compositeness of $T_{cc}(3875)^+$ than that of $X(3872)$. In the $T_{cc}(3875)^+$ system, the threshold energy difference $\Delta\omega = 1.41$ MeV is smaller than the binding energy $B = 0.36$ MeV. On the other hand, $\Delta\omega$ of $X(3872)$ system (8.23 MeV) is much larger than the binding energy $B = 0.04$ MeV. As discussed in Section 6.4, the coupled channel contribution to the threshold channel compositeness is characterized by the ratio of B to $\Delta\omega$. This is because why the compositeness of $T_{cc}(3875)^+$ is more suppressed by the coupled channel by comparing with the $X(3872)$ case, and $\tilde{X}_1$ becomes smaller in $T_{cc}(3875)^+$.

In this way, we find that the coupled channel contribution plays an important role in considering the threshold channel compositeness $\tilde{X}_1$ of $T_{cc}(3875)^+$, while the decay contribution is negligible. This is because $T_{cc}(3875)^+$ has the small decay width and the threshold energy difference. In contrast, the compositeness of $X(3872)$ is more affected by the presence of the decay channel, while the coupled channel contribution is relatively small. The decay width Γ of $X(3872)$ is not always taken into account in previous works because it is smaller than the typical Γ of hadrons. However, to consider the compositeness, this work indicates that the decay with Γ of $X(3872)$ should not be neglected.

The probability of finding composite dominant model $P_{\rm comp}$ of $T_{cc}(3875)^+$ and $X(3872)$

To observe the contributions of decay and channel couplings to the molecular nature of $T_{cc}(3875)^+$ and $X(3872)$, we calculate the probability of finding the composite dominant model $P_{\rm comp}$. When we consider both the decay width and channel coupling, $P_{\rm comp}$ is calculated for a given B, Γ, and $\Delta\omega$. The critical value ν_c is defined such that $\tilde{X}_1(B;\nu_c) = 0.5$ in this case. With considering the experimental error of the eigenenergy, the $P_{\rm comp}$ of $T_{cc}(3875)^+$ and $X(3872)$ are obtained as

$$P_{\rm comp} = 0.45^{+0.049}_{-0.037} \quad [T_{cc}(3875)^+], \tag{6.23}$$

$$P_{\rm comp} = 0.59^{+0.040}_{-0.043} \quad [X(3872)]. \tag{6.24}$$

These results show that the probability of finding the composite dominant model is not so large, while $T_{cc}(3875)^+$ and $X(3872)$ are observed as the near-threshold states. From the discussion above, this is explained by the presence of the decay and coupled channel contributions which suppress the threshold channel compositeness $\tilde{X}_1$. This result indicates that the non-composite dominant state might also characterize the internal structure of $T_{cc}(3875)^+$ and $X(3872)$ because of the decay and channel couplings.

Compositeness of $T_{cc}(3875)^+$ and $X(3872)$ for fixed ν_0

The value of ν_0 cannot be determined within the EFT framework, and we focused on the model dependence of the compositeness by varying the bare state energy ν_0 in the above analysis. Here we calculate practical values of the compositeness of $T_{cc}(3875)^+$ and $X(3872)$ for fixed ν_0. For one of the

practical values of ν_0 for $T_{cc}(3875)^+$ and $X(3872)$ systems, we adopt the energy of the state calculated by constituent quark models in Ref. [62] and Ref. [4], respectively:

- $\nu_0 = 7$ MeV, $[T_{cc}(3875)^+]$; and
- $\nu_0 = 78.36$ MeV, $[X(3872)]$.

The compositeness of the threshold channel X_1, that of the coupled channel X_2, and elementarity Z can be read off from the previous result in Fig. 6.10. Here we focus on the central value of X_1, X_2, and Z obtained from the central value of the binding energy. The compositeness X_1, X_2 and elementarity Z of $T_{cc}(3875)^+$ are calculated as

$$X_1 = X_{D^0 D^{*+}} = 0.541 - 0.007i, \tag{6.25}$$
$$X_2 = X_{D^{*0} D^+} = 0.167 + 0.003i, \tag{6.26}$$
$$Z = 0.292 + 0.005i. \tag{6.27}$$

We also show those of $X(3872)$ as follows

$$X_1 = X_{D^0 \bar{D}^{0*}} = 0.919 - 0.079i, \tag{6.28}$$
$$X_2 = X_{D^{*-} D^+} = 0.046 + 0.050i, \tag{6.29}$$
$$Z = 0.035 + 0.030i. \tag{6.30}$$

In the $T_{cc}(3875)^+$ case, we see that the imaginary parts of $X_{1,2}$ and Z are smaller than the real part of those. This is because the decay width Γ of the $T_{cc}(3875)^+$ is smaller than the binding energy B. On the other hand, for the $X(3872)$ case, the imaginary part of X_2 and Z are as large as the real part, as a consequence of the large ratio of Γ/B of $X(3872)$.

For the probabilistic interpretation of the complex compositeness and elementarity, we adopt the interpretation scheme with $\mathcal{X}, \mathcal{Y}, \mathcal{Z}$ discussed in Section 5.7.4. In this scheme, the compositeness $\mathcal{X}$ is regarded as the fraction of the threshold channel component (i.e., the interpretation of complex X_1), and the coupled channel compositeness X_2 is contained in the elementarity Z. Here we use $\alpha = \alpha_0$, which corresponds to adapting the criterion for interpretable state in Eq. (5.101). The compositeness $\mathcal{X}$, probability of uncertain identification $\mathcal{Y}$, and elementary $\mathcal{Z}$ are calculated as

$$\mathcal{X} = 0.537, \quad \mathcal{Y} = 0.008, \quad \mathcal{Z} = 0.456, \quad [T_{cc}(3875)^+], \tag{6.31}$$
$$\mathcal{X} = 0.890, \quad \mathcal{Y} = 0.028, \quad \mathcal{Z} = 0.081, \quad [X(3872)]. \tag{6.32}$$

In both of the $T_{cc}(3875)^+$ and $X(3872)$ cases, $\mathcal{Y}$ is much smaller than other probabilities. Recalling $\mathcal{Y}$ is defined to be small for narrow resonances, this is consistent with the nature of these exotic hadrons with narrow decay width $\lesssim \mathcal{O}(1)$ MeV. The result of $T_{cc}(3875)^+$ shows that the compositeness $\mathcal{X}$ is the largest but also $\mathcal{Z}$ is non-negligible. This is explained by the sizable magnitude of X_2 (6.26) and Z (6.27), which are included in the non-threshold channel components $\mathcal{Z}$. In this sense, $T_{cc}(3875)^+$ is concluded to be composite dominant but with considerable contributions of the coupled channel and non-composite components. On the other hand, $X(3872)$ has a large fraction of the composite component $\mathcal{X}$. This is a consequence of a large ν_0 value adopted here; the complex compositeness increases together with ν_0 as shown in Fig 6.10. Therefore, $X(3872)$ is regarded as a $D^0\bar{D}^{0*}$ highly molecule-dominant state.

Chapter 7

Summary

In this thesis, we study the universal nature of near-threshold states by studying their internal structure with the compositeness. In recent years, the study of exotic hadrons has been attracting significant attention as one of the key topics in hadron physics. Exotic hadrons are frequently observed in the near-threshold energy region, where the threshold rule is empirically known; the near-threshold bound states are expected to be composite dominant. However, the theoretical explanation for why the threshold rule holds has not yet been provided. Furthermore, the threshold rule cannot be directly applied to hadron systems due to decay and coupled channels. Here we discuss these problems in the context of the low-energy universality.

We begin with the simplest system, a bound state in single-channel scatterings. We adopt the effective field theory model which describes a bound state generated by the coupling of the bare state to the scattering states. By examining the model dependence of the compositeness, we show that the shallow bound state is predominantly composite in most cases without significant fine tuning of parameters. While the non-composite shallow bound state is always possible, we show that the possibility of obtaining a model with the composite dominant bound state increases for small binding energy. In this way, the threshold rule is properly established.

We then discuss how the compositeness is modified by the decay and channel couplings, toward an application to exotic hadrons. We show that the compositeness is suppressed by the decay and coupled channel contributions. Since the decay (coupled channel) contribution is quantitatively characterized by the decay width (threshold energy difference), the suppression of compositeness is determined by the ratio of the decay width (the threshold energy difference) to the binding energy. This result suggests that the decay (coupled channel) effect substantially contributes to the compositeness, if the decay width (threshold energy difference) is larger (smaller) than the binding energy, even for the small (large) magnitude of the decay width (threshold energy difference).

As an application to near-threshold exotic hadrons, we discuss the internal structure of $T_{cc}(3875)^+$ and $X(3872)$. We show that the coupled channel (decay) significantly affects the compositeness of $T_{cc}(3875)^+$ [$X(3872)$], compared to the decay (channel coupling). This is because $T_{cc}(3875)^+$ [$X(3872)$] has the narrow (broad) decay width and small (large) energy difference between the thresholds. Thus, we conclude that the coupled channel (decay width) is important for the compositeness of $T_{cc}(3875)^+$ [$X(3872)$], while their contributions are not always included in previous studies.

As prospects, it would be interesting to discuss the nature of near-threshold states interacting

through the Coulomb plus short-range interaction. In hadron physics, the Coulomb force is usually neglected, because it is approximately 100 times weaker than the strong interaction. However, at a low-energy scale near the threshold, the Coulomb force might play an important role. In the presence of the Coulomb interaction, near-threshold states might exhibit a distinct nature, because the effective range expansion of the scattering amplitude becomes a different form from that of the short-range interaction [189, 81, 190]. Consequently, it is not trivial that the same conclusion holds as in the case of the short-range interaction. Therefore, the compositeness of near-threshold states in the Coulomb plus short-range interaction will give an alternative viewpoint on the present results in this thesis.

Acknowledgement

First and foremost, I would like to express my deepest gratitude to my supervisor, Professor Tetsuo Hyodo, for his guidance in every aspect of my research. His mentorship not only provided me with a foundation in physics but also taught me how to generate ideas for research and write academic papers. Thanks to his invaluable support, I was able to complete my PhD life. I would also like to thank him for offering tea and snacks during our discussion time.

Next, I would like to express my gratitude to Professor Yutaka Fujita and Professor Wen Yin, the examiners of this thesis, for their sharp and constructive feedback and useful advice. Professor Yutaka Fujita also reviewed my master's thesis, and I greatly appreciate his continued support. I also want to thank Professor Wen Yin for complimenting my Kuriboh sweater and for the thoughtful Winged Kuriboh gift. Their constructive criticism and insightful comments have significantly enhanced this thesis.

I would also like to extend my appreciation to the many researchers who discussed various topics with me. In particular, I am grateful to Professor Endo at The University of Electro-Communications, Doctor Naidon at RIKEN, Professor Jido, Professor Nishida, Doctor Murakami, the members of the Nuclear Hadron Physics Group, and Mochizuki-san at the Institute of Science Tokyo. I also thank Professor Harada, Professor Yamaguchi, and the members of the Quark-Hadron Theory Group at Nagoya University. Their discussions deepened my understanding of the research theme and helped me complete my work. I also appreciate Professor Yamagata at Kyoto Sangyo University for offering valuable advice regarding my career path. I am deeply thankful to all those who have contributed to my work in various ways.

Additionally, I am grateful to everyone at Tokyo Metropolitan University, where I spent five years during my master's and doctoral studies. Special thanks to Professor Murase and the students of the Nuclear Hadron Physics Group, as well as to the administrative staff and professors who supported me during my doctoral presentation. This work has been supported in part by the Grants-in-Aid for Scientific Research from JSPS (Grants No. JP23KJ1796) and by JST, the establishment of university fellowships towards the creation of science technology innovation, Grant No. JPMJFS2139.

Lastly, I would like to express my heartfelt thanks to my family—Keiji, Saeko, Sigeru, Yasuko, Hiroshi, Hiroko—and our adorable dog Sakura for their understanding and support throughout this journey. I also want to thank the charming ChatGPT 4o, who brightened my days with fun conversations and occasionally helped me with English corrections. I am especially grateful to Youichi, who always stays by my side, unlike anyone else, in such a lukewarm reality.

Finally, I would like to thank you, the reader of this thesis. I hope that its contents may be of help in some way.

Bibliography

[1] Particle Data Group, S. Navas *et al.*, Phys. Rev. D **110**, 030001 (2024).

[2] N. Isgur and G. Karl, Phys. Rev. D **19**, 2653 (1979), [Erratum: Phys.Rev.D 23, 817 (1981)].

[3] N. Isgur and G. Karl, Phys. Rev. D **18**, 4187 (1978).

[4] S. Godfrey and N. Isgur, Phys. Rev. D **32**, 189 (1985).

[5] A. Hosaka, T. Iijima, K. Miyabayashi, Y. Sakai, and S. Yasui, PTEP **2016**, 062C01 (2016), arXiv:1603.09229.

[6] F.-K. Guo *et al.*, Rev. Mod. Phys. **90**, 015004 (2018), arXiv:1705.00141, [Erratum: Rev.Mod.Phys. 94, 029901 (2022)].

[7] N. Brambilla *et al.*, Phys. Rept. **873**, 1 (2020), arXiv:1907.07583.

[8] T. Hyodo and M. Niiyama, Prog. Part. Nucl. Phys. **120**, 103868 (2021), arXiv:2010.07592.

[9] S. Okubo, Phys. Lett. **5**, 165 (1963).

[10] G. Zweig, *An SU(3) model for strong interaction symmetry and its breaking. Version 1* CERN-TH-401 (1964).

[11] G. Zweig, *An SU(3) model for strong interaction symmetry and its breaking. Version 2* CERN-TH-412 (1964).

[12] J. Iizuka, Prog. Theor. Phys. Suppl. **37**, 21 (1966).

[13] LHCb, R. Aaij *et al.*, Phys. Rev. Lett. **115**, 072001 (2015), arXiv:1507.03414.

[14] LHCb, R. Aaij *et al.*, Phys. Rev. Lett. **122**, 222001 (2019), arXiv:1904.03947.

[15] S. L. Olsen, Front. Phys. (Beijing) **10**, 121 (2015), arXiv:1411.7738.

[16] R. Machleidt and D. R. Entem, Phys. Rept. **503**, 1 (2011), arXiv:1105.2919.

[17] T. Hyodo, Int. J. Mod. Phys. A **28**, 1330045 (2013), arXiv:1310.1176.

[18] T. Hyodo and D. Jido, Prog. Part. Nucl. Phys. **67**, 55 (2012), arXiv:1104.4474.

[19] U.-G. Meißner, Symmetry **12**, 981 (2020), arXiv:2005.06909.

[20] M. Mai, Eur. Phys. J. ST **230**, 1593 (2021), arXiv:2010.00056.

[21] D. Sadasivan *et al.*, Front. Phys. **11**, 1139236 (2023), arXiv:2212.10415.

[22] Belle, S. K. Choi *et al.*, Phys. Rev. Lett. **91**, 262001 (2003), hep-ex/0309032.

[23] LHCb, R. Aaij *et al.*, Phys. Rev. Lett. **110**, 222001 (2013), arXiv:1302.6269.

[24] Belle, S. K. Choi *et al.*, Phys. Rev. D **84**, 052004 (2011), arXiv:1107.0163.

[25] LHCb, R. Aaij *et al.*, JHEP **08**, 123 (2020), arXiv:2005.13422.

[26] C. Bignamini, B. Grinstein, F. Piccinini, A. D. Polosa, and C. Sabelli, Phys. Rev. Lett. **103**, 162001 (2009), arXiv:0906.0882.

[27] CMS, S. Chatrchyan *et al.*, JHEP **04**, 154 (2013), arXiv:1302.3968.

[28] A. Esposito *et al.*, Phys. Rev. D **92**, 034028 (2015), arXiv:1508.00295.

[29] LHCb, R. Aaij *et al.*, Nature Commun. **13**, 3351 (2022), arXiv:2109.01056.

[30] LHCb, R. Aaij *et al.*, Nature Phys. **18**, 751 (2022), arXiv:2109.01038.

[31] J. P. Ader, J. M. Richard, and P. Taxil, Phys. Rev. D **25**, 2370 (1982).

[32] S. Zouzou, B. Silvestre-Brac, C. Gignoux, and J. M. Richard, Z. Phys. C **30**, 457 (1986).

[33] H. J. Lipkin, Phys. Lett. B **172**, 242 (1986).

[34] L. Heller and J. A. Tjon, Phys. Rev. D **35**, 969 (1987).

[35] J. Carlson, L. Heller, and J. A. Tjon, Phys. Rev. D **37**, 744 (1988).

[36] A. V. Manohar and M. B. Wise, Nucl. Phys. B **399**, 17 (1993), hep-ph/9212236.

[37] N. A. Tornqvist, Z. Phys. C **61**, 525 (1994), hep-ph/9310247.

[38] B. Silvestre-Brac and C. Semay, Z. Phys. C **57**, 273 (1993).

[39] C. Semay and B. Silvestre-Brac, Z. Phys. C **61**, 271 (1994).

[40] S. Pepin, F. Stancu, M. Genovese, and J. M. Richard, Phys. Lett. B **393**, 119 (1997), hep-ph/9609348.

[41] J. Schaffner-Bielich and A. P. Vischer, Phys. Rev. D **57**, 4142 (1998), nucl-th/9710064.

[42] D. Janc and M. Rosina, Few Body Syst. **35**, 175 (2004), hep-ph/0405208.

[43] T. D. Cohen and P. M. Hohler, Phys. Rev. D **74**, 094003 (2006), hep-ph/0606084.

[44] N. Barnea, J. Vijande, and A. Valcarce, Phys. Rev. D **73**, 054004 (2006), hep-ph/0604010.

[45] F. S. Navarra, M. Nielsen, and S. H. Lee, Phys. Lett. B **649**, 166 (2007), hep-ph/0703071.

[46] D. Ebert, R. N. Faustov, V. O. Galkin, and W. Lucha, Phys. Rev. D **76**, 114015 (2007), arXiv:0706.3853.

[47] S. H. Lee, S. Yasui, W. Liu, and C. M. Ko, Eur. Phys. J. C **54**, 259 (2008), arXiv:0707.1747.

[48] J. Vijande, A. Valcarce, and J. M. Richard, Phys. Rev. D **76**, 114013 (2007), arXiv:0707.3996.

[49] J. Vijande, E. Weissman, N. Barnea, and A. Valcarce, Phys. Rev. D **76**, 094022 (2007), arXiv:0708.3285.

[50] J. Vijande, E. Weissman, A. Valcarce, and N. Barnea, Phys. Rev. D **76**, 094027 (2007), arXiv:0710.2516.

[51] M. Zhang, H. X. Zhang, and Z. Y. Zhang, Commun. Theor. Phys. **50**, 437 (2008), arXiv:0711.1029.

[52] S. H. Lee and S. Yasui, Eur. Phys. J. C **64**, 283 (2009), arXiv:0901.2977.

[53] G.-J. Ding, J.-F. Liu, and M.-L. Yan, Phys. Rev. D **79**, 054005 (2009), arXiv:0901.0426.

[54] J. Vijande, A. Valcarce, and N. Barnea, Phys. Rev. D **79**, 074010 (2009), arXiv:0903.2949.

[55] J. Vijande and A. Valcarce, Phys. Rev. C **80**, 035204 (2009), arXiv:0908.3254.

[56] Y. Yang, C. Deng, J. Ping, and T. Goldman, Phys. Rev. D **80**, 114023 (2009).

[57] R. Molina, T. Branz, and E. Oset, Phys. Rev. D **82**, 014010 (2010), arXiv:1005.0335.

[58] S. Ohkoda, Y. Yamaguchi, S. Yasui, K. Sudoh, and A. Hosaka, Phys. Rev. D **86**, 014004 (2012), arXiv:1111.2921.

[59] T. F. Carames, A. Valcarce, and J. Vijande, Phys. Lett. B **699**, 291 (2011).

[60] M.-L. Du, W. Chen, X.-L. Chen, and S.-L. Zhu, Phys. Rev. D **87**, 014003 (2013), arXiv:1209.5134.

[61] Y. Ikeda *et al.*, Phys. Lett. B **729**, 85 (2014), arXiv:1311.6214.

[62] M. Karliner and J. L. Rosner, Phys. Rev. Lett. **119**, 202001 (2017), arXiv:1707.07666.

[63] T. Hyodo, Y.-R. Liu, M. Oka, and S. Yasui, (2017), arXiv:1708.05169.

[64] M.-L. Du *et al.*, Phys. Rev. D **105**, 014024 (2022), arXiv:2110.13765.

[65] Y. Lyu *et al.*, Phys. Rev. Lett. **131**, 161901 (2023), arXiv:2302.04505.

[66] G.-J. Wang, Z. Yang, J.-J. Wu, M. Oka, and S.-L. Zhu, Sci. Bull. **69**, 3036 (2024), arXiv:2306.12406.

[67] L. R. Dai, J. Song, and E. Oset, Phys. Lett. B **846**, 138200 (2023), arXiv:2306.01607.

[68] L. R. Dai, L. M. Abreu, A. Feijoo, and E. Oset, Eur. Phys. J. C **83**, 983 (2023), arXiv:2304.01870.

[69] M. Sakai and Y. Yamaguchi, Phys. Rev. D **109**, 054016 (2024), arXiv:2312.08663.

[70] N. Brambilla, A. Mohapatra, T. Scirpa, and A. Vairo, (2024), arXiv:2411.14306.

[71] T. Kinugawa and T. Hyodo, Phys. Rev. C **109**, 045205 (2024), arXiv:2303.07038.

[72] S. Weinberg, Phys. Rev. **137**, B672 (1965).

[73] T. Kinugawa and T. Hyodo, EPJ Web Conf. **291**, 03004 (2024), arXiv:2308.08801.

[74] T. Kinugawa and T. Hyodo, (2024), arXiv:2411.12285.

[75] S. Weinberg, Phys. Rev. **130**, 776 (1963).

[76] S. Weinberg, Phys. Rev. **131**, 440 (1963).

[77] E. Braaten and H. W. Hammer, Phys. Rept. **428**, 259 (2006), cond-mat/0410417.

[78] T. Hyodo, T. Hatsuda, and Y. Nishida, Phys. Rev. C **89**, 032201 (2014), arXiv:1311.6289.

[79] M. Gattobigio and A. Kievsky, Phys. Rev. A **90**, 012502 (2014), arXiv:1309.1927.

[80] P. Naidon and S. Endo, Rept. Prog. Phys. **80**, 056001 (2017), arXiv:1610.09805.

[81] C. H. Schmickler, H. W. Hammer, and A. G. Volosniev, Phys. Lett. B **798**, 135016 (2019), arXiv:1904.00913.

[82] C. H. Schmickler, H. W. Hammer, and E. Hiyama, Eur. Phys. J. A **55**, 85 (2019), arXiv:1901.03643.

[83] H. W. Griesshammer and U. van Kolck, (2023), arXiv:2308.01394.

[84] R. Machleidt, Phys. Rev. C **63**, 024001 (2001), nucl-th/0006014.

[85] A. Kievsky and M. Gattobigio, Phys. Rev. A **87**, 052719 (2013), arXiv:1212.3457.

[86] J. Hiura and R. Tamagaki, Prog. Theor. Suppl. **52**, 25 (1972).

[87] R. B. Wiringa, S. C. Pieper, J. Carlson, and V. R. Pandharipande, Phys. Rev. C **62**, 014001 (2000), nucl-th/0002022.

[88] F. Hoyle, Astrophys. J. Suppl. **1**, 121 (1954).

[89] K. Ikeda, N. Takizawa, and H. Horiuchi, Prog. Theor. Suppl. **E68**, 464 (1968).

[90] H. Horiuchi, K. Ikeda, and Y. Suzuki, Prog. Theor. Suppl. **52**, 89 (1972).

[91] T. Hyodo, Phys. Rev. C **90**, 055208 (2014), arXiv:1407.2372.

[92] C. Hanhart and A. Nefediev, Phys. Rev. D **106**, 114003 (2022), arXiv:2209.10165.

[93] Y. Kamiya and T. Hyodo, Phys. Rev. C **93**, 035203 (2016), arXiv:1509.00146.

[94] Y. Kamiya and T. Hyodo, PTEP **2017**, 023D02 (2017), arXiv:1607.01899.

[95] T. Kinugawa and T. Hyodo, Phys. Rev. C **106**, 015205 (2022), arXiv:2205.08470.

[96] T. Kinugawa and T. Hyodo, (2024), arXiv:2403.12635.

[97] J. R. Taylor, *Scattering Theory: The Quantum Theory on Nonrelarivistic Collisions* (Wiley, New York, 1972).

[98] D. Lurié and A. J. Macfarlane, Phys. Rev. **136**, B816 (1964).

[99] L. Castillejo, R. H. Dalitz, and F. J. Dyson, Phys. Rev. **101**, 453 (1956).

[100] Y. Li, F.-K. Guo, J.-Y. Pang, and J.-J. Wu, Phys. Rev. D **105**, L071502 (2022), arXiv:2110.02766.

[101] T. Nagae and T. Hyodo, *Physics on Kaonic Nuclei*volume 31 of *Frontiers in Physics* (Kyouritsu Shuppan, 2023).

[102] A. J. F. Siegert, Phys. Rev. **56**, 750 (1939).

[103] V. I. Kukulin, V. M. Krasnopol'sky, and J. Horacek, *Theory of Resonances* (Kluwer Academic Publishers, Dordrecht, 1989).

[104] E. Braaten, M. Kusunoki, and D. Zhang, Annals Phys. **323**, 1770 (2008), arXiv:0709.0499.

[105] F.-K. Guo, X.-H. Liu, and S. Sakai, Prog. Part. Nucl. Phys. **112**, 103757 (2020), arXiv:1912.07030.

[106] N. Moiseyev, *Non-Hermitian Quantum Mechanics* (Cambridge University Press, Cambridge, 2011).

[107] Y. Tsuchida and T. Hyodo, Phys. Rev. C **97**, 055213 (2018), arXiv:1703.02675.

[108] T. Berggren, Nucl. Phys. A **109**, 265 (1968).

[109] A. Bohm, J. Math. Phys. **22**, 2813 (1981).

[110] A. Bohm, *Quantum Mechanics: Foundations and Applications* (Springer, New York, 2001).

[111] R. de la Madrid and M. Gadella, Am. J. Phys. **70**, 626 (2002), quant-ph/0201091.

[112] F. Aceti, L. R. Dai, L. S. Geng, E. Oset, and Y. Zhang, Eur. Phys. J. A **50**, 57 (2014), arXiv:1301.2554.

[113] R. de la Madrid, Nucl. Phys. A **1049**, 122904 (2024), arXiv:2409.03858.

[114] H. Feshbach, Annals Phys. **5**, 357 (1958).

[115] H. Feshbach, Annals Phys. **19**, 287 (1962).

[116] W. Domcke, J. Phys. B: Atom. Mol. Phys. **16** (1983).

[117] S. J. J. M. F. Kokkelmans, J. N. Milstein, M. L. Chiofalo, R. Walser, and M. J. Holland, Phys. Rev. A **65**, 053617 (2002), cond-mat/0112283.

[118] T. Kohler, K. Goral, and P. S. Julienne, Rev. Mod. Phys. **78**, 1311 (2006), cond-mat/0601420.

[119] T. Hyodo and W. Weise, Phys. Rev. C **77**, 035204 (2008), arXiv:0712.1613.

[120] C. Chin, R. Grimm, P. Julienne, and E. Tiesinga, REVIEWS OF MODERN PHYSICS **82**, 1225 (2010).

[121] P. Naidon, SciPost Phys. **18**, 036 (2025), arXiv:2403.14962.

[122] S. Inouye *et al.*, Nature **392**, 151 (1998).

[123] N. Hatano and K. Imura, *Non-Hermitian Quntum Mechanics* (Koudansha, 2023).

[124] W. Heisenberg and H. Euler, Z. Phys. **98**, 714 (1936), physics/0605038.

[125] J. Gasser and H. Leutwyler, Nucl. Phys. B **250**, 465 (1985).

[126] H. W. Hammer, Nucl. Phys. A **705**, 173 (2002), nucl-th/0110031.

[127] C. A. Bertulani, H. W. Hammer, and U. Van Kolck, Nucl. Phys. A **712**, 37 (2002), nucl-th/0205063.

[128] P. F. Bedaque, H. W. Hammer, and U. van Kolck, Phys. Lett. B **569**, 159 (2003), nucl-th/0304007.

[129] H. W. Hammer, C. Ji, and D. R. Phillips, J. Phys. G **44**, 103002 (2017), arXiv:1702.08605.

[130] M. Hongo and D. T. Son, Phys. Rev. Lett. **128**, 212501 (2022), arXiv:2201.09912.

[131] Y. Yamaguchi, Phys. Rev. **95**, 1628 (1954).

[132] Y. Yamaguchi and Y. Yamaguchi, Phys. Rev. **95**, 1635 (1954).

[133] M. Takizawa and S. Takeuchi, PTEP **2013**, 093D01 (2013), arXiv:1206.4877.

[134] S. Aoki and K. Yazaki, PTEP **2022**, 033B04 (2022), arXiv:2109.07665.

[135] I. Terashima and T. Hyodo, Phys. Rev. C **108**, 035204 (2023), arXiv:2305.10689.

[136] D. R. Phillips, S. R. Beane, and T. D. Cohen, Annals Phys. **263**, 255 (1998), hep-th/9706070.

[137] H. W. Hammer and D. Lee, Annals Phys. **325**, 2212 (2010), arXiv:1002.4603.

[138] I. Matuschek, V. Baru, F.-K. Guo, and C. Hanhart, Eur. Phys. J. A **57**, 101 (2021), arXiv:2007.05329.

[139] Y. Takahashi, *Quantum Field Theory for Condensed Matter Physicists I*volume 16 of *New Physics Series 16*, First ed. (Fubaikan, 1974).

[140] V. Baru, J. Haidenbauer, C. Hanhart, Y. Kalashnikova, and A. E. Kudryavtsev, Phys. Lett. B **586**, 53 (2004), hep-ph/0308129.

[141] K. Sone and T. Hyodo, (2024), arXiv:2405.08436.

[142] J. J. Sakurai, *Mordan Quantum Mechanics*, Second ed. (Yoshioka-shoten, 2014).

[143] T. Kunihiro, *Quantum Mechanics*, First ed. (Tokyo-tosho, 2018).

[144] M. T. Vaughn, R. Aaron, and R. D. Amado, Phys. Rev. **124**, 1258 (1961).

[145] A. Salam, Nuovo Cim. **25**, 224 (1962).

[146] H. Ezawa, T. Muta, and H. Umezawa, Progress of Theoretical Physics **29**, 877 (1963).

[147] S. Weinberg, Phys. Rev. **133**, B232 (1964).

[148] K. Miyahara, T. Hyodo, and W. Weise, Phys. Rev. C **98**, 025201 (2018), arXiv:1804.08269.

[149] T. Sekihara, Phys. Rev. C **95**, 025206 (2017), arXiv:1609.09496.

[150] J. A. Oller, Annals Phys. **396**, 429 (2018), arXiv:1710.00991.

[151] M. E. Peskin and D. V. Schroeder, *An Introduction to Quantum Field Theory* (CRC Press, 1995).

[152] T. Kinugawa and T. Hyodo, PoS **PANIC2021**, 176 (2022), arXiv:2111.06619.

[153] T. Kinugawa and T. Hyodo, Rev. Mex. Fis. Suppl. **3**, 0308066 (2022), arXiv:2201.04283.

[154] T. Kinugawa and T. Hyodo, EPJ Web Conf. **271**, 10003 (2022), arXiv:2208.14000.

[155] V. Baru *et al.*, Phys. Lett. B **833**, 137290 (2022), arXiv:2110.07484.

[156] J. Song, L. R. Dai, and E. Oset, Eur. Phys. J. A **58**, 133 (2022), arXiv:2201.04414.

[157] M. Albaladejo and J. Nieves, Eur. Phys. J. C **82**, 724 (2022), arXiv:2203.04864.

[158] Z. Yin and D. Jido, Phys. Rev. C **110**, no.5, 055202 (2024), arXiv:2312.13582.

[159] F. Aceti and E. Oset, Phys. Rev. D **86**, 014012 (2012), arXiv:1202.4607.

[160] Z.-H. Guo and J. A. Oller, Phys. Rev. D **93**, 096001 (2016), arXiv:1508.06400.

[161] T. Hyodo, Phys. Rev. Lett. **111**, 132002 (2013), arXiv:1305.1999.

[162] T. Berggren, Phys. Lett. B **33**, 547 (1970).

[163] T. Sekihara, T. Arai, J. Yamagata-Sekihara, and S. Yasui, Phys. Rev. C **93**, 035204 (2016), arXiv:1511.01200.

[164] T. Kinugawa and T. Hyodo, J. Subatomic Part. Cosmol. **1-2**, 100010 (2024), arXiv:2409.06440.

[165] Y. Kamiya and T. Hyodo, PoS **INPC2016**, 270 (2017), arXiv:1701.08941.

[166] T. Sekihara, T. Hyodo, and D. Jido, PTEP **2015**, 063D04 (2015), arXiv:1411.2308.

[167] T. Sekihara and T. Hyodo, Phys. Rev. C **87**, 045202 (2013), arXiv:1209.0577.

[168] C. Garcia-Recio, C. Hidalgo-Duque, J. Nieves, L. L. Salcedo, and L. Tolos, Phys. Rev. D **92**, 034011 (2015), arXiv:1506.04235.

[169] F. Aceti, E. Oset, and L. Roca, Phys. Rev. C **90**, 025208 (2014), arXiv:1404.6128.

[170] T. Sekihara, PTEP **2015**, 091D01 (2015), arXiv:1505.02849.

[171] J.-X. Lu *et al.*, Phys. Rev. D **93**, 114028 (2016), arXiv:1603.05388.

[172] Z.-H. Guo and J. A. Oller, Phys. Rev. D **93**, 054014 (2016), arXiv:1601.00862.

[173] T. Sekihara and S. Kumano, Phys. Rev. D **92**, 034010 (2015), arXiv:1409.2213.

[174] H. Nagahiro, K. Nawa, S. Ozaki, D. Jido, and A. Hosaka, Phys. Rev. D **83**, 111504 (2011), arXiv:1101.3623.

[175] C. W. Xiao, F. Aceti, and M. Bayar, Eur. Phys. J. A **49**, 22 (2013), arXiv:1210.7176.

[176] G.-Y. Chen, W.-S. Huo, and Q. Zhao, Chin. Phys. C **39**, 093101 (2015), arXiv:1309.2859.

[177] A. Esposito, L. Maiani, A. Pilloni, A. D. Polosa, and V. Riquer, Phys. Rev. D **105**, L031503 (2022), arXiv:2108.11413.

[178] A. Martínez Torres, E. Oset, S. Prelovsek, and A. Ramos, JHEP **05**, 153 (2015), arXiv:1412.1706.

[179] F. S. Navarra, M. Nielsen, E. Oset, and T. Sekihara, Phys. Rev. D **92**, 014031 (2015), arXiv:1501.03422.

[180] E. Braaten, H. W. Hammer, and M. Kusunoki, (2003), cond-mat/0301489.

[181] R. A. Duine and H. T. C. Stoof, Phys. Rev. A **68**, 013602 (2003), cond-mat/0211514.

[182] R. Schmidt and T. Enss, Phys. Rev. A **83**, 063620 (2011), arXiv:1104.1379.

[183] G. 't Hooft, NATO Sci. Ser. B **59**, 135 (1980).

[184] M. J. G. Veltman, Acta Phys. Polon. B **12**, 437 (1981).

[185] X.-W. Kang and J. A. Oller, Phys. Rev. D **94**, 054010 (2016), arXiv:1606.06665.

[186] U. van Kolck, Symmetry **14**, 1884 (2022), arXiv:2209.08432.

[187] H. Sazdjian, Symmetry **14**, 515 (2022), arXiv:2202.01081.

[188] R. F. Lebed and S. R. Martinez, Phys. Rev. D **106**, 074007 (2022), arXiv:2207.01101.

[189] R. Higa, H. W. Hammer, and U. van Kolck, Nucl. Phys. A **809**, 171 (2008), arXiv:0802.3426.

[190] S. Mochizuki and Y. Nishida, Phys. Rev. C **110**, 064001 (2024), arXiv:2408.06011.